Optimization-based Approaches for Fault Detection and Estimation with applications to health-monitoring of energy systems

Dong, J.

DOI
10.4233/uuid:32f02090-19d2-4c6f-a8bf-9cbfb7cffd45

Publication date
2023

Document Version
Final published version

Citation (APA)
Dong, J. (2023). *Optimization-based Approaches for Fault Detection and Estimation: with applications to health-monitoring of energy systems*. [Dissertation (TU Delft), Delft University of Technology]. https://doi.org/10.4233/uuid:32f02090-19d2-4c6f-a8bf-9cbfb7cffd45

Important note
To cite this publication, please use the final published version (if applicable).
Please check the document version above.

Optimization-based Approaches for Fault Detection and Estimation

with applications to health-monitoring of energy systems

Optimization-based Approaches for Fault Detection and Estimation

with applications to health-monitoring of energy systems

Dissertation

for the purpose of obtaining the degree of doctor
at Delft University of Technology,
by the authority of the Rector Magnificus, prof.dr.ir. T.H.J.J. van der Hagen,
chair of the Board for Doctorates,
to be defended publicly on
Wednesday 06 September 2023 at 10:00 o'clock

by

Jingwei DONG

Master of Engineering in Control Science and Engineering,
Harbin Institute of Technology, China
born in Lianyungang, China

This dissertation has been approved by the promotors.

Composition of the doctoral committee:

Rector Magnificus,	Chairperson
Prof.dr.ir. T. Keviczky,	Delft University of Technology, promotor
Dr. P. Mohajerin Esfahani,	Delft University of Technology, promotor
Independent members:	
Prof.dr.ir. M.H.G. Verhaegen,	Delft University of Technology
Prof.dr.ir. M. Popov,	Delft University of Technology
Prof.dr. S. Yin,	Norwegian University of Science and Technology
Dr. A.M.H. Teixeira,	Uppsala University
Dr. S.D.G.M. Pequito,	Uppsala University

This research was financially supported by China Scholarship Council.

Keywords: Robust fault detection and estimation, Probabilistic certificates, Filter design, Optimization methods, Energy systems
Printed by: Ridderprint

ISBN 978-94-6483-378-2

An electronic version of this dissertation is available at
`http://repository.tudelft.nl/`.

To my parents.

Contents

Summary

Advancements in technology and societal demands have led to increasing complexity, size, and automation in modern industrial systems. This trend makes these systems more safety-critical, as the occurrence of faults in system components or subsystems may cause the entire system to fail, resulting in significant economic losses and casualties. Consequently, developing an effective fault diagnosis method is crucial for ensuring the reliability, safety, and performance of industrial systems, especially energy systems, which are so relevant to our lives. However, most model-based fault diagnosis systems developed based on observers and parity space relations have the same order as that of the system. This can cause a significant computational burden when dealing with large-scale and high-dimensional systems.

This thesis is dedicated to the design of fault diagnosis filters in the framework of differential-algebraic equations, which produce scalable residual generators with design flexibility. Meanwhile, we consider the impact of disturbances and stochastic noise on diagnosis results, as well as the fault diagnosis problem within the finite frequency domain. In order to design filters capable of handling these issues, we solve filter parameters through optimization problems that are constructed based on specific diagnosis requirements. The main research contents are as follows.

First, we propose a diagnosis scheme to reliably detect the active mode of switched affine systems with measurement noise. We take into account the delay between the active mode and its corresponding controller caused by the detection process, which is known as asynchronous switching. Following the mindset of the generalized observer scheme, we develop an optimization framework to solve a bank of filters, where each residual is sensitive to all but only one mode. The $\mathcal{H}_2$ norm method is adopted to deal with the stochastic noise. The derived optimization problem is tractable because it can be safely approximated through linear matrix inequalities. We further develop a determination method of thresholds along with probabilistic false-alarm guarantees. Additionally, we provide an estimate of the time required for the diagnosis component to recognize the correct mode.

Second, in light of the conservatism associated with fault diagnosis methods developed for the entire frequency domain, for the first time, we study the design of fault detection and estimation filters in the framework of differential-algebraic equations in the finite frequency domain. To tackle this problem, we introduce mixed $\mathcal{H}_2/\mathcal{H}_-$ performance indices and formulate the design of fault detection filters with residuals of arbitrary dimensions into an optimization problem. We propose a threshold determination method that provides probabilistic guarantees on both false alarms and missing detection rates. Then, we replace the $\mathcal{H}_-$ index with the finite-frequency $\mathcal{H}_\infty$ norm to characterize the estimation performance in the proposed optimization framework. This enables us to obtain a design method for the fault estimation filter in the finite frequency domain. To reduce computational complexity,

we further relax the design requirements and formulate the design of the fault estimation filter into a quadratic programming problem with an analytical solution.

Lastly, we consider ground fault detection for inverter-based microgrid systems. This problem is challenging since the fault current deviates slightly from its nominal value and the effect of the disturbance is similar to that of the fault. We design fault detection filters for the following two scenarios: (i) the disturbance can be completely decoupled, and (ii) the disturbance cannot be completely decoupled. In the case where the disturbance can be completely decoupled, the problem is a special case of the mode detection problem mentioned before. When the disturbance cannot be completely decoupled, we use available disturbance patterns to train the filter and enhance its robustness. The filter design is formulated into a quadratic programming problem that has an approximate analytical solution. This solution can be made arbitrarily precise and used to update the filter parameters online.

Samenvatting

De technologische vooruitgang en de maatschappelijke eisen hebben geleid tot een toenemende complexiteit, omvang en automatisering van moderne industriële systemen. Deze trend maakt deze systemen meer veiligheidskritisch, aangezien het optreden van fouten in systeemcomponenten of subsystemen kan leiden tot het falen van het gehele systeem, met aanzienlijke economische verliezen en slachtoffers tot gevolg. Bijgevolg is de ontwikkeling van een doeltreffende foutendiagnosemethode cruciaal om de betrouwbaarheid, veiligheid en prestaties van industriële systemen te garanderen. De meeste modelgebaseerde foutendiagnosesystemen die zijn ontwikkeld op basis van waarnemers en pariteitsruimte-relaties hebben echter dezelfde orde als die van het systeem. Dit kan een aanzienlijke rekenlast veroorzaken bij grootschalige en hoog-dimensionale systemen.

Dit proefschrift is gewijd aan het ontwerp van foutdiagnosefilters in het kader van differentiaalalgebraïsche vergelijkingen, die schaalbare residugeneratoren met ontwerpflexibiliteit produceren. Ondertussen houden we rekening met de invloed van storingen en stochastische ruis op de diagnoseresultaten en met het probleem van foutdiagnose binnen het eindige frequentiedomein. Om filters te ontwerpen die deze problemen aankunnen, lossen we filterparameters op via optimalisatieproblemen die zijn geconstrueerd op basis van verschillende ontwerpeisen. De belangrijkste onderzoeksinhouden zijn als volgt.

Ten eerste stellen wij een diagnoseschema voor om de actieve modus van geschakelde affiene systemen met asynchrone schakelingen en meetruis betrouwbaar te detecteren. Naar het voorbeeld van het schema van de veralgemeende waarnemer ontwikkelen wij een optimalisatiekader om een reeks filters op te lossen, waarbij elk residu gevoelig is voor alle, maar slechts één modus. De $\mathcal{H}_2$ normmethode wordt toegepast om met de stochastische ruis om te gaan. Het afgeleide optimalisatieprobleem is hanteerbaar omdat het veilig kan worden benaderd via lineaire matrixongelijkheden. Verder ontwikkelen we een methode voor het bepalen van drempels, samen met probabilistische garanties voor vals alarm. Bovendien geven wij een schatting van de tijd die de diagnosecomponent nodig heeft om de juiste modus te herkennen.

Ten tweede bestuderen we, in het licht van het conservatisme dat gepaard gaat met foutdiagnosemethoden die ontwikkeld zijn voor het gehele frequentiedomein, voor het eerst het ontwerp van foutdetectie- en schattingsfilters in het kader van differentiaalalgebraïsche vergelijkingen in het eindige frequentiedomein. Om dit probleem aan te pakken, introduceren we gemengde prestatie-indices van $\mathcal{H}_2/\mathcal{H}_-$ en formuleren we het ontwerp van foutdetectiefilters met residuen van willekeurige afmetingen als een optimalisatieprobleem. We stellen een drempelbepalingsmethode voor die probabilistische garanties biedt voor zowel vals alarm als ontbrekende detectiepercentages. Vervolgens vervangen we de index $\mathcal{H}_-$ door de norm voor eindige frequenties $\mathcal{H}_\infty$ om de schattingsprestaties in het voorgestelde optimalisatiekader te karakteriseren en de ontwerpmethode voor het foutschattingsfilter in het eindige frequentiedomein te verkrijgen. Om de computationele complexiteit te verminderen, versoepelen we de ontwerpeisen en formuleren we het

ontwerp van het foutschattingsfilter in een kwadratisch programmeerprobleem met een analytische oplossing.

Ten slotte beschouwen we aardfoutdetectie voor op omvormers gebaseerde microgridsystemen. Dit is een uitdagend probleem omdat de foutstroom licht afwijkt van de nominale waarde en het effect van de storing vergelijkbaar is met dat van de fout. We ontwerpen filters voor foutdetectie voor de volgende twee scenario's: (i) de storing kan volledig ontkoppeld worden, en (ii) de storing kan niet volledig ontkoppeld worden. In het geval dat de storing volledig ontkoppeld kan worden, is het probleem een speciaal geval van het eerder genoemde modedetectieprobleem. Als de storing niet volledig ontkoppeld kan worden, gebruiken we beschikbare storingspatronen om het filter te trainen en zijn robuustheid te verbeteren. Het filterontwerp is geformuleerd in een kwadratisch programmeerprobleem dat een analytische oplossing heeft. Deze oplossing kan willekeurig nauwkeurig gemaakt worden en gebruikt worden om de filterparameters online bij te werken.

Acknowledgements

Looking back at my PhD study, I am glad that I made the decision to embark on the path of pursuing a doctoral degree at TU Delft five years ago. I am deeply grateful to all those who have supported and encouraged me throughout this incredible journey.

First of all, my deepest thankfulness goes to my supervisors Peyman Mohajerin Esfahani and Tamás Keviczky. I feel fortunate to have the opportunity to work and study under Peyman's guidance and support. He has set an example for me in academics through his unwavering passion for research, his adept approach to problem-solving, and his profound and extensive knowledge. I will never forget the time we went to the library to revise our first journal paper after the 3ME building closed. I would like to express my gratitude to Tamás for his prompt support in my time of need. His advice during my go/no-go meeting has been instrumental. I am also grateful to Sérgio Pequito for his assistance during the last two years of my PhD study. As my copromotor, he offered numerous insightful ideas and provided essential guidance for paper revision.

My sincere thanks to the defense committee members, Prof. Michel Verhaegen, Prof. Marjan Popov, Prof. Shen Yin, and Dr. André Teixeira, for their acceptance to be part of the committee and for their constructive comments that improved the quality of this dissertation.

I would like to thank all my colleagues from Peyman's group. Thanks to Arman for his instruction on the writing of the first conference paper. Thanks to Amin for his help when I just started my PhD study. Thanks to Kaikai for his valuable advice on academics and all the discussions. Thanks to Yucheng for the collaborative results that form Chapter 4 of this dissertation. Thanks to my office mates Shabnam and Rayyan for the friendly working atmosphere. I would also like to thank Pedro, Max, Reza, Mohammad, etc.

I want to express thanks to all my friends during these few years in Delft. Thanks to Chengpeng, Yingfu, and Xiujie, we started life in Delft together and left lots of memorable moments. Thanks to my friends from DCSC, Dingshan, Ximan, Xiaoyu, Yun, Luyao, Kanghui, Shengling, Zhixin, Yongxia, Tian, Jianfeng, Maolong, Suad, Raja, and Changrui, for all the dinner parties and enjoyable moments. Thanks to Jianing and Jiaxiang, I always enjoy playing basketball with you. Thanks to Shuo, Xiuli, Hongpeng, Haiwei, and Bo. It is great to know you all.

I would like to thank my friends, Yuchen, Zhihao, Zhen, and Wanyu. Thank you for all the conversations we had during these years that helped me get through some tough times and inspired me to move on. I wish you all the best in the future.

Finally, I would like to thank my family. Thanks to my parents for their constant and unconditional support and care, which has allowed me to pursue studies without distractions these years. Thanks to my little sister, even though I cannot be with her all the time, it has been a pleasure watching her grow up and I wish her all the happiness in the world. Thanks to my grandparents. Regrettably, due to the pandemic, I was unable to see

my grandfather before his passing. I believe he would take pride in my PhD achievement. May he find peace, and may my grandmother remain in good health.

Jingwei Dong
Delft, August 2023

List of Notations

$\mathbb{R}$	the set of reals
$\mathbb{R}_+$	the set of positive reals
$\mathbb{R}^n$	the space of n dimensional real-valued vectors
$\mathcal{S}^n$	the space of $n \times n$ symmetric matrices
$\mathcal{M}^n$	the space of $n \times n$ non-singular matrices
$\mathbb{H}^n$	the space of $n \times n$ Hermitian matrices
$\mathbb{N}$	the set of non-negative integers
$\mathbb{N}_+$	the set of positive integers
I	the identity matrix with an appropriate dimension
Θ	the frequency range
$\mathbb{T}$	the transfer function
$\mathbb{T}[s]$	the output of the system in response to the input signal s
$\|\mathbb{T}\|_{\mathcal{H}_2}$	the $\mathcal{H}_2$ norm of the transfer function $\mathbb{T}$
$\|\mathbb{T}\|_{\mathcal{H}_\infty}$	the $\mathcal{H}_\infty$ norm of the transfer function $\mathbb{T}$
$\|\mathbb{T}\|_{\mathcal{H}_-(\Theta)}$	the $\mathcal{H}_-$ index of the transfer function $\mathbb{T}$ over Θ
$\|\mathbb{T}\|_{\mathcal{H}_\infty(\Theta)}$	the finite-frequency $\mathcal{H}_\infty$ norm of the transfer function $\mathbb{T}$ ove Θ
$[\mathbb{T}]_{\text{ss}}$	the steady-state gain of the transfer function $\mathbb{T}$
$\|v\|_2$	the 2-norm of the vector v
$\|v\|_\infty$	the infinity-norm of the vector v
$\|s\|_{\mathcal{L}_2}$	the $\mathcal{L}_2$-norm of the signal s
$\mathbf{Pr}[\chi]$	the probability law of the random variable χ
$\mathbf{E}[\chi]$	the expectation of the random variable χ
$M^\top$	the transpose of the matrix M
M^{-1}	the inverse of the matrix M
$M^\dagger$	the pseudo-inverse of the matrix M
M^*	the conjugate transpose of the matrix M

$\|M\|_2$	the largest singular value of the matrix M
$\text{Trace}(M)$	the trace of the matrix M
$\|M\|_F$	the Frobenius norm of the matrix M
$\text{Rank}(M)$	the rank of the matrix M
$\Lambda(M)$	the eigenvalues of the matrix M
$*$	the off-diagonal elements in symmetric matrices
$\text{diag}(\cdot)$	the diagonalization operator
$\mathbf{0}_{m\times n}$	the zero matrix with m rows and n columns
$\mathfrak{q}$	the time-shift operator

List of Abbreviations

DAE	Differential-algebraic equations
FDE	Fault detection and estimation
FDI	Fault detection and isolation
LMI	Linear matrix inequality
LTI	Linear time-invariant
GOS	Generalized observer scheme
UIO	Unknown input observer
LP	Linear programming
QP	Quadratic programming
GKYP	Generalized Kalman-Yakubovich-Popov
FAR	False alarm rate
FDR	Fault detection rate
AO	Alternating optimization
LS	Least squares
iid	independent and identically distributed
IUIE	Inversion-based unknown input estimation
ER	Exact reformulation
RR	Relaxed requirement
DG	distributed generator

1

Introduction

1

1.1 Introduction to Fault Diagnosis

The reliability of industrial systems has always been a concern for both researchers and engineers. With the advances in technology and the growing demands of society, modern industrial systems, such as power systems, transport systems, and building systems, have been evolving with higher complexity and degree of automation. This makes modern industrial systems more safety-critical because there are a large number of sensors, actuators, and communication devices integrated into these systems, which results in an increased probability of faults. Furthermore, these faults can lead to degradation in system performance, economic loss, and even personal safety issues [1, 2].

In fact, faults in some parts of the systems are unnoticed until they have serious consequences that negatively impact our lives. Take a recent incident that happened nearby as an example. In February 2023, one water pump in the heating system of building section C of 3ME in TU Delft, where the Delft Center for Systems and Control is located, malfunctioned. As a result, the entire section lost heat, and the building manager had to provide electric heaters for each room as a temporary solution. Unfortunately, the excessive use of electric heaters led to an overload in the power system, resulting in a power outage on one side of the building. This incident affected our normal work and study for several days.

Faults in large-scale industrial systems can cause more serious consequences. It was reported that the United States incurs nearly 20 billion dollars in property losses each year due to various accidents just in the chemical industry, while similar incidents annually cause economic losses of up to 27 billion dollars to the United Kingdom [3]. In 2003, due to a short circuit of cable, the northeastern United States and eastern Canada experienced the largest power outage in North American history. About 50 million people were affected, and at least 8 people died from this accident [4]. In 2015, a passenger plane of Taiwan's TransAsia Airways crashed due to engine failure, which claimed 8 lives [5].

As a result, improving the reliability and safety of industrial systems while guaranteeing their performance has been the focus of research in the last several decades. Fault diagnosis methods have emerged as one of the solutions to this issue. By detecting faults early and accurately, industrial operators can take corrective actions to prevent or minimize the impact of faults on system performance, productivity, and safety. Fault diagnosis also plays a crucial role in predictive maintenance, which helps to reduce maintenance costs, extend equipment lifespan, and improve overall system efficiency. For instance, fault diagnosis tools can help operators identify and correct faults that affect energy consumption and performance of buildings, resulting in up to 10% energy savings and leading to a more sustainable and efficient building operation [6]. According to the statistics, the annual cost of equipment maintenance in China is up to 25 billion RMB. Effective fault diagnosis and fault-tolerant control technology can reduce the accident rate by 50% to 70% and save costs by 10% to 30%, which can bring considerable economic benefits. The advantages of health monitoring systems and their expected percentages of improvement are summarized in Table I [7].

For the sake of clarity, let us introduce the following definition of faults.

Definition 1.1.1 (Fault [8])**.** *A fault is an unpermitted deviation of at least one characteristic property or parameter of the system from the acceptable/usual/standard condition.*

Consider a controlled system as depicted in Figure 1.1, where x, u, and y denote the state, the control input, and the measurement, respectively. The notation d represents the disturbance while ω represents measurement noise. Notations f_p, f_s, and f_a denote faults that happen in different parts of the system. Generally, people classify these faults into the following three categories [9]:

- **Plant faults f_p.** They are used to indicate faults within the process, such as the disconnection of a system component, which is also called component faults or parameter faults;
- **Sensor faults f_s.** These are issues that occur within sensors, which can cause a sensor to become stuck at a particular value or exhibit a variation in its scalar factor;
- **Actuator faults f_a.** These faults cause changes in actuators, such as the blocking or partial failure of an actuator.

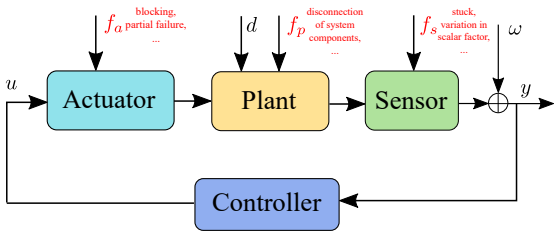

Figure 1.1: The structure of dynamical systems with different faults.

The goal of fault diagnosis is to monitor industrial processes and systems to detect and identify any faults that may occur. In order to achieve this goal, fault diagnosis typically involves three main tasks [2]:

- **Fault detection.** The building block of the fault diagnosis system is used to detect and report the occurrence of faults in the system;
- **Fault isolation.** It entails the localization and classification of different faults that have been detected;
- **Fault estimation.** It provides the description of a fault that could entail characteristics such as size and shape. Fault estimation is critical for identifying the root cause of the fault and for devising appropriate actions to restore healthy system functionality.

There are mainly two ways to implement fault diagnosis: hardware redundancy and analytical redundancy (also called software redundancy). The basic idea of hardware redundancy is to incorporate identical and redundant hardware components for a process component, where the input to the redundant hardware is the same as that of the process component. If there is a fault in the process component, it can be detected by comparing its output to that of its redundancy. If the outputs are different, it indicates faults in the process component, and the redundancy circuitry overtakes the functional process to ensure normal

function. Hardware redundancy is reliable and useful for the protection of key components. However, this scheme can increase the complexity of systems, occupy more space, and result in high costs due to the acquisition of new hardware and maintenance.

Different from hardware redundancy, the analytical redundancy method replaces the redundant component with a process model implemented in the software form, as illustrated in the diagnosis component in Figure 1.2. The model is constructed based on prior knowledge of the dynamical system, which enables the reconstruction of system behavior online. When applying the diagnosis algorithm, the diagnosis component utilizes the control input and output of the real-time process, which contain feature information, as input. Then, it compares the behavior of the real-time process with that of the fault-free system to generate diagnosis results (also called consistency checking). This scheme is cost-effective and has become the mainstream of fault diagnosis research [10, 11].

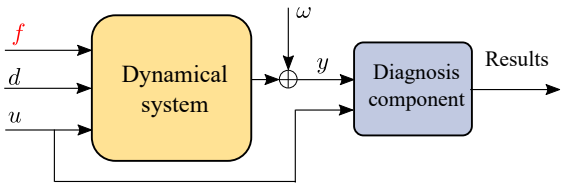

Figure 1.2: The structure of fault diagnosis systems.

1.2 A Review on Fault Diagnosis Methods

Fault diagnosis methods based on analytical redundancy can be divided into three categories: model-based methods, signal processing techniques, and knowledge-based methods [12]. Model-based fault diagnosis methods involve creating an abstract model of the system and computing the difference between its predicted behavior and the actual measurement, known as the *residual*. By analyzing the residual, faults can be detected and diagnosed. Model-based methods make full use of the intrinsic physical information of the system, and therefore, they usually provide satisfactory fault diagnosis performance for systems with a precise mathematical model. However, complex industrial systems often exhibit characteristics of strong coupling and nonlinearity. This makes it extremely challenging, and in some cases, impossible to establish accurate analytical models. As a result, model-based fault diagnosis methods show limitations when applied to complex industrial systems.

In contrast, methods based on signal processing techniques do not need to build a mathematical model of the system. People usually extract the time domain (e.g., mean, trends, standard deviation, and magnitudes) and frequency-domain (e.g., spectrum) features of the measured signals. Then, they use methods like wavelet analysis [13] and spectral analysis [14] to analyze changes in the measured signals for fault diagnosis. Signal processing techniques have achieved great success in the fault detection of rotating machinery systems, such as motor rotors and bearings [15, 16]. However, one obstacle to the widespread popularization of wavelet analysis is the absence of a standard or general method for selecting the appropriate wavelet function for different tasks [17]. Spectral analysis methods, like fast Fourier transform, have difficulties in handling complex systems with non-stationary signals and closely spaced fault frequencies. In order to deal with

non-stationary signals, several time-frequency analysis methods have been developed, whose advantages and disadvantages are summarized in [18].

Knowledge-based methods utilize prior knowledge to build a qualitative model of the system instead of a precise mathematical model. The derived qualitative model can capture the interconnections between different components of the system and illustrate the potential pathways for fault propagation. When faults occur, search algorithms such as inference and deduction are employed for fault diagnosis [19]. Commonly used qualitative models include three subcategories: fault tree [20], signed digraph [21], and expert systems [22]. Although knowledge-based methods do not require a precise mathematical model, they still have limitations in the face of complex industrial systems. On one hand, it is difficult to obtain a qualitative model due to the complexity of systems. The search algorithms and inference rules become complex as well, which easily leads to low search efficiency because of combinatorial explosions. On the other hand, knowledge-based methods are mainly based on human experience to understand the internal mechanism of the system. The lack of basic extraction of the underlying physics of the system makes it difficult to update the algorithms to adapt to changes in the system.

In recent years, the development of physical sensors enables the acquisition of large amounts of offline and online data. This motivates researchers to explore how to use the available historical data for fault diagnosis, which has led to the rapid development of data-driven fault diagnosis methods. Compared to model-based methods, data-driven approaches for fault diagnosis do not require prior knowledge about the system. They obtain information about systems and faults by analyzing historical data with some advanced techniques [23, 24]. It is clear that data-driven methods are suitable for large-scale and complex systems. However, the diagnosis performance of data-driven fault diagnosis methods relies heavily on the quality of the data, while data collected directly in industrial processes suffers from problems like sampling time, missing data, outliers, and so forth. Thus, data preprocessing is necessary. Additionally, the lack of labeled data is also a challenge due to the low frequency of failures [25].

In what follows, we provide an overview of the two most widely used fault diagnosis techniques: model-based and data-driven methods. Additionally, for readers interested in signal processing-based and knowledge-based approaches, we suggest referring to review papers [24, 26–28].

1. Model-based methods. In 1971, Beard [29] introduced a novel fault diagnosis approach that relies on mathematical modeling rather than hardware redundancy to generate residuals. Since then, various model-based fault diagnosis methods that rely on different residual generation approaches are developed. Frank [12] classified these model-based fault diagnosis methods into three categories: observer-based methods, parity space methods, and parameter identification methods.

Specifically, observer-based fault diagnosis methods employ different types of observers, such as Luenberger observers [29], unknown input observers [30–32], sliding mode observers [33, 34], and adaptive observers [35, 36], to design fault diagnosis schemes that cater to specific problems and requirements. For instance, an unknown input observer is typically used to decouple disturbances from the residual, while a sliding mode observer can handle disturbances robustly and ensure a fast convergence rate. Additionally, one can achieve fault isolation by designing a bank of observers and making each residual sensitive

to specific faults while being insensitive to others. Common fault isolation strategies include dedicated observer schemes [37] and generalized observer schemes [38].

The fault diagnosis method developed based on the parity space approach was first proposed in [39]. This method establishes an equivalence between the input and output variables in the mathematical model of the system. Then, it tests whether the actual input and output variables satisfy the equivalence relation for the purpose of fault diagnosis. Compared to observer-based methods, parity space approaches simplify the design of residual generators, as they only require finding solutions to linear equations or linear optimization problems. In [40], the authors investigate the robustness problem of parity relation-based fault detection and demonstrate that increasing the order of the parity relation could improve the robustness. More results related to parity space-based fault diagnosis approaches can be found in [1, 41].

Parameter identification-based fault diagnosis methods often represent faults as multiplicative or additive parameters that affect system parameters. This approach involves online identification of the actual process parameters and comparing them with reference parameters obtained under fault-free conditions to detect faults [2]. The least square method is a primary approach for parameter identification, offering the advantages of simplicity and robustness [42]. Another well-known method is constructing an augmented state observer, which treats faults as system states and estimates the augmented states [43]. However, this approach often requires assumptions on the derivatives of fault signals.

It is worth emphasizing that residual generators obtained through observer-based and parity space methods often have the same order as that of the system, leading to a significant computational burden when dealing with large-scale or high-dimensional systems. However, in [44], the authors propose a polynomial framework approach similar to parity space methods that can construct residual generators with the potentially lower order. This approach was later extended to linear differential-algebraic equations (DAE) in their subsequent work [45]. This expands the scope of fault diagnosis approaches as DAE models encompass various types of models, such as transfer functions, state-space models, and descriptor models. With this extension, the approach can address a wider range of fault diagnosis problems with reduced computational complexity.

All these model-based methods mentioned above rely on an accurate mathematical model of the system. However, there are always unknown uncertainties, disturbances, and stochastic noise that cannot be accurately modeled as analyzed before. These factors can pose significant challenges in fault diagnosis tasks, leading to false alarms and missing detection of faults. To tackle these challenges, researchers adopt indices such as $\mathcal{H}_2$ and $\mathcal{H}_\infty$ norms to characterize the effects of these disturbing factors on residuals. In specific, the $\mathcal{H}_2$ norm is useful in addressing stochastic aspects such as measurement noise and random disturbances, while the $\mathcal{H}_\infty$ norm is effective in achieving robustness against uncertainties with deterministic bounds and meeting frequency-domain specifications [46]. With these indices, the parameters of residual generators are generally solved through multi-objective optimization problems within the robust control framework, ensuring the robustness of the derived residual generators [47–49].

The previous results are for fault diagnosis of linear systems. For fault diagnosis of nonlinear systems, a commonly used and simple approach is to linearize systems at local operating points and treat higher-order nonlinear terms as uncertainties or disturbances.

Linearization simplifies the analysis and allows for the use of techniques developed for linear systems, see for example [50] and [51]. However, the limitation of using linearization-based approaches is their inability to effectively handle systems with a wide dynamic operating range. This is because linearization can result in a significant model mismatch in such cases. To address the limitations imposed by linearization and improve the ability to handle nonlinear terms, researchers in [52] have developed adaptive estimators to approximate the nonlinear terms. The authors in [53] propose a framework based on DAE to design fault diagnosis filters for nonlinear systems. They develop tractable optimization-based approaches and use available nonlinearity signatures to train the filter and make it robust to nonlinear terms.

In recent years, data-driven approaches have become increasingly prevalent in fault diagnosis for nonlinear systems, such as [54, 55]. This is because data-driven approaches can effectively make use of the data generated by systems and deal with nonlinear terms. In the following part, we will provide an overview of fault diagnosis methods based on data-driven approaches.

2. **Data-driven methods.** To obtain information about systems and faults, data-driven fault diagnosis methods employ techniques including system identification, multivariate statistical methods, and machine learning to process the historical data. The subspace identification technique is one of the widely used system identification methods applied to fault diagnosis. It first identifies the state-space model of the system. Model-based approaches are then used to design fault diagnosis schemes based on the derived model. In [56], the authors present the "direct identification and design" approach, which greatly reduces the complexity of system design and improves the reliability of process monitoring systems compared to the previous "identification-first, design-later" approach. Subspace identification-based process monitoring methods have attracted interest in recent years because they can utilize analytical model-based theories and methods. Some additional discussion can be found in the references [57–60].

The core idea of multivariate statistical methods is to uncover the relations between process variables and identify unique patterns in a large amount of historical industrial data. Then, they use the obtained relations or patterns to detect faults in the process by checking whether the online data satisfies the statistical relations. Multivariate statistical process monitoring methods, with representative approaches including principal component analysis (PCA) [61–64] and partial least squares (PLS) [65, 66], are more suitable for large-scale and complex industrial systems [67, 68]. This is due to their ability to handle large numbers of highly correlated variables. However, traditional PCA and PLS are linear methods while most real processes are nonlinear. Researchers have extended PCA and PLS to nonlinear systems by (i) employing polynomials or neural networks to represent nonlinearity, or (ii) using kernel methods. For example, authors in [69] develop kernel PCA which uses nonlinear kernel functions to compute the principal components. A kernel PLS method is developed in [70] to address challenges caused by nonlinear characteristics in fault diagnosis problems.

Traditional machine learning methods train artificial neural networks (ANN) or support vector machines (SVM) with healthy and faulty samples offline. When executing diagnosis tasks online, faults are detected and diagnosed by identifying the category to which the samples belong. There are several different ANN that are used to complete diagnosis tasks,

such as radial basis function networks [71], wavelet neural networks [72], probabilistic neural networks [73], and so on. The strong self-learning capability of ANN enables the ANN-based diagnosis systems automatically learn diagnosis knowledge from the data by minimizing the empirical risk. However, ANN-based fault diagnosis methods suffer from the interpretability issue because they are black boxes that lack rigorous theoretical support.

SVM-based methods have better interpretability compared to ANN, as they minimize structural risk. To recognize multiple faults and improve the accuracy of SVM-based methods, several modified SVM-based fault diagnosis methods are developed in the literature [74]. The drawbacks associated with SVM-based methods encompass inefficiency in managing massive datasets, susceptibility to kernel parameter choices, and complexity when tackling multi-class classification tasks. Other traditional machine learning methods like k-nearest neighbor [75] and probabilistic graphical model [76] are used to design fault diagnosis systems as well.

It is worth mentioning that traditional machine learning methods require human expertise and signal processing techniques to design a feature extractor. However, there is no standard design procedure for the feature extractor for different tasks [77]. Besides, the volume of data has been dramatically growing due to the development of industry technology in recent years, which can provide more sufficient information. Unfortunately, traditional machine learning methods are not suitable for big data scenarios because of their shallow structures. They have limited ability to learn the nonlinear relations between extracted features [78].

Deep learning methods employ deep architectures with multiple layers of neural networks to automatically extract complex features from the raw data, and further establish the relations between the learned features and the target output directly [79]. In comparison with traditional machine learning methods, no human expertise is required. The advantages of deep learning methods have led to their wide application in the field of fault diagnosis. Deep learning fault diagnosis methods first employ hierarchical networks, such as stacked autoencoders (AE), deep belief networks (DBN), and convolutional neural networks (CNN), to learn abstracted features layer by layer. After feature extraction, the output of hierarchical networks (i.e., the learned features) serves as the input of an ANN-based classifier to recognize the healthy states of machines [74].

Authors in [78] used the stacked AE to automatically extract features from the data of rolling element bearings and gears, and then constructed the fault diagnosis system. This is one of the earliest studies on the applications of AE in the fault diagnosis field. The proposed approach is able to handle massive monitoring data and obtain higher diagnosis accuracy compared to ANN-based and SVM-based diagnosis methods. To further improve the performance of fault diagnosis methods based on the stacked AE, people started to study the optimization algorithms of AE, see for example [80–82]. Note that the stacked AE approach cannot be directly applied to fault diagnosis as it is an unsupervised learning method. Thus, a classification layer and sufficient labeled samples are required for the construction of the diagnosis system based on the stacked AE.

Similar to the stacked AE approach, DBN consists of a set of restricted Boltzmann machines (a special type of generative stochastic neural network). Fault diagnosis approaches developed based on DBN could automatically learn features from the data. In order to

recognize faults, DBN-based methods map the learned features into the labeled space by adding a classification layer. Researchers developed DBN-based fault diagnosis methods for fault diagnosis of rolling element bearings in [83]. By improving the optimization algorithm, like using adaptive learning rate and momentum [84] and selecting the structure with the particle warm [85], the improved DBN-based methods can achieve higher diagnosis accuracy than the standard DBN. This method requires sufficient labeled samples to obtain convincing diagnosis results as well.

CNN is a supervised learning method that comprises convolutional layers, pooling layers, and full-connected layers [86]. It has been widely used in speech recognition and image identification with many achievements. Applications of CNN to fault diagnosis can be divided into 2-dimensional (2D) and 1-dimensional (1D) methods according to the architectures of CNN. Since the standard 2D CNN used for image identification is unable to deal with 1D signals, like vibration data in bearings. To address this issue, researchers adopt signal processing techniques, such as the wavelet packet [87], continue wavelet transform [88], and synchrosqueezing transform [89], to convert the 1D data to the time-frequency domain. Then, CNN can handle the 2D time-frequency spectrum for fault diagnosis. There are also some results [90, 91] manually reshape the input data to align with the requirements of CNN-based diagnosis methods. Additionally, 1D CNN has been employed to process raw data without preprocessing too. Researchers have used it to construct the end-to-end diagnosis methods for rolling element bearings [92] and gears [93].

Other deep learning methods, like ResNet, have also been used to construct fault diagnosis systems [94]. More results based on learning-based fault diagnosis methods can be found in survey papers [24, 74, 95] and course book [25]. We would like to point out that the deep learning methods mentioned before mostly assume that there are sufficient labeled data and contain complete healthy data of systems. However, such an assumption is unrealistic in engineering scenarios. Besides, since it is easier to obtain healthy data than faulty data, it also leads to seriously imbalanced datasets. Therefore, using deep learning with limited and imbalanced data to design reliable diagnosis methods for engineering scenarios is still a challenging problem.

1.3 Thesis Outline

In this thesis, our focus is on developing model-based fault diagnosis techniques for linear systems that can operate effectively even in the presence of disturbances and noise. In light of the discussion on existing model-based fault diagnosis methods, we will consider the following issues when designing fault diagnosis methods:

- **Scalability of residual generators.** The order of the residual generator obtained by common observer-based and parity space-based methods is usually the same as that of the system, which results in a substantial computational workload when dealing with large-scale systems. Therefore, a simple and scalable residual generator is more desirable for online implementation and large-scale systems.

- **Stochastic disturbance signals.** Most fault diagnosis methods in the literature usually consider model mismatches including uncertainties, disturbances, and noise,

with deterministic bounds. Then, they design residual generators to be robust to these model mismatches only through the support information. However, it is generally difficult to obtain such bounds, and the results obtained are highly conservative. Therefore, it is meaningful to find solutions to deal with stochastic model mismatches and study their effects on diagnosis results.

- **Probabilistic diagnosis performance.** To achieve successful fault diagnosis, it is essential to design residual evaluation strategies and determine detection thresholds, as the residuals are often corrupted by disturbances and noise. However, due to the random nature of disturbance signals, false alarms and missing detection of faults are inevitable. Therefore, designing residual evaluation strategies and thresholds that can provide guarantees on false alarms and missing detection rates is of utmost importance. Unfortunately, research on probabilistic diagnosis performance is limited at present.
- **Finite frequency domain design.** Most existing model-based fault diagnosis methods are designed for the entire frequency domain. However, in engineering practice, practitioners may only be interested in the performance of the control system within a specific frequency range. Moreover, actual system signals, such as external disturbances, measurement noise, and fault signals, often appear in specific frequency ranges. Therefore, by designing fault diagnosis strategies in a finite frequency domain, it is possible to attain better diagnosis performance with less design conservatism compared to methods for the entire frequency domain.

Motivated by the aforementioned needs, we propose design approaches for fault diagnosis filters within the framework of differential-algebraic equations. This offers design flexibility and the potential for constructing low-order filters. We further determine the parameters of the filters through optimization problems to ensure that the resulting filters meet various design requirements. Considering the importance of energy systems, we take energy systems, such as power systems and building radiant systems, as experimental subjects to validate the effectiveness of our proposed approaches. The structure of the thesis is as follows.

Chapter 2. In this chapter, we consider the switching detection and mode identification problem for switched affine systems, while taking into account asynchronous switchings and measurement noise. This problem becomes particularly relevant in fault diagnosis scenarios, where an unexpected transition from a healthy mode to a faulty mode can be treated as an unknown switching. Therefore, the problem can also be viewed as a fault detection and isolation problem. To tackle this problem, we propose a diagnosis scheme that comprises a bank of filters and a diagnosis rule based on residual/threshold analysis. Specifically, we follow the mindset of the generalized observer scheme for mode isolation, where each residual is sensitive to all but only one mode. Furthermore, the $\mathcal{H}_2$ norm method from the robust control theory is utilized here to mitigate the impact of stochastic noise on the residuals. We formulate the design of the bank of filters into a finite optimization problem, which can be safely approximated through linear matrix inequalities and, thus, tractable.

In the threshold determination part, we consider the random nature of the residuals and develop a thresholding policy along with probabilistic false-alarm guarantees to estimate

the active system mode in real-time. Compared to the existing results, the guarantees improve from a polynomial dependency in the probability of false-alarm to a logarithmic form. This improvement is achieved by assuming that the noise satisfies sub-Gaussianity distributions, which is common in many practical applications. In addition, we estimate the time required for our proposed diagnosis component to isolate the correct mode. This is rarely studied in previous literature. To validate the effectiveness of our approach, we present a numerical example and an application of the building radiant system.

Chapter 3. In this chapter, we consider fault detection and estimation for discrete-time linear time-invariant systems in the finite frequency domain. This is motivated by the fact that some practical faults are in the finite frequency domain, such as stuck and incipient faults. To enhance fault sensitivity in the frequency domain of interest, we utilize the $\mathcal{H}_-$ index and the generalized Kalman-Yakubovich-Popov lemma. We develop an exact optimization framework to solve the fault detection filter that meets the requirements for mixed $\mathcal{H}_2/\mathcal{H}_-$ performance indices, which simultaneously suppress noise, decouple unknown inputs and improve fault sensitivity. Additionally, we propose a threshold determination method that provides probabilistic guarantees on the diagnosis performance. In comparison with the results presented in **Chapter 2**, which only consider one-dimensional residuals, the proposed filter design method here allows for residuals of arbitrary dimensions and can handle the simultaneous occurrence of multiple faults. Additionally, we compute the probability of missing detection, which is not studied in **Chapter 2**.

Furthermore, by adjusting the constraints in the proposed optimization framework, we obtain the design method for the fault estimation filter in the finite frequency domain, where the finite-frequency $\mathcal{H}_\infty$ norm is adopted to measure the estimation performance. We relax further the fault estimation conditions to reduce computational complexity and formulate a quadratic programming problem to solve the desired fault estimation filter. To our knowledge, this is the first attempt to tackle fault estimation filter design in the finite frequency domain, while taking into account both unknown inputs and stochastic noise. The effectiveness of our proposed methodologies is demonstrated through an application on a synthetic non-minimum phase system and a multi-area power system.

Chapter 4[1]**.** In this chapter, we focus on the detection of ground faults in inverter-based microgrid systems. The presence of a fault current limiter in the inverter controller causes the fault current to deviate slightly from its nominal value, making fault detection challenging. Additionally, distinguishing ground faults from disturbances based solely on the output current can be difficult, as the effect of disturbances on the output current is similar to that of ground faults. To address this challenge, we begin by obtaining the state-space model of inverter-based microgrid systems in both healthy and faulty modes. As this problem only involves two modes, we can consider it as a special case of the mode detection problem discussed in **Chapter 2**. This allows us to apply fault diagnosis methods that have been previously developed to address the current problem when disturbances can be fully decoupled. However, in contrast to the results presented in **Chapter 2** and **Chapter 3**, this problem involves disturbances that cannot be fully decoupled. To develop fault detection filters that are robust to such disturbances, we use available disturbance patterns to train the filters. We formulate the filter design as a quadratic programming

[1]The results in this chapter are also used in the master thesis: Y. Liao, "Monitoring Techniques in Modern Industrial Systems: Fault detection and non-intrusive load monitoring".

problem that has an approximate analytical solution. This approximate analytical solution can be arbitrarily precise and used to update filter parameters in real-time. We also establish a threshold to ensure the desired probabilistic diagnosis performance.

Chapter 5. In this chapter, we revisit the main results of this thesis and also discuss possible future research directions.

2

Multimode Diagnosis for Switched Affine Systems with Noisy Measurement

This chapter is based on *J. Dong, A.S.Kolarijani, P. Mohajerin Esfahani. Multimode diagnosis for switched affine systems with noisy measurement. Automatica, 2023, 151: 110898.* [96].

2.1 Introduction

Over the last two decades, special attention has been paid to switched affine systems because they can be used to effectively model a wide range of practical systems, such as chemical plants [97], aeronautic systems [98] and smart buildings [99]. These systems are usually difficult to be exactly described by a single model because of their nonlinear and complex dynamic characteristics. Research on switched systems is mainly focused on model identification [100, 101], state estimation [102], stability analysis and controller design [103, 104]. The prior knowledge of the switching signal that indicates the evolution of modes is crucial to theoretical results in these research topics. For example, a general approach to controlling switched systems is to employ mode-dependent controllers, where the activation of a proper controller depends on the switching signal. There are, however, several scenarios in which the switching signal is not a priori known. In fault diagnosis scenarios, an unexpected transition from a healthy mode to a faulty mode can be treated as an unknown switching. Thus, one needs to detect the active mode of switched systems as the detection process results in a delay between the active mode and its corresponding controller.

The problem of mode detection for switched affine systems has been studied for decades. The proposed approaches can be grouped into two categories: data-based and model-based approaches. The data-based approaches are most adopted when the parameters of each mode are unknown. In that case, the parameters need to be identified from a collection of input-output data. Then, the new data is associated with the most suitable mode through data classification techniques. A number of results on data-based approaches have been achieved. We refer the interested readers to [100] and the references therein.

Model-based fault diagnosis: In model-based approaches, one leverages tools from the fault detection and isolation (FDI) field to detect and isolate changes caused by switchings or faults. The most widely used FDI methods are based on residual generation, where certain residual signals are generated by observer-based or parity space methods to characterize the occurrence of changes quantitatively [2]. Beard [29] proposes the original observer-based diagnosis approach to replace the hardware redundancy in 1971. Subsequently, many observer-based diagnosis approaches are developed. To deal with disturbances or measurement noise, the authors in [105] construct an optimization problem to design the parameters of the observer, in which the influence of disturbances on residuals characterized by $\mathcal{H}_\infty$ norm is minimized. The parity space approach is proposed in [39], which generates residuals to check the consistency between the model and the measurements.

It is worth noting that the derived residual generators usually have the same order as that of the systems. This makes the generators complex and computationally demanding when dealing with high-dimensional or large-scale systems. Frisk [44] proposes a parity-space-like approach in a polynomial framework that produces residual generators with possibly low order. In their following work [45], the previous approach is extended to the linear differential-algebraic equations (DAE, difference-algebraic equations in the discrete-time case). This extension enlarges the application range of FDI approaches because DAE models cover several classes of models, e.g., transfer functions, state-space models, or descriptor models. The above approaches are for linear systems. For the fault detection of nonlinear systems, a natural way is to linearize nonlinear systems at local operating points and decouple the disturbances together with the higher-order terms from

the residuals, see for example [50, 51]. Another method is to develop adaptive nonlinear estimators to approximate the nonlinear terms [52, 106]. More recently, the authors in [53, 107] develop tractable optimization-based approaches in the DAE framework to design FDI filters to deal with disturbances and nonlinear terms.

Multi-mode diagnosis: Note that the aforementioned approaches are applicable to systems with a single model. A bank of residuals is usually required to deal with systems consisting of several modes. Moreover, the systems need to satisfy certain rank conditions to guarantee that any two subsystems can be distinguished from each other. This is the distinguishability (also called discernibility or observability) of switched systems [108, 109]. To detect the active mode, the idea that makes each residual sensitive to all but only one mode is usually adopted, which is called *generalized observer scheme* (GOS) [12]. Following a GOS mindset, results on mode detection are achieved based on basic residual generation methods, such as parity space approaches [110], unknown input observers [111], and sliding mode observers [112, 113]. Note that the computational complexity of these residual generation methods increases significantly as the system dimension and the number of modes increase. In this work, we propose a design perspective in the DAE framework that relies on a bank of filters whose dimension does not necessarily scale up with the dimension of the system. This feature enables the possibility of low-ordered filters compared to the existing literature.

Another class of mode detection methods is the set-membership method which computes the reachable set of each subsystem. Then, the output is compared to the reachable sets to determine the mode [114–116]. The authors in [114] and [115] develop active diagnosis approaches in which an optimal separating input sequence is designed to guarantee that output sets of different subsystems are separated. In [116], a model invalidation approach is proposed to compare the input-output data to the nominal behaviors of the system, where the set-membership check is reduced to the feasibility of a mixed-integer linear programming problem. The set-membership methods are generally computationally demanding because they require solving optimization problems at each step. Also, the residual generation and set-membership methods mentioned above either neglect the noise or treat them as robust only through the support information. This viewpoint often leads to conservative diagnosis guarantees. In fact, the measurement noise introduces a unique challenge to the detection task where the reachable sets of healthy residuals may well overlap with the faulty ones. This challenge is one of the focus points of this study.

Main contributions: In light of the literature reviewed above, the main message of this chapter revolves around a diagnosis scheme to detect the active mode of asynchronously switched affine systems in real-time. The diagnosis scheme consists of a bank of filters and a residual/threshold-based diagnosis rule. The bank of filters comprises as many filters as the admissible mode transitions, while the diagnosis rule prescribes conditions under which we estimate the transition based on the behaviors of the residuals. The main contributions of this chapter are summarized as follows.

- **Exact characterization of an optimal bank of filters:** Building on residual-based detection and $\mathcal{H}_2$ norm approaches in the DAE framework, we formulate the optimal bank of filters design problem as a finite optimization problem in which the objective is the noise contribution to the residuals (Theorem 2.3.1). We also provide necessary

and sufficient conditions that ensure the feasibility of the resulting optimization problem (Proposition 2.3.3).

- **Tractable convex restriction:** We provide a sufficient condition for the nonlinear constraint in the exact optimization problem of the filter design based on linear matrix inequalities (LMI), leading to a tractable approximation of the original problem (Proposition 2.3.2).

- **Probabilistic performance bounds:** We further propose diagnosis thresholds along with probabilistic false-alarm guarantees to estimate the active system mode (Theorem 2.3.8). The proposed bound admits a logarithmic dependency with respect to the desired reliability level, which is better than the polynomial rate in the existing works [117]. This improvement comes under the sub-Gaussianity assumption on the noise distribution, a regularity requirement expected to hold in many real-world applications.

The rest of the chapter is organized as follows. The problem formulation and the proposed architecture of the diagnosis scheme are introduced in Section 2.2. In Section 2.3, we present an optimization-based approach to design the filters along with some performance analysis of the proposed scheme. To improve the flow of the chapter and its accessibility, we postpone all technical proofs to Section 2.4. The proposed scheme is applied to a numerical example and a building radiant system in Section 2.5 to validate its effectiveness. Finally, Section 2.6 concludes the chapter with some remarks and future directions.

2.2 Model Description and Problem Statement

In this section, we provide a formal description of discrete-time asynchronously switched affine systems. Then, we present the architecture of the proposed mode detector and formulate the problems studied in this work.

2.2.1 Model Description

Consider a discrete-time switched affine system that consists of n subsystems:

$$\begin{aligned} x(k+1) &= A_{\sigma(k)}x(k) + B_{\sigma(k)}u(k) + E_{\sigma(k)}d(k) + W_{\sigma(k)}\omega(k) \\ y(k) &= C_{\sigma(k)}x(k) + D_{\sigma(k)}\omega(k), \end{aligned} \tag{2.1}$$

where $x(k) \in \mathbb{R}^{n_x}$, $u(k) \in \mathbb{R}^{n_u}$ and $y(k) \in \mathbb{R}^{n_y}$ are the state, control input and output, resp. The signal $d(k) \in \mathbb{R}^{n_d}$ and $\omega(k) \in \mathbb{R}^{n_\omega}$ represent the reference and noise signals, resp. For simplicity of analysis, we consider a one-dimensional reference signal, i.e., $n_d = 1$. Throughout this study, the noise $\omega(k)$ is assumed to be independent and identically distributed (iid). We define the set $\{1,\dots,n\}$ by $\mathcal{N}$. The switching law $\sigma(k) \in \mathcal{N}$ indicates the active mode at each instant k. Matrices $A_{\sigma(k)}$, $B_{\sigma(k)}$, $E_{\sigma(k)}$, $W_{\sigma(k)}$, $C_{\sigma(k)}$ and $D_{\sigma(k)}$ are all known with appropriate dimensions, and matrices $E_i \neq 0$. For each mode $i \in \mathcal{N}$, we consider the static output-feedback controller

$$u(k) = K_i y(k), \tag{2.2}$$

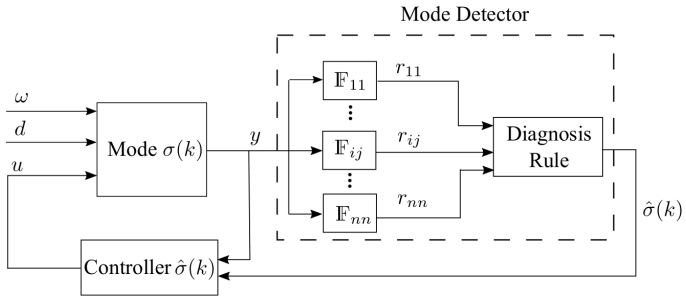

Figure 2.1: Structure of the closed-loop dynamics and the mode detector.

where K_i is a constant controller gain; see [118] for a design approach to K_i. Let $\{t_0, \dots, t_s, \dots\}$ denote the sequence of switching time instants of the system mode $\sigma(k)$, i.e., by definition we have $\sigma(t_s - 1) \neq \sigma(t_s)$.

In this study, we consider the setting that the switching law $\sigma(k)$ and the switching instant t_s are both unknown to the controller. The main objective is to estimate the active mode $\sigma(k)$, hereafter denoted by $\hat{\sigma}(k)$, through the noisy measurement y in real-time. As depicted in Figure 2.1, our proposed scheme to accomplish this goal builds on a bank of filters where each filter is intended to detect a possible pair of $\hat{\sigma}(k) = i, \sigma(k) = j$ for any $i, j \in \mathcal{N}$; we use the notation S_{ij} to represent this status of the closed-loop system. For each pair (i, j), the filter is assumed to be a linear time-invariant (LTI) system (described by a transfer function) denoted by $\mathbb{F}_{ij}$ whose output (also called residual) is a scalar-valued signal $r_{ij} := \mathbb{F}_{ij}[y]$. We note that in our setting, the current controller mode $\hat{\sigma}(k) = i$ is always known, whereas the system mode $\sigma(k)$ is unknown and the object of interest. Suppose that the system transitions to the status S_{ih} at t_s (i.e., $\hat{\sigma}(t_s) = i, \sigma(t_s) = h$), thanks to the linearity of the dynamics, the residual r_{ij} can be written as

$$r_{ij} = \underbrace{\mathbb{F}_{ij}\mathbb{T}_{dy}^{S_{ih}}[d]}_{d \mapsto r_{ij}} + \underbrace{\mathbb{F}_{ij}\mathbb{T}_{\omega y}^{S_{ih}}[\omega]}_{\omega \mapsto r_{ij}} + \underbrace{\mathcal{I}(x(t_s), \bar{x}_{ij}(t_s))}_{\text{initial condition}}, \tag{2.3}$$

where $\mathbb{T}_{dy}^{S_{ih}}$ and $\mathbb{T}_{\omega y}^{S_{ih}}$ are the LTI systems from the external signals (d, ω) to y, and $\mathcal{I}(\cdot)$ is the contribution of the internal states of the system $x(t_s)$ and the filter $\bar{x}_{ij}(t_s)$. From the classical system theory, we know that the initial condition contribution vanishes exponentially fast under appropriate asymptotic stability conditions. To isolate the active mode, we adopt the same mindset as GOS and opt to decouple the contribution of the reference signal d (i.e., the first term in the right-hand side of (2.3)) for the matched mode $j = h$, and make sure that it is significantly high when $j \neq h$. With regards to the latter, we look at the steady-state behavior of the filters, motivated by the fact that in many important applications the reference signal d is effectively constant between two switching instants. Furthermore, we opt to suppress the noise contribution (the second term in the right-hand side of (2.3)) for all $h \in \mathcal{N}$. These steps will be formalized in the next part.

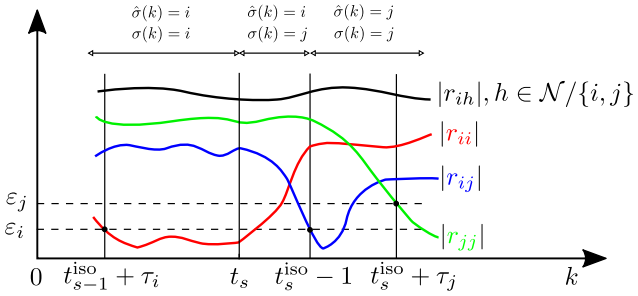

Figure 2.2: Illustration of the diagnosis process.

2.2.2 Problem Statement

We consider a setting consisting of two components to perform the diagnosis task: (i) bank of filters, as briefly described in the previous section, and (ii) diagnosis rule, which is essentially a thresholding technique to estimate the system mode from the residuals. We then present two problems concerning each of these components. For each pair (i, j) and the respective filter $\mathbb{F}_{ij}$, the desired properties of $d \mapsto r_{ij}$ and $\omega \mapsto r_{ij}$ (the first two terms in the right-hand side of (2.3)) can be formalized as follows:

$$\mathbb{F}_{ij}\mathbb{T}_{dy}^{S_{ij}} = 0, \tag{2.4a}$$

$$\left|\left[\mathbb{F}_{ij}\mathbb{T}_{dy}^{S_{ih'}}\right]_{\text{ss}}\right| \geq 1, \qquad h' \in \mathcal{N} \setminus \{j\}, \tag{2.4b}$$

$$\left\|\mathbb{F}_{ij}\mathbb{T}_{\omega y}^{S_{ih}}\right\|_{\mathcal{H}_2}^2 \leq \eta_{ijh}, \quad h \in \mathcal{N}. \tag{2.4c}$$

Let us briefly elaborate on each condition in (2.4): The equality constraint (2.4a) decouples d from r_{ij} when the closed-loop status is S_{ij}. The condition (2.4b) ensures that the absolute value of the steady-state gain of $\mathbb{F}_{ij}\mathbb{T}_{dy}^{S_{ih'}}$ remains larger than or equal to 1, and as such, the contribution of d to r_{ij} is notably nonzero when the closed-loop status is $S_{ih'}$ for all $h' \in \mathcal{N} \setminus \{j\}$. Recall that the $\mathcal{H}_2$ norm of a transfer function is the asymptotic variance of the white noise response [46]. Then, the constant η_{ijh} in (2.4c) is an upper bound for the variance of the noise contribution to the residual. In view of the desired properties (2.4), we proceed with our first problem.

Problem 1. (Optimal bank of filters) Consider the closed-loop dynamics (2.1)-(2.2) and the mode detector in Figure 2.1. Given $i, j \in \mathcal{N}$ and an admissible family of the filters $\mathbb{F}_{ij}$, find the optimal filter defined through the optimization program

$$\min_{\mathbb{F}_{ij},\, \eta_{ijh}} \left\{ \sum_{h=1}^{n} \eta_{ijh} \,:\, (2.4a),\ (2.4b),\ (2.4c) \right\}. \tag{2.5}$$

Given the filters as an (approximate) solution to (2.5), we now shift our attention to the diagnosis rule component in Figure 2.1. Consider a transition from mode i to mode j at time instant t_s (i.e., $\hat{\sigma}(t_s) = i, \sigma(t_s) = j$), where $i, j \in \mathcal{N}$. There are two key parameters during the diagnosis process of the transition: (i) the threshold $\varepsilon_i \in \mathbb{R}_+$, and (ii) the waiting

time $\tau_j \in \mathbb{N}_+$. The behavior of the trajectories, as well as the design parameters ε_i, τ_j, are pictorially illustrated in Figure 2.2. In the following, the role of each of the design parameters is discussed:

(1) *Threshold* ε_i: As formalized in (2.4), the matched residual $r_{\hat{\sigma}\sigma}(k)$ should be close to zero, while the other residuals are notably away from zero. Recall that the current controller mode $\hat{\sigma}(k)$ is known, and the system mode $\sigma(k)$ is the detection target. Hence, we monitor the residuals $r_{\hat{\sigma}h}(k)$ for all $h \in \mathcal{N}$, and compare them with the threshold $\varepsilon_{\hat{\sigma}}$ to isolate the matched residual (the one with the smallest absolute value). More specifically, we opt to single out one candidate from all the other possible modes. This procedure can be formally described by introducing the following conditions

$$j^*(k) = \arg\min_{h\in\mathcal{N}} |r_{\hat{\sigma}h}(k)|, \tag{2.6a}$$

$$|r_{\hat{\sigma}j^*}(k)| \le \varepsilon_{\hat{\sigma}(k)} < \min_{h'\in\mathcal{N}\setminus\{j^*(k)\}} |r_{\hat{\sigma}h'}(k)|. \tag{2.6b}$$

The mode $j^*(k)$ defined in (2.6a) is our best candidate to estimate the system mode $\sigma(k)$, and (2.6b) is essentially a requirement to ensure that the threshold only selects one candidate. Once the conditions (2.6) are fulfilled at a time instant k, then the diagnosis component updates $\hat{\sigma}(k+1) = j^*(k)$, otherwise, it still retains the old mode $\hat{\sigma}(k+1) = \hat{\sigma}(k)$. In Figure 2.2, note the period prior to t_s^{iso}, the *isolation* time of the transition at t_s; this will be formally defined in the next part in (2.7).

(2) *Waiting time* τ_j: Once we update $\hat{\sigma}$ at t_s^{iso}, the conditions (2.6) are violated immediately since the controller mode changes. Thus, we need to wait for sufficiently large time to pass the transient behavior of the system caused by the initial condition (the third term in the right-hand side of (2.3)); see the "waiting period" $[t_s^{\text{iso}}, t_s^{\text{iso}} + \tau_j)$ in Figure 2.2. The controller mode $\hat{\sigma}$ remains unchanged during this period (i.e., $\hat{\sigma}(k+1) = \hat{\sigma}(k)$) until $|r_{jj}(k)|$ reaches the respective threshold ε_j; see Figure 2.2 and the time instant $t_s^{\text{iso}} + \tau_j$. To determine whether the diagnosis process is in the waiting period or not, we record the last isolation time instant through

$$t^{\text{iso}}(k) := \max\Big\{ t \in \mathbb{N}_+ : \hat{\sigma}(t) \neq \hat{\sigma}(t-1),\ k \ge t \Big\}. \tag{2.7}$$

We use the shorthand notation $t^{\text{iso}}(k) = t_s^{\text{iso}}$ for $k \in [t_s^{\text{iso}}, t_{s+1}^{\text{iso}})$.

In summary, the diagnosis rule of the second component can be mathematically described by

$$\hat{\sigma}(k+1) = \begin{cases} j^*(k), \text{ if (2.6) and } k \ge t^{\text{iso}}(k) + \tau_{\hat{\sigma}(k)}, \\ \hat{\sigma}(k), \text{ otherwise.} \end{cases} \tag{2.8}$$

Note that ε_i in (2.6) and τ_j in (2.8) are the design parameters, and their objective is to detect the current system mode $\sigma(k)$. In view of the update rule (2.8), this objective is formalized in our next problem in terms of the behavior of the matched filter residual $r_{ij}(k)$.

Problem 2. (Probabilistic performance certificates) Suppose that the transition from mode i to j occurs at t_s (i.e., $\hat{\sigma}(t_s) = i$ and $\sigma(t_s) = j$). Given the filters constructed from Problem 1

and a reliability level $\beta \in (0,1]$, determine the threshold ε_i and the estimated matched time T_{ij} such that

$$\mathbf{Pr}\left[|r_{ij}(t)| \le \varepsilon_i \;\middle|\; \begin{bmatrix}\hat{\sigma}(k)\\ \sigma(k)\end{bmatrix} = \begin{bmatrix} i \\ j\end{bmatrix}, k \ge t_s\right] \ge 1-\beta, \quad \forall\, t \ge t_s + T_{ij}. \tag{2.9}$$

The initial condition $\mathcal{I}(x(t_s), \bar{x}_{ij}(t_s))$ determines the time that $|r_{ij}|$ takes to reach ε_i. However, the internal system state $x(t_s)$ and switching instant t_s are unknown. Moreover, if the next transition occurs before $t_s + T_{ij}$, the guarantee in (2.9) is no longer useful. Thus, we assume that the time between two consecutive transitions (the so-called *dwell time* [104]) is large enough so that the system reaches its steady-state before the next transition. It is a reasonable assumption as the dwell time of many real-world applications is longer than the time available for the controller to detect the mode. In this setting, the probabilistic guarantee (2.9) can be obtained, and the internal state $x(t_s)$ can be estimated by its steady-state value.

Remark 2.2.1. *(Waiting time) The waiting time τ_j depicted in Figure 2.2 is indeed a special case of the estimated matched time introduced in Problem 2, where the controller and the system mode coincide, i.e., $\hat{\sigma}(t_s^{\text{iso}}) = \sigma(t_s^{\text{iso}}) = j$, and as such $\tau_j = T_{jj}$.*

2.3 Main Results

In this section, the structure and design method of the filters are presented. Then, computation methods of the thresholds and the estimated matched time are given to provide probabilistic guarantees on the diagnosis performance. All proofs are relegated to Section 2.4 to improve readability.

2.3.1 Filter Design: An Optimization-based Method

Suppose the current status is S_{ih}, i.e., $\hat{\sigma}(k) = i, \sigma(k) = h$. The closed-loop dynamics (2.1)-(2.2) can be written as

$$\begin{aligned} x(k+1) &= A_{ih}^{cl} x(k) + E_h d(k) + (W_h + B_h K_i D_h)\omega(k) \\ y(k) &= C_h x(k) + D_h \omega(k), \end{aligned} \tag{2.10}$$

where $A_{ih}^{cl} = A_h + B_h K_i C_h$. We further reformulate (2.10) into the DAE format, which is

$$H_{ih}(\mathfrak{q}) \begin{bmatrix} x \\ d \end{bmatrix} + L(\mathfrak{q})[y] + G_{ih}(\mathfrak{q})[\omega] = 0, \tag{2.11}$$

where the operator $\mathfrak{q}$ is a time-shift operator, i.e., $x(k+1) = \mathfrak{q}x(k)$. The polynomial matrices $H_{ih}(\mathfrak{q})$, $L(\mathfrak{q})$ and $G_{ih}(\mathfrak{q})$ are given by

$$H_{ih}(\mathfrak{q}) = H_{ih,1}\mathfrak{q} + H_{ih,0} = \begin{bmatrix} -\mathfrak{q}I + A_{ih}^{cl} & E_h \\ C_h & 0 \end{bmatrix}, \; L(\mathfrak{q}) = L_0 = \begin{bmatrix} 0 \\ -I \end{bmatrix}, \text{ and}$$

$$G_{ih}(\mathfrak{q}) = G_{ih,0} = \begin{bmatrix} W_h + B_h K_i D_h \\ D_h \end{bmatrix}.$$

Inspired by [45] and [53], the filter $\mathbb{F}_{ij}$ is defined as

$$\mathbb{F}_{ij}(\mathfrak{q}) = a^{-1}(\mathfrak{q}) N_{ij}(\mathfrak{q}) L(\mathfrak{q}), \tag{2.12}$$

where the polynomial row vector $N_{ij}(\mathfrak{q}) = \sum_{m=0}^{d_N} N_{ij,m}\mathfrak{q}^m$, each $N_{ij,m} \in \mathbb{R}^{1\times(n_x+n_y)}$ is a constant row vector, d_N denotes the degree of $N_{ij}(\mathfrak{q})$, and $a(\mathfrak{q})$ is a (d_N+1)-th order polynomial with all roots inside the unit disk. We define

$$a(\mathfrak{q}) = \mathfrak{q}^{d_N+1} + a_{d_N}\mathfrak{q}^{d_N} + \cdots + a_1\mathfrak{q} + a_0, \tag{2.13}$$

where a_m is a constant coefficient for each $m \in \{0, 1, \ldots, d_N\}$. Notice that the role of $a(\mathfrak{q})$ is to ensure that the filter $\mathbb{F}_{ij}$ is strictly proper and stable. To simplify the design process, we fix $a(\mathfrak{q})$ and d_N, and suppose that all the filters are of the same degree. The coefficients of the numerator, i.e., $N_{ij,m}$ for $m \in \{0, 1, \ldots, d_N\}$, are the design parameters. Multiplying the left-hand side of (2.11) by $a^{-1}(\mathfrak{q})N_{ij}(\mathfrak{q})$ yields

$$r_{ij} = \frac{N_{ij}(\mathfrak{q})L(\mathfrak{q})}{a(\mathfrak{q})}[y] = -\frac{N_{ij}(\mathfrak{q})H_{ih}(\mathfrak{q})}{a(\mathfrak{q})}\begin{bmatrix} x \\ d \end{bmatrix} - \frac{N_{ij}(\mathfrak{q})G_{ih}(\mathfrak{q})}{a(\mathfrak{q})}[\omega]. \tag{2.14}$$

To bound the $\mathcal{H}_2$ norm of the transfer function from ω to r_{ij}, we derive the observable canonical form of $\mathbb{F}_{ij}(\mathfrak{q})$ from (2.12)

$$\begin{aligned} \bar{x}_{ij}(k+1) &= A_r\bar{x}_{ij}(k) + B_{r_{ij}}y(k) \\ r_{ij}(k) &= C_r\bar{x}_{ij}(k), \end{aligned} \tag{2.15}$$

where $\bar{x}_{ij}(k) \in \mathbb{R}^{d_N+1}$ denotes the state. Matrices $A_r, B_{r_{ij}}, C_r$ are given by

$$A_r = \begin{bmatrix} 0 & \ldots & 0 & -a_0 \\ 1 & \ldots & 0 & -a_1 \\ \vdots & \ddots & \vdots & \vdots \\ 0 & \ldots & 1 & -a_{d_N} \end{bmatrix}, \; B_{r_{ij}} = \begin{bmatrix} N_{ij,0} \\ N_{ij,1} \\ \vdots \\ N_{ij,d_N} \end{bmatrix} L_0, \text{ and } C_r = \begin{bmatrix} 0 \ldots 0 & 1 \end{bmatrix}. \tag{2.16}$$

The parameters $N_{ij,m}$ are reformulated into $B_{r_{ij}}$ here. Let us introduce an augmented state $\mathcal{X}_{ij}(k) := \left[x(k)^\top \; \bar{x}_{ij}(k)^\top\right]^\top$. The dynamics of $\mathcal{X}_{ij}$ can be derived from (2.10) and (2.15),

which is

$$\begin{aligned}\mathcal{X}_{ij}(k+1) &= \mathcal{A}_{ijh}\mathcal{X}_{ij}(k) + \mathcal{E}_h d(k) + \mathcal{D}_{ijh}\omega(k)\\ r_{ij}(k) &= \mathcal{C}_r\mathcal{X}_{ij}(k),\end{aligned} \tag{2.17}$$

where

$$\mathcal{A}_{ijh} = \begin{bmatrix} A_{ih}^{cl} & 0 \\ B_{r_{ij}}C_h & A_r \end{bmatrix},\ \mathcal{E}_h = \begin{bmatrix} E_h \\ 0 \end{bmatrix},\ \mathcal{D}_{ijh} = \begin{bmatrix} W_h + B_h K_i D_h \\ B_{r_{ij}} D_h \end{bmatrix},\ \text{and } \mathcal{C}_r = \begin{bmatrix} 0 & C_r \end{bmatrix}.$$

To design filters satisfying conditions in Problem 1, we formulate an optimization problem in the following theorem. For clarity of exposition, we allocate the first two lines to the decision variables in the optimization problem.

Theorem 2.3.1 (Optimal bank of filters: exact finite reformulation)**.** *Consider the closed-loop dynamics* (2.1)-(2.2) *and the filter* $\mathbb{F}_{ij}$ *proposed in* (2.12) *with the state-space realization* $(A_r, B_{r_{ij}}, C_r)$ *as defined in* (2.16)*. Given the order* d_N*, coefficients of* $a(\mathfrak{q})$*, and a sufficiently small* $\vartheta \in \mathbb{R}_+$*, Problem 1 as defined in* (2.5) *can be equivalently translated into the following finite optimization program:*

$$\begin{aligned}
&\min \sum_{h=1}^{n} \eta_{ijh}\\
&\text{s.t. } N_{ij,m} \in \mathbb{R}^{1\times(n_x+n_y)},\ m \in \{0,1,\dots,d_N\},\ \eta_{ijh} \in \mathbb{R}_+,\ h \in \mathcal{N},\\
&\quad P_{ij} \in \mathcal{S}^{d_N+1},\ P_{ijh'} \in \mathcal{S}^{n_x+d_N+1},\ h' \in \mathcal{N}\setminus\{j\}\\
&\quad \bar{N}_{ij}\bar{H}_{ij} = 0, && \text{(2.18a)}\\
&\quad \left|a^{-1}(1)\bar{N}_{ij}\mathcal{L}_{ih'}\right| \geq 1, && \text{(2.18b)}\\
&\quad \begin{bmatrix} P_{ij} & A_r P_{ij} & \mathcal{B}_{ij} \\ * & P_{ij} & 0 \\ * & * & I \end{bmatrix} \succeq \vartheta I,\ \begin{bmatrix} \eta_{ijj} & C_r P_{ij} \\ * & P_{ij} \end{bmatrix} \succeq \vartheta I, && \text{(2.18c)}\\
&\quad \begin{bmatrix} P_{ijh'} & \mathcal{A}_{ijh'}P_{ijh'} & \mathcal{D}_{ijh'} \\ * & P_{ijh'} & 0 \\ * & * & I \end{bmatrix} \succeq \vartheta I,\ \begin{bmatrix} \eta_{ijh'} & \mathcal{C}_r P_{ijh'} \\ * & P_{ijh'} \end{bmatrix} \succeq \vartheta I, && \text{(2.18d)}
\end{aligned}$$

where the involved matrices are given by

$$\bar{N}_{ij} = [N_{ij,0}\ N_{ij,1}\ \dots\ N_{ij,d_N}],\ \mathcal{L}_{ih'} = \bar{L}[\overbrace{I\ \dots\ I}^{d_N+1}]^\top C_{h'}\left(I - A_{ih'}^{cl}\right)^{-1}E_{h'},$$

$$\bar{H}_{ij} = \begin{bmatrix} H_{ij,0} & H_{ij,1} & \dots & 0 \\ \vdots & \ddots & \ddots & \vdots \\ 0 & \dots & H_{ij,0} & H_{ij,1} \end{bmatrix},\ \mathcal{B}_{ij} = -\begin{bmatrix} N_{ij,0} \\ \vdots \\ N_{ij,d_N} \end{bmatrix} G_{ij,0},\ \textit{and } \bar{L} = \begin{bmatrix} L_0, & \dots, & 0 \\ \vdots & \ddots & \vdots \\ 0 & \dots & L_0 \end{bmatrix}.$$

Proof. The proof is provided in Section 2.4.1. □

Note that if $N^*_{ij,0},\dots,N^*_{ij,d_N}$ are feasible solutions to (2.18), then so are $-N^*_{ij,0},\dots,-N^*_{ij,d_N}$ with the same objective values. This directly holds for constraints (2.18a) and (2.18b) and can be proved through Schur complement for the matrix inequalities constraints (2.18c) and (2.18d). Thus, we can drop the absolute value of (2.18b) without loss of generality.

The following proposition shows that the nonlinear matrix inequality in (2.18d) can be safely approximated with an LMI.

Proposition 2.3.2 (Optimal bank of filters: safe convex approximation)**.** *Consider the optimization problem* (2.18)*. Given $\alpha \in \mathbb{R}$ and $\gamma \in \mathbb{R}_+$, the nonlinear inequality constraint as the first term in* (2.18d) *can be safely approximated by the following LMI constraint if there exist matrices $\mathcal{G}_{ijh',1} \in \mathcal{M}^{n_x+d_N+1}$, $\mathcal{G}_{ijh',2} \in \mathcal{M}^{n_\omega}$ such that:*

$$\begin{bmatrix} P_{ijh'} & \hat{A}_{ih'}\mathcal{G}_{ijh'} & \hat{B}_{r_{ij}} & 0 \\ * & \Xi_{ijh'} & 0 & \left(\hat{D}_{h'}\mathcal{G}_{ijh'}\right)^\top \\ * & * & \frac{1}{\gamma}I & 0 \\ * & * & * & \gamma I \end{bmatrix} \succeq \vartheta I, \tag{2.19}$$

where the involved matrices are defined as

$$\hat{A}_{ih'} = \begin{bmatrix} \begin{bmatrix} A^{cl}_{ih'} & 0 \\ 0 & A_r \end{bmatrix} & \begin{bmatrix} W_{h'} + B_{h'}K_iD_{h'} \\ 0 \end{bmatrix} \end{bmatrix},\ \mathcal{G}_{ijh'} = \begin{bmatrix} \mathcal{G}_{ijh',1} & 0 \\ 0 & \mathcal{G}_{ijh',2} \end{bmatrix},$$

$$\hat{D}_{h'} = \begin{bmatrix} \begin{bmatrix} C_{h'} & 0 \end{bmatrix} & D_{h'} \end{bmatrix},\ \hat{B}_{r_{ij}} = \begin{bmatrix} 0 \\ -B_{r_{ij}} \end{bmatrix},\ \text{and } \Xi_{ijh'} = \alpha\mathcal{G}_{ijh'} + \alpha\mathcal{G}^\top_{ijh'} - \alpha^2 \begin{bmatrix} P_{ijh'} & 0 \\ * & I \end{bmatrix}.$$

Proof. The proof is provided in Section 4.1. □

It is worth pointing out that the linear approximation (2.19) provides a sufficient condition for the nonlinear matrix inequality in (2.18d). This means that any feasible solution to (2.19) is necessarily a feasible solution to the nonlinear constraint.

Furthermore, we provide necessary and sufficient conditions for the feasibility of the optimization problem (2.18) in the following proposition. Here, the rank and eigenvalues of a matrix A are denoted by $\mathrm{Rank}(A)$ and $\Lambda(A)$, resp.

Proposition 2.3.3 (Optimal bank of filters: feasibility)**.** *The optimization problem* (2.18) *is feasible if and only if the following conditions are satisfied:*

$$(d_N+1)(n_x+n_y) > \mathrm{Rank}\left(\bar{H}_{ij}\right), \tag{2.20a}$$

$$\mathrm{Rank}\left(\begin{bmatrix}\bar{H}_{ij} & \mathcal{L}_{ih'}\end{bmatrix}\right) > \mathrm{Rank}\left(\bar{H}_{ij}\right), \tag{2.20b}$$

$$|\Lambda(A_r)| < 1,\ |\Lambda(A^{cl}_{ih'})| < 1,\ \text{(i.e., } A_r \text{ and } A^{cl}_{ih'} \text{ are stable)}. \tag{2.20c}$$

Proof. The proof is provided in Section 2.4.1. □

Note that the inequality (2.20a) provides a way to find the minimum filter order d_N. According to (2.20c), $|\Lambda(A^{cl}_{ih'})| < 1$ ensures that (2.18d) is feasible. However, $A^{cl}_{ih'}$ could be unstable because the mode and the controller are unmatched. Hence, the constraints in (2.18d) with unstable $A^{cl}_{ih'}$ should be excluded. Since the unmatched residuals of those unstable modes diverge from zero, removing those constraints does not affect the mode detection task.

Remark 2.3.4 (Observability)**.** *The conditions* (2.20a) *and* (2.20b) *are related to the observability of switched affine systems theoretically [109]. In particular, the mode can be determined deterministically without noise if the two conditions are satisfied. Also, observability of each mode is not necessary, which is consistent with the result in [109, Theorem 8].*

We close this section with the following remark on different sources of conservatism for the proposed filter design:

Remark 2.3.5 (Conservatism analysis)**.** *The conservatism of the proposed approximate solution stems from three different sources:*

(i) Reference signal dimension: We only focus on one-dimensional reference signals, but instead, we do not require any further prior assumptions on their values. As shown in [119], this restriction is inevitable when the filter residual is one-dimensional since different elements of a multi-dimensional reference signal may cancel out each other's contributions;

(ii) Filters denominator: To simplify the design, the filters denominator $a(\mathfrak{q})$ are all fixed, which reduces design freedom;

(iii) Non-convexity: The exact reformulation of Problem 1 is a non-convex optimization problem (Theorem 2.3.1), for which we propose a safe convex approximation (Proposition 2.3.2).

2.3.2 Performance Certificates

With the filters designed by using (2.18), we now determine the threshold ε_i and waiting time τ_j to ensure proper detection task governed by (2.8). Considering the stochastic measurement noise ω, we resort to the probabilistic guarantees depicted in (2.9). Let us introduce the following lemma and assumption.

Lemma 2.3.6 (Sub-Gaussian concentration [120, Proposition 2.5.2])**.** *Let ω be an $\mathbb{R}^{n_\omega}$-valued sub-Gaussian random vector with positive parameter λ_ω, i.e., $\mathbf{E}\left[\mathrm{e}^{\phi v^\top(\omega-\mathbf{E}[\omega])}\right] \leq \mathrm{e}^{\lambda_\omega^2\phi^2/2}$ for all $\phi \in \mathbb{R}$ and $v \in \mathbb{R}^{n_\omega}$ where $\|v\|_2 = 1$. Then, we have*

$$\mathbf{Pr}\left[\|\omega - \mathbf{E}[\omega]\|_\infty \leq \varepsilon\right] \geq 1 - 2n_\omega \,\mathrm{e}^{-\varepsilon^2/(2\lambda_\omega{}^2)}, \quad \forall \varepsilon \in \mathbb{R}_+. \tag{2.21}$$

Assumption 2.3.7 (Sub-Gaussian noise)**.** *The measurement noise ω is an iid sub-Gaussian signal with zero mean and parameter $\lambda_\omega \in \mathbb{R}_+$ as defined in Lemma 2.3.6.*

From (2.21), the tails of sub-Gaussian distributions decay exponentially. Moreover, the class of sub-Gaussian distributions is broad, containing Gaussian, Bernoulli, and all bounded distributions. In the following results, the noise is assumed to be sub-Gaussian. To improve readability, we further introduce several notations. Let the polynomial row vector $N_{ij}(\mathfrak{q}) := \left[\hat{N}_{ij}(\mathfrak{q})\ \check{N}_{ij}(\mathfrak{q})\right]$, where $\hat{N}_{ij}(\mathfrak{q})$ and $\check{N}_{ij}(\mathfrak{q})$ have dimensions n_x and n_y, resp.

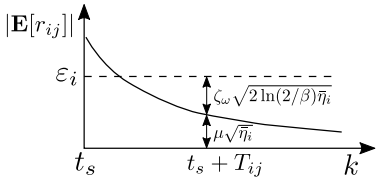

Figure 2.3: Estimated matched time.

Define $\rho_{\max} := \max_{m\in\{1,\dots,d_{N+1}\}}|\rho_m|$, where ρ_m is a root of $a(\mathfrak{q})$ defined in (2.13). These roots are chosen to be distinct, i.e., $\rho_m \neq \rho_n$ for $m \neq n$. The following theorem provides conditions for the probabilistic performance certificates.

Theorem 2.3.8 (Probabilistic performance certificates)**.** *Suppose Assumption 2.3.7 holds and the dwell time is large enough. Consider the closed-loop dynamics* (2.1)-(2.2) *and the filter* $\mathbb{F}_{ij}$ *with the poles* $\rho_m,\ m\in\{1,\dots,d_{N+1}\}$*, and the numerator designed by using* (2.18) *with the corresponding optimal solutions* η^*_{ijj}*. Given a reliability level* $\beta\in(0,1]$ *and a constant* $\mu\in\mathbb{R}_+$*, the probabilistic performance* (2.9) *in Problem 2 is satisfied, if the threshold* ε_i *is set as*

$$\varepsilon_i = \left(\mu+\lambda_\omega\sqrt{2\ln(2/\beta)}\right)\sqrt{\bar{\eta}_i},\quad \bar{\eta}_i = \max_{j\in\hat{\mathcal{N}}}\eta^*_{ijj}, \tag{2.22}$$

and the estimated matched time T_{ij} *equals to*

$$T_{ij} = \left\lceil \frac{\log\left(\psi_{ij}\left(\mathbb{F}_{ij},\mathcal{X}_{ij}(t_s)\right)/\left(\mu\sqrt{\bar{\eta}_i}\right)\right)}{\log\rho^{-1}_{\max}}\right\rceil, \tag{2.23}$$

where $\psi_{ij}\left(\mathbb{F}_{ij},\mathcal{X}_{ij}(t_s)\right) = \sqrt{d_N+1}\left(1+\rho^{-1}_{\max}\|\bar{B}_{ij}\|_2\right)\left\|\mathbf{E}\left[\mathcal{X}_{ij}(t_s)\right]\right\|_2$*. The matrix* $\bar{B}_{ij}$ *is defined as*

$$\bar{B}_{ij} = \begin{bmatrix} b_{ij,11} & \dots & b_{ij,1n_x}\\ \vdots & \ddots & \vdots\\ b_{ij,(d_N+1)1} & \dots & b_{ij,(d_N+1)n_x}\end{bmatrix},$$

where $b_{ij,\ell h} = -\sum_{m=0}^{d_N}\hat{N}_{ij,m}(h)\rho^m_\ell\Big/\left(\prod_{\tilde{\ell}\neq\ell}(\rho_{\tilde{\ell}}-\rho_\ell)\right)$ *for* $h\in\{1,\dots,n_x\},\ \ell,\ \tilde{\ell}\in\{1,\dots,d_N+1\}$*, and* $\hat{N}_{ij,m}(h)$ *denotes the h-th element of* $\hat{N}_{ij,m}$*.*

Proof. The proof is provided in Section 2.4.2. □

The estimated matched time T_{ij} in (2.23) is actually an upper bound for the time that $|\mathbf{E}[r_{ij}]|$ takes to arrive at $\mu\sqrt{\bar{\eta}_i}$ after transition happens (as shown in Figure 2.3). Then, we set the confidence interval according to β, such that ε_i is determined.

Remark 2.3.9 (Threshold vs estimated matched time trade-off)**.** *There is a trade-off in selecting* μ *and* β *in* (2.22)*: A smaller threshold* ε_i *provides high guarantees on excluding the unmatched residuals. We can decrease* ε_i *with smaller* μ *or larger* β *from* (2.22)*. However, a smaller* μ *can lead to a more conservative estimated matched time* T_{ij} *from* (2.23)*. Also, a larger* β *increases the chance of false isolation.*

Remark 2.3.10 (Comparison with Chebyshev based bounds)**.** *We highlight that the threshold* (2.22) *depends logarithmically on the reliability parameter, i.e.,* $\sqrt{\ln(2/\beta)}$*. This is a significant improvement in comparison with the results based on Chebyshev's inequality (e.g., [117, Section III.B]) in which the threshold scales polynomially by the factor* $\sqrt{1/\beta}$*.*

2

As a special case of T_{ij} in Theorem 2.3.8, the waiting time τ_j can be determined by

$$\tau_j = \left\lceil \frac{\log\left(\psi_{jj}\left(\mathbb{F}_{jj}, \mathcal{X}_{jj}(t_s^{\mathrm{iso}})\right) / \left(\mu\sqrt{\bar{\eta}_j}\right)\right)}{\log \rho_{\max}^{-1}} \right\rceil, \tag{2.24}$$

where $\psi_{jj}\left(\mathbb{F}_{jj}, \mathcal{X}_{jj}(t_s^{\mathrm{iso}})\right) = \sqrt{d_N+1}\left(1+\rho_{\max}^{-1}\|\bar{B}_{jj}\|_2\right)\left\|\mathbf{E}\left[\mathcal{X}_{jj}\left(t_s^{\mathrm{iso}}\right)\right]\right\|_2$.

Observe that the expected values of $\mathcal{X}_{ij}(t_s)$ and $\mathcal{X}_{jj}(t_s^{\mathrm{iso}})$ are required in (2.23) and (2.24). Recall that we assume that the dwell time is large enough and the system can reach the steady state before the next transition. The constant reference signal d is considered during the dwell time, i.e., $d(k) = \bar{d}$ for $k \in [t_s, t_{s+1})$. Then, $\mathbf{E}\left[\mathcal{X}_{ij}(t_s)\right]$ can be estimated by its steady-state value $\mathbf{E}\left[\mathcal{X}_{ij}(t_s)\right] = \left(I - \mathcal{A}_{iji}\right)^{-1}\mathcal{E}_i\bar{d}$. For $\mathbf{E}\left[\mathcal{X}_{jj}(t_s^{\mathrm{iso}})\right]$, since the actual diagnosis time is a random value, we first compute the steady-state value of $\mathbf{E}\left[\mathcal{X}_{jj}(t_s)\right]$. Then, according to the dynamics (2.17), we compute $\max_{i\in\mathcal{N}}\|\mathbf{E}\left[\mathcal{X}_{jj}(t_s+T_{ij})\right]\|_2$ as a conservative estimate of $\|\mathbf{E}[\mathcal{X}_{jj}(t_s^{\mathrm{iso}})]\|_2$.

According to the diagnosis rule (2.8), one still needs to let the unmatched residuals be outside the threshold interval. Suppose the status is S_{ij}. Inspired by the active fault diagnosis method [114], we can design the reference signal d such that the unmatched residuals $r_{ih'}$ for $h' \in \mathcal{N}\setminus\{j\}$ satisfy $|\mathbf{E}[r_{ih'}]| \geq \varepsilon_i + \bar{\mu}\sqrt{\bar{\eta}_i}$ in the steady state, where $\bar{\mu} \in \mathbb{R}_+$ is a constant. From the closed-loop dynamics (2.10) and (2.14), the expected value of $r_{ih'}$ can be written as

$$\mathbf{E}[r_{ih'}] = \frac{N_{ih'}(\mathfrak{q})L(\mathfrak{q})}{a(\mathfrak{q})} C_j\left(\mathfrak{q}I - A_{ij}^{cl}\right)^{-1}E_j\bar{d}. \tag{2.25}$$

According to (2.25), the requirement $|\mathbf{E}[r_{ih'}]| \geq \varepsilon_i + \bar{\mu}\sqrt{\bar{\eta}_i}$ is equivalent to choosing $\bar{d}$ such that

$$\left|a^{-1}(1)\bar{N}_{ih'}\mathcal{L}_{ij}\bar{d}\right| \geq \varepsilon_i + \bar{\mu}\sqrt{\bar{\eta}_i}. \tag{2.26}$$

In the light of Lemma 2.3.6, we have $|r_{ih'}| > \varepsilon_i$ with guaranteed probability in the steady state if (2.26) is satisfied.

Remark 2.3.11 (Regularities on the reference input)**.** *When designing the filters and thresholds, the value of the reference signal is not necessary. However, this value is required when computing the estimated matched time* T_{ij}*. Moreover, in order to separate the residuals of different modes in the presence of noise, the reference signal* $\bar{d}$ *should satisfy* (2.26)*. Such constraint is not novel in the distinguishability problem for switched affine systems [121]. This also can be interpreted as the persistence of excitation.*

Remark 2.3.12 (Extension to nonlinear switched systems)**.** *There are several ways to extend the proposed diagnosis method to nonlinear systems. The most straightforward approach is to linearize each subsystem at the operating point and decouple the disturbances together with*

the higher-order nonlinear terms. However, linearization is only applicable to systems with a narrow operating range, and it is impossible to completely decouple the nonlinear terms in practice. One can leverage the idea from [53], where the authors robustify the filter to the nonlinearity signatures by exploiting the statistical properties of the disturbance signals. Another option is to use polynomials to approximate the nonlinear terms [122]. Thus, when formulating the residual generator, it becomes possible to integrate the approximation of nonlinear terms into the objective function. This integration serves to mitigate the impact of these nonlinear elements on the residuals.

2.4 Technical Proofs of Main Results

This section presents the technical proofs of the theoretical results in Section 2.3.

2.4.1 Proofs of Results in Filter Design

Let us start with two lemmas required for the proof of Theorem 2.3.1.

Lemma 2.4.1. *(Multiplication of polynomial matrices [53, Section III-A]) Let $Q_1(\mathfrak{q})$ and $Q_2(\mathfrak{q})$ be polynomial matrices of degree d_1 and d_2, resp., and defined by*

$$Q_1(\mathfrak{q}) = \sum_{m=0}^{d_1} Q_{1,m}\mathfrak{q}^m, \quad Q_2(\mathfrak{q}) = \sum_{m=0}^{d_2} Q_{2,m}\mathfrak{q}^m,$$

where $Q_{1,m} \in \mathbb{R}^{n_1 \times n_2}$ and $Q_{2,m} \in \mathbb{R}^{n_2 \times n_3}$ are the matrices of constant coefficients. The multiplication of $Q_1(\mathfrak{q})$ and $Q_2(\mathfrak{q})$ is equivalent to

$$Q_1(\mathfrak{q})Q_2(\mathfrak{q}) = \bar{Q}_1\bar{Q}_2 \left[I \ \mathfrak{q}I \ \dots \ \mathfrak{q}^{d_1+d_2}I\right]^\top,$$

where $\bar{Q}_1 = \begin{bmatrix} Q_{1,0} & Q_{1,1} & \dots & Q_{1,d_1} \end{bmatrix}$ *and*

$$\bar{Q}_2 = \begin{bmatrix} Q_{2,0} & Q_{2,1} & \dots & Q_{2,d_2} & 0 & \dots & 0 \\ 0 & Q_{2,0} & Q_{2,1} & \dots & Q_{2,d_2} & 0 & \vdots \\ \vdots & & \ddots & \ddots & & \ddots & 0 \\ 0 & 0 & \dots & Q_{2,0} & Q_{2,1} & \dots & Q_{2,d_2} \end{bmatrix}.$$

The following lemma is a slight modification of the standard result concerning the $\mathcal{H}_2$ norm of the stable LTI systems.

Lemma 2.4.2. *($\mathcal{H}_2$ norm [123, Lemma 1]) Consider the linear transfer function $\mathbb{T}(\mathfrak{q}) = C(\mathfrak{q}I - A)^{-1}B$. For any constant η, the system is stable and $\|\mathbb{T}(\mathfrak{q})\|_{\mathcal{H}_2}^2 < \eta$ if and only if for all sufficiently small $\vartheta \in \mathbb{R}_+$, there exist P, $Z \in \mathcal{S}$ such that the following LMIs are feasible:*

$$\begin{bmatrix} P & AP & B \\ * & P & 0 \\ * & * & I \end{bmatrix} \succeq \vartheta I, \ \begin{bmatrix} Z & CP \\ * & P \end{bmatrix} \succeq \vartheta I, \ \text{Trace}(Z) \leq \eta - \vartheta.$$

Proof of Theorem 2.3.1. First, we show that the equality (2.18a) guarantees the satisfaction of the property (2.4a). According to Lemma 2.4.1, it holds that

$$N_{ij}(\mathfrak{q})H_{ij}(\mathfrak{q}) = \bar{N}_{ij}\bar{H}_{ij}\left[I\ \mathfrak{q}I\ \ldots\ \mathfrak{q}^{d_N+1}I\right]^\top.$$

Hence, (2.18a) implies that $N_{ij}(\mathfrak{q})H_{ij}(\mathfrak{q}) = 0$. The contribution of d to r_{ij} is completely canceled when the status is S_{ij} ($h = j$ in (2.14)). This concludes the first part of the proof.

In the second part of the proof, we show that the constraint (2.18b) implies the satisfaction of the property (2.4b). Suppose the status is $S_{ih'}$ for $h' \in \mathcal{N}\setminus\{j\}$. According to the closed-loop dynamics (2.10), we have

$$y = C_{h'}\left(\mathfrak{q}I - A^{cl}_{ih'}\right)^{-1}E_{h'}[d] + \left[C_{h'}\left(\mathfrak{q}I - A^{cl}_{ih'}\right)^{-1}(W_{h'} + B_{h'}K_iD_{h'}) + D_{h'}\right][\omega].$$

By virtue of (2.14) and the expression of y, the transfer function from d to r_{ij} can be written as

$$\begin{aligned}\mathbb{F}_{ij}\mathbb{T}^{S_{ih'}}_{dy}(\mathfrak{q}) &= a^{-1}(\mathfrak{q})N_{ij}(\mathfrak{q})L(\mathfrak{q})C_{h'}\left(\mathfrak{q}I - A^{cl}_{ih'}\right)^{-1}E_{h'}\\ &= a^{-1}(\mathfrak{q})\bar{N}_{ij}\bar{L}\left[I\ \mathfrak{q}I\ \ldots\ \mathfrak{q}^{d_N}I\right]^\top C_{h'}\left(\mathfrak{q}I - A^{cl}_{ih'}\right)^{-1}E_{h'},\end{aligned}$$

where Lemma 2.4.1 is used in the second equality. Then, we enforce the absolute value of the steady-state gain of $\mathbb{F}_{ij}\mathbb{T}^{S_{ih'}}_{dy}$ to be larger than or equal to 1, which is

$$\left|\left[\mathbb{F}_{ij}\mathbb{T}^{S_{ih'}}_{dy}\right]_{ss}\right| = \left|a^{-1}(1)\bar{N}_{ij}\mathcal{L}_{ih'}\right| \geq 1.$$

This concludes the second part of the proof.

In the third part, we show that the inequalities (2.18c) and (2.18d) enforce the desired property (2.4c). When the status is S_{ij}, as shown in (2.14), the transfer function from ω to r_{ij} becomes

$$\mathbb{F}_{ij}\mathbb{T}^{S_{ij}}_{\omega y}(\mathfrak{q}) = -a^{-1}(\mathfrak{q})N_{ij}(\mathfrak{q})G_{ij}(\mathfrak{q}), \tag{2.27}$$

where $[x^\top\ d^\top]^\top$ is decoupled by (2.4a). Let $(A_r, \mathcal{B}_{ij}, C_r)$ be the observable canonical realization of (2.27), whose derivation process is similar to that of (2.16). According to Lemma 2.4.2, the inequalities (2.18c) imply $\left\|\mathbb{F}_{ij}\mathbb{T}^{S_{ij}}_{\omega y}\right\|^2_{\mathcal{H}_2} < \eta_{ijj}$ directly. Note that the slack variable Z shown in Lemma 2.4.2 has one dimension in this problem, thus the third inequality is dropped. When the status is $S_{ih'}$ for $h' \in \mathcal{N}\setminus\{j\}$, the transfer function from ω to r_{ij} can be obtained from (2.17). Again, according to Lemma 2.4.2, the inequalities (2.18d) imply $\left\|\mathbb{F}_{ij}\mathbb{T}^{S_{ih'}}_{\omega y}\right\|^2_{\mathcal{H}_2} < \eta_{ijh'}$. Then, we take the sum of η_{ijh} for all $h \in \mathcal{N}$ as the objective function to minimize the effect of ω on r_{ij}. This completes the proof. □

Proof of Proposition 2.3.2. This proof is to show that (2.19) ensures the satisfaction of the nonlinear matrix inequality in (2.18d). By applying Schur complement to (2.19), we have

$$\begin{aligned}&\begin{bmatrix}P_{ijh'} & \hat{A}_{ih'}\mathcal{G}_{ijh'}\\ * & \Xi_{ijh'}\end{bmatrix} - \begin{bmatrix}\hat{B}_{r_{ij}} & 0\\ * & \left(\hat{D}_{h'}\mathcal{G}_{ijh'}\right)^\top\end{bmatrix}\begin{bmatrix}\gamma I & 0\\ * & \frac{1}{\gamma}I\end{bmatrix}\begin{bmatrix}\hat{B}^\top_{r_{ij}} & 0\\ * & \hat{D}_{h'}\mathcal{G}_{ijh'}\end{bmatrix}\\ =&\begin{bmatrix}P_{ijh'} & \hat{A}_{ih'}\mathcal{G}_{ijh'}\\ * & \Xi_{ijh'}\end{bmatrix} - \gamma\begin{bmatrix}\hat{B}_{r_{ij}}\\ 0\end{bmatrix}\begin{bmatrix}\hat{B}^\top_{r_{ij}} & 0\end{bmatrix} - \frac{1}{\gamma}\begin{bmatrix}0\\ \left(\hat{D}_{h'}\mathcal{G}_{ijh'}\right)^\top\end{bmatrix}\begin{bmatrix}0 & \hat{D}_{h'}\mathcal{G}_{ijh'}\end{bmatrix} \succeq \vartheta I.\end{aligned} \tag{2.28}$$

Note that, for matrices A, B with appropriate dimensions and any scalar $\gamma > 0$, it holds that $\gamma AA^\top + \frac{1}{\gamma} B^\top B \succeq AB + B^\top A^\top$ [118, Lemma 1]. We have

$$\begin{aligned}
&-\begin{bmatrix} \hat{B}_{r_{ij}} \\ 0 \end{bmatrix} \begin{bmatrix} 0 & \hat{D}_{h'} \mathcal{G}_{ijh'} \end{bmatrix} - \begin{bmatrix} 0 \\ \left(\hat{D}_{h'} \mathcal{G}_{ijh'}\right)^\top \end{bmatrix} \begin{bmatrix} \hat{B}_{r_{ij}}^\top & 0 \end{bmatrix} \\
&\succeq -\gamma \begin{bmatrix} \hat{B}_{r_{ij}} \\ 0 \end{bmatrix} \begin{bmatrix} \hat{B}_{r_{ij}}^\top & 0 \end{bmatrix} - \frac{1}{\gamma} \begin{bmatrix} 0 \\ \left(\hat{D}_{h'} \mathcal{G}_{ijh'}\right)^\top \end{bmatrix} \begin{bmatrix} 0 & \hat{D}_{h'} \mathcal{G}_{ijh'} \end{bmatrix}.
\end{aligned}$$

Thus, the inequality (2.28) can be written as

$$\begin{aligned}
&\begin{bmatrix} P_{ijh'} & \hat{A}_{ih'} \mathcal{G}_{ijh'} \\ * & \Xi_{ijh'} \end{bmatrix} - \begin{bmatrix} \hat{B}_{r_{ij}} \\ 0 \end{bmatrix} \begin{bmatrix} 0 & \hat{D}_{h'} \mathcal{G}_{ijh'} \end{bmatrix} - \begin{bmatrix} 0 \\ \left(\hat{D}_{h'} \mathcal{G}_{ijh'}\right)^\top \end{bmatrix} \begin{bmatrix} \hat{B}_{r_{ij}}^\top & 0 \end{bmatrix} \\
&= \begin{bmatrix} P_{ijh'} & \hat{A}_{ih'} \mathcal{G}_{ijh'} - \hat{B}_{r_{ij}} \hat{D}_{h'} \mathcal{G}_{ijh'} \\ * & \Xi_{ijh'} \end{bmatrix} \succeq \vartheta I. \qquad (2.29)
\end{aligned}$$

Expanding $\hat{A}_{ih'} \mathcal{G}_{ijh'} - \hat{B}_{r_{ij}} \hat{D}_{h'} \mathcal{G}_{ijh'}$ leads to

$$\begin{aligned}
&\left[\begin{bmatrix} A_{ih'}^{cl} & 0 \\ 0 & A_r \end{bmatrix} \mathcal{G}_{ijh',1} \quad \begin{bmatrix} W_{h'} + B_{h'} K_i D_{h'} \\ 0 \end{bmatrix} \mathcal{G}_{ijh',2}\right] - \left[\begin{bmatrix} 0 \\ -B_{r_{ij}} \end{bmatrix} \begin{bmatrix} C_{h'} & 0 \end{bmatrix} \mathcal{G}_{ijh',1} \quad \begin{bmatrix} 0 \\ -B_{r_{ij}} \end{bmatrix} D_{h'} \mathcal{G}_{ijh',2}\right] \\
&= \left[\begin{bmatrix} A_{ih'}^{cl} & 0 \\ B_{r_{ij}} C_{h'} & Ar \end{bmatrix} \mathcal{G}_{ijh',1} \quad \begin{bmatrix} W_{h'} + B_{h'} K_i D_{h'} \\ B_{r_{ij}} D_{h'} \end{bmatrix} \mathcal{G}_{ijh',2}\right] \\
&= \begin{bmatrix} \mathcal{A}_{ijh'} & \mathcal{D}_{ijh'} \end{bmatrix} \mathcal{G}_{ijh'}. \qquad (2.30)
\end{aligned}$$

From (2.30), the inequality (2.29) is equivalent to

$$\begin{bmatrix} P_{ijh'} & \begin{bmatrix} \mathcal{A}_{ijh'} & \mathcal{D}_{ijh'} \end{bmatrix} \mathcal{G}_{ijh'} \\ * & \Xi_{ijh'} \end{bmatrix} \succeq \vartheta I. \qquad (2.31)$$

For a scalar $\alpha \in \mathbb{R}$, matrices A, B with appropriate dimensions, and $A \succ 0$, note that $(B - \alpha A)^\top A^{-1} (B - \alpha A) \succeq 0$ implies $B^\top A^{-1} B \succeq \alpha B + \alpha B^\top - \alpha^2 A$. Thus, we have

$$\mathcal{G}_{ijh'}{}^\top \begin{bmatrix} P_{ijh'} & 0 \\ * & I \end{bmatrix}^{-1} \mathcal{G}_{ijh'} \succeq \Xi_{ijh'}. \qquad (2.32)$$

By combining (2.31) and (2.32), we obtain

$$\begin{bmatrix} P_{ijh'} & \begin{bmatrix} \mathcal{A}_{ijh'} & \mathcal{D}_{ijh'} \end{bmatrix} \mathcal{G}_{ijh'} \\ * & \mathcal{G}_{ijh'}{}^\top \begin{bmatrix} P_{ijh'} & 0 \\ * & I \end{bmatrix}^{-1} \mathcal{G}_{ijh'} \end{bmatrix} \succeq \vartheta I. \qquad (2.33)$$

Pre- and post-multiplying (2.33) by $\mathrm{diag}(I, \mathcal{G}_{ijh'}{}^{-\top})$ and $\mathrm{diag}(I, P_{ijh'}, I)$ and their transpose successively, we arrive at

$$\begin{bmatrix} P_{ijh'} & \mathcal{A}_{ijh'}P_{ijh'} & \mathcal{D}_{ijh'} \\ * & P_{ijh'} & 0 \\ * & * & I \end{bmatrix} \succeq \vartheta I.$$

This completes the proof. □

Proof of Proposition 2.3.3. We first show that the inequality (2.20a) is a necessary and sufficient condition for the constraint (2.18a) having non-trivial solutions. According to Rank Plus Nullity Theorem [124, Chapter 4], it holds that

$$(d_N+1)(n_x+n_y) = \mathrm{Rank}\left(\bar{H}_{ij}\right) + \mathrm{Null}\left(\bar{H}_{ij}\right),$$

where $\mathrm{Null}\left(\bar{H}_{ij}\right)$ denotes the dimension of the left null space of $\bar{H}_{ij}$. Thus, (2.18a) having non-trivial solutions is equivalent to $\mathrm{Null}\left(\bar{H}_{ij}\right)$ being nonzero. This concludes the first part of the proof.

Second, we show that (2.20b) is equivalent to (2.18b) when (2.20a) holds. (⇒) We proceed with the proof by contradiction. Suppose that (2.18b) holds but (2.20b) is not satisfied, we have $\mathrm{Rank}\left(\begin{bmatrix}\bar{H}_{ij} & \mathcal{L}_{ih'}\end{bmatrix}\right) = \mathrm{Rank}\left(\bar{H}_{ij}\right)$. This means that $\mathcal{L}_{ih'}$ belongs to the column range space of $\bar{H}_{ij}$. In other words, there exists a vector $\xi \in \mathbb{R}^{(n_x+n_d)(d_N+2)}$, such that $\mathcal{L}_{ih'} = \bar{H}_{ij}\xi$. Since $\bar{N}_{ij}$ satisfying $\bar{N}_{ij}\bar{H}_{ij} = 0$, we have $\bar{N}_{ij}\mathcal{L}_{ih'} = \bar{N}_{ij}\bar{H}_{ij}\xi = 0$, which contradicts to (2.18b). (⇐) Assume that (2.20b) holds. This means that the left null space of $\bar{H}_{ij}$ and $\mathcal{L}_{ih'}$ are not the same. Thus, one can find a $\bar{N}_{ij}$ which satisfies (2.18a) and (2.18b) at the same time. This completes the second part of the proof.

Finally, it is known from Lemma 2.4.2 that $|\Lambda(A_r)| < 1$, and $|\Lambda(\mathcal{A}_{ijh'})| < 1$ are necessary and sufficient conditions for the feasibility of (2.18c) and (2.18d), resp. Recalling the definition of $\mathcal{A}_{ijh'}$ in (2.17), $|\Lambda(\mathcal{A}_{ijh'})| < 1$ if and only if $|\Lambda(A_r)| < 1$ and $|\Lambda(A^{cl}_{ih'})| < 1$. This completes the proof. □

2.4.2 Proofs of Probabilistic Certificates

We introduce the following lemma to be used to prove Theorem 2.3.8.

Lemma 2.4.3 (Linear transformation of sub-Gaussian signals)**.** *Suppose $\mathbb{T}_{\omega r}$ is a transfer function from ω to r with the state-space realization (A,B,C), i.e., $r = \mathbb{T}_{\omega r}[\omega] = C(\mathrm{q}I - A)^{-1}B[\omega]$. If the input ω is an iid sub-Gaussian signal with zero mean and parameter λ_ω, the output r is also sub-Gaussian with zero mean and the respective parameter $\lambda_r = \|\mathbb{T}_{\omega r}\|_{\mathcal{H}_2}\lambda_\omega$.*

Proof. From the linear system theory we know that $r(k) - \mathbf{E}[r(k)] = C\sum_{m=0}^{k-1} A^{k-1-m}B\omega(m)$. Then, for any constant $\phi \in \mathbb{R}$ and a unit vector ν with an appropriate dimension, we have

$$\begin{aligned}\mathbf{E}\left[\mathrm{e}^{\phi\nu^\top(r(k)-\mathbf{E}[r(k)])}\right] &= \mathbf{E}\left[\mathrm{e}^{\phi\nu^\top C\sum_{m=0}^{k-1}A^{k-1-m}B\omega(m)}\right] \\ &= \prod_{m=0}^{k-1}\mathbf{E}\left[\mathrm{e}^{\phi\nu^\top CA^{k-1-m}B\omega(m)}\right]. \end{aligned} \tag{2.34}$$

Since ω is sub-Gaussian, according to Lemma 2.3.6, it holds that

$$\mathbf{E}\left[\mathrm{e}^{\phi v^\top CA^{k-1-m}B\omega(m)}\right] \le \mathrm{e}^{\phi^2\|v^\top\|_2^2\|CA^{k-1-m}B\|_2^2\lambda_\omega^2/2}.$$

Recall that $\|v\|_2 = 1$. Thus, equality (2.34) satisfies

$$\mathbf{E}\left[\mathrm{e}^{\phi v^\top(r(k)-\mathbf{E}[r(k)])}\right] \le \prod_{m=0}^{k-1}\mathrm{e}^{\phi^2\|CA^{k-1-m}B\|_2^2\lambda_\omega^2/2} = \mathrm{e}^{\phi^2\sum_{m=0}^{k-1}\|CA^{k-1-m}B\|_2^2\lambda_\omega^2/2}.$$

By matrix norm definitions, we know $\|A\|_2^2 \le \mathrm{Trace}(A^\top A)$ for all real-valued matrix A, and, thus,

$$\begin{aligned}\mathbf{E}\left[\mathrm{e}^{\phi v^\top(r(k)-\mathbf{E}[r(k)])}\right] &\le \mathrm{e}^{\phi^2\sum_{m=0}^{k-1}\mathrm{Trace}\left(CA^{k-1-m}BB^\top A^{\top k-1-m}C^\top\right)\lambda_\omega^2/2}\\ &\le \mathrm{e}^{\phi^2\|\mathbb{T}_{\omega r}\|_{\mathcal{H}_2}^2\lambda_\omega^2/2},\end{aligned}$$

where the last inequality follows from Parseval's Theorem and the $\mathcal{H}_2$ norm definition. □

Proof of Theorem 2.3.8. The main idea builds on the probabilistic relation between the concentration of a random variable and its expectation. Since the noise ω is sub-Gaussian, according to Lemma 2.4.3, the matched residual r_{ij} is also sub-Gaussian with the parameter $\lambda_{r_{ij}} = \left\|\mathbb{T}_{\omega r_{ij}}^{S_{ij}}\right\|_{\mathcal{H}_2}\lambda_\omega < \sqrt{\bar\eta_i}\lambda_\omega$. We first show that the performance guarantee (2.9) holds when $|\mathbf{E}[r_{ij}(k)]| \le \mu\sqrt{\bar\eta_i}$. According to (2.22), we have

$$\varepsilon_i - \left|\mathbf{E}[r_{ij}(k)]\right| \ge \varepsilon_i - \mu\sqrt{\bar\eta_i} = \lambda_\omega\sqrt{2\ln(2/\beta)\bar\eta_i}.$$

Since it also holds that $\left|r_{ij}(k)\right| - \left|\mathbf{E}[r_{ij}(k)]\right| \le \left|r_{ij}(k) - \mathbf{E}[r_{ij}(k)]\right|$, we have

$$\begin{aligned}&\mathbf{Pr}\left[\left|r_{ij}(k)\right| \le \varepsilon_i \middle| \begin{bmatrix}\hat\sigma(k)\\ \sigma(k)\end{bmatrix} = \begin{bmatrix}i\\ j\end{bmatrix}, k \ge t_s\right]\\ =&\mathbf{Pr}\left[\left|r_{ij}(k)\right| - \left|\mathbf{E}[r_{ij}(k)]\right| \le \varepsilon_i - \left|\mathbf{E}[r_{ij}(k)]\right| \middle| \begin{bmatrix}\hat\sigma(k)\\ \sigma(k)\end{bmatrix} = \begin{bmatrix}i\\ j\end{bmatrix}, k \ge t_s\right]\\ \ge&\mathbf{Pr}\left[\left|r_{ij}(k) - \mathbf{E}[r_{ij}(k)]\right| \le \lambda_\omega\sqrt{2\ln(2/\beta)\bar\eta_i} \middle| \begin{bmatrix}\hat\sigma(k)\\ \sigma(k)\end{bmatrix} = \begin{bmatrix}i\\ j\end{bmatrix}, k \ge t_s\right]\\ \ge&1 - 2\mathrm{e}^{-2\ln(2/\beta)\bar\eta_i\lambda_\omega^2\Big/\left(2\|\mathbb{T}_{\omega r_{ij}}^{S_{ij}}\|_{\mathcal{H}_2}^2\lambda_\omega^2\right)} \ge 1-\beta,\end{aligned}$$

where the concentration inequality (2.21) in Lemma 2.3.6 is used to get the second inequality. This completes the first part of the proof.

Next, we show that $|\mathbf{E}[r_{ij}(k)]| \le \mu\sqrt{\bar\eta_i}$ when $k \ge t_s + T_{ij}$. Let us incorporate the initial state $x(t_s)$ into the expression of $\mathbf{E}[r_{ij}(k)]$, where $x(t_s)$ is viewed as an input to the system

that only has a nonzero value at t_s. According to the closed-loop dynamics (2.10), for $k = t_s + \Delta k$ where $\Delta k \in [0, t_s^{\text{iso}})$, we have

$$\begin{aligned} x(k+1) &= A_{ij}^{cl} x(k) + E_j d(k) + (W_j + B_j K_i D_j)\omega(k) + x(t_s), \\ y(k) &= C_j x(k) + D_j \omega(k). \end{aligned} \tag{2.35}$$

We reformulate (2.35) into the DAE format, which is

$$\begin{bmatrix} -\mathfrak{q} I + A_{ij}^{cl} & E_j & I \\ C_j & 0 & 0 \end{bmatrix} \begin{bmatrix} x \\ d \\ x(t_s) \end{bmatrix} + L(\mathfrak{q})[y] + G_{ij}(\mathfrak{q})[\omega] = 0. \tag{2.36}$$

Multiplying the left hand-side of (2.36) by $a^{-1}(\mathfrak{q}) N_{ij}(\mathfrak{q})$ leads to

$$\begin{aligned} r_{ij} &= \frac{N_{ij}(\mathfrak{q}) L(\mathfrak{q})}{a(\mathfrak{q})}[y] \\ &= -\frac{N_{ij}(\mathfrak{q})}{a(\mathfrak{q})} \begin{bmatrix} -\mathfrak{q} I + A_{ij}^{cl} & E_j & I \\ C_j & 0 & 0 \end{bmatrix} \begin{bmatrix} x \\ d \\ x(t_s) \end{bmatrix} - \frac{N_{ij}(\mathfrak{q}) G_{ij}(\mathfrak{q})}{a(\mathfrak{q})}[\omega]. \end{aligned} \tag{2.37}$$

Recall that $N_{ij}(\mathfrak{q}) H_{ij}(\mathfrak{q}) = 0$ in Theorem 2.3.1. By substituting $N_{ij}(\mathfrak{q}) = \left[\hat{N}_{ij}(\mathfrak{q}) \; \check{N}_{ij}(\mathfrak{q})\right]$ into (2.37), we have

$$r_{ij} = -\frac{\hat{N}_{ij}(\mathfrak{q})}{a(\mathfrak{q})} x(t_s) - \frac{N_{ij}(\mathfrak{q}) G_{ij}(\mathfrak{q})}{a(\mathfrak{q})}[\omega].$$

Hence, the expected value of r_{ij} is

$$\mathbf{E}[r_{ij}] = -a^{-1}(\mathfrak{q}) \hat{N}_{ij}(\mathfrak{q}) \mathbf{E}[x(t_s)].$$

To compute T_{ij}, following the idea of [125, Lemma 3.4], we transform $-a^{-1}(\mathfrak{q})\hat{N}_{ij}(\mathfrak{q})$ to its Jordan canonical form denoted by $(\bar{A}, \bar{B}_{ij}, \bar{C})$. The transfer function $-a^{-1}(\mathfrak{q})\hat{N}_{ij}(\mathfrak{q})$ can be expanded as

$$-\frac{\hat{N}_{ij}(\mathfrak{q})}{a(\mathfrak{q})} = \left[-\frac{\sum_{m=0}^{d_N} \hat{N}_{ij,m}(1)\mathfrak{q}^m}{a(\mathfrak{q})}, \ldots, -\frac{\sum_{m=0}^{d_N} \hat{N}_{ij,m}(n_x)\mathfrak{q}^m}{a(\mathfrak{q})} \right].$$

Recall that $a(\mathfrak{q}) = \prod_{\ell=1}^{d_N+1}(\mathfrak{q} - \rho_\ell)$. The factorization of the h-th element of $-a^{-1}(\mathfrak{q})\hat{N}_{ij}(\mathfrak{q})$ is

$$-\frac{\sum_{m=0}^{d_N} \hat{N}_{ij,m}(h)\mathfrak{q}^m}{a(\mathfrak{q})} = \sum_{\ell=1}^{d_N+1} \frac{b_{ij,\ell h}}{\mathfrak{q} - \rho_\ell},$$

where $b_{ij,\ell h} = -\frac{\sum_{m=0}^{d_N} \hat{N}_{ij,m}(h)\rho_\ell^m}{\prod_{\bar{\ell} \neq \ell}(\rho_{\bar{\ell}} - \rho_\ell)}$.

The Jordan canonical form of $-a^{-1}(\mathfrak{q})\sum_{m=0}^{d_N}\hat{N}_{ij,m}(h)\mathfrak{q}^m$ is denoted by $(\bar{A}_h, \bar{B}_{ij,h}, \bar{C}_h)$, where

$$\bar{A}_h = \text{diag}([\rho_1, \ldots, \rho_{d_N+1}]),\ \bar{B}_{ij,h} = [b_{ij,1h}, \ldots, b_{ij,(d_N+1)h}]^\top,\ \text{and}\ \bar{C}_h = [1, \ldots, 1].$$

According to the superposition property of linear systems, we have

$$\bar{A} = \text{diag}([\rho_1, \ldots, \rho_{d_N+1}]),\ \bar{B}_{ij} = [\bar{B}_{ij,1}, \ldots, \bar{B}_{ij,n_x}],\ \text{and}\ \bar{C} = [1, \ldots, 1].$$

With the state-space description, $\mathbf{E}[r_{ij}(k)]$ can be written as

$$\begin{aligned}\mathbf{E}[r_{ij}(k)] &= \bar{C}\bar{A}^{\Delta k}\mathbf{E}[\bar{x}_{ij}(t_s)] + \bar{C}\sum_{m=0}^{\Delta k-1}\bar{A}^{\Delta k-1-m}\bar{B}_{ij}\mathbf{E}[x(t_s)] \\ &= \bar{C}\bar{A}^{\Delta k}\mathbf{E}[\bar{x}_{ij}(t_s)] + \bar{C}\bar{A}^{\Delta k-1}\bar{B}_{ij}\mathbf{E}[x(t_s)],\end{aligned}$$

where $\bar{x}_{ij}(t_s)$ is the filter state at the switching instance t_s.

Since $\bar{A}$ is a diagonal matrix, we have $\|\bar{A}\|_2 = \rho_{\max}$. Based on the triangle property of norms, $|\mathbf{E}[r_{ij}(k)]|$ is bounded by

$$\begin{aligned}|\mathbf{E}[r_{ij}(k)]| &\le \|\bar{C}\|_2\|\bar{A}\|_2^{\Delta k}\|\mathbf{E}[\bar{x}_{ij}(t_s)]\|_2 + \|\bar{C}\|_2\|\bar{A}\|_2^{\Delta k-1}\|\bar{B}_{ij}\|_2\|\mathbf{E}[x(t_s)]\|_2 \\ &\le \sqrt{d_N+1}(1+\rho_{\max}^{-1}\|\bar{B}_{ij}\|_2)\|\mathbf{E}[\mathcal{X}_{ij}(t_s)]\|_2\rho_{\max}^{\Delta k} \\ &= \psi_{ij}\left(\mathbb{F}_{ij}, \mathcal{X}_{ij}(t_s)\right)\rho_{\max}^{\Delta k}.\end{aligned}$$

Finally, by setting $\mu\sqrt{\bar{\eta}_i} \ge \psi_{ij}\left(\mathbb{F}_{ij}, \mathcal{X}_{ij}(t_s)\right)\rho_{\max}^{\Delta k}$, we arrive at

$$\Delta k \ge T_{ij} = \left\lfloor \log_{\rho_{\max}} \frac{\mu\sqrt{\bar{\eta}_i}}{\psi_{ij}\left(\mathbb{F}_{ij}, \mathcal{X}_{ij}(t_s)\right)} \right\rfloor.$$

□

2.5 Simulation Results

In this section, we consider a numerical example and a practical application on building radiant systems to illustrate the effectiveness of the proposed diagnosis scheme.

2.5.1 Numerical Results

Consider a switched system with three linear subsystems. The system matrices are

$$A_1 = \begin{bmatrix}0.5 & 0\\ 0 & -0.4\end{bmatrix},\ A_2 = \begin{bmatrix}0.5 & -0.2\\ 0 & -0.4\end{bmatrix},\ A_3 = \begin{bmatrix}-0.5 & 0\\ 0.1 & -0.4\end{bmatrix},\ B_1 = \begin{bmatrix}0\\ 1\end{bmatrix},$$

$$B_2 = \begin{bmatrix}1\\ 1\end{bmatrix},\ B_3 = \begin{bmatrix}1\\ 0\end{bmatrix},\ E_1 = E_2 = E_3 = \begin{bmatrix}1\\ 1\end{bmatrix},\ W_1 = W_2 = W_3 = 0,$$

$$C_1 = C_3 = \begin{bmatrix}1 & 0\\ 0 & 1\end{bmatrix},\ C_2 = \begin{bmatrix}1 & 0\\ 0 & 0\end{bmatrix},\ \text{and}\ D_1 = D_2 = D_3 = \begin{bmatrix}0.01 & 0\\ 0.01 & -0.01\end{bmatrix}.$$

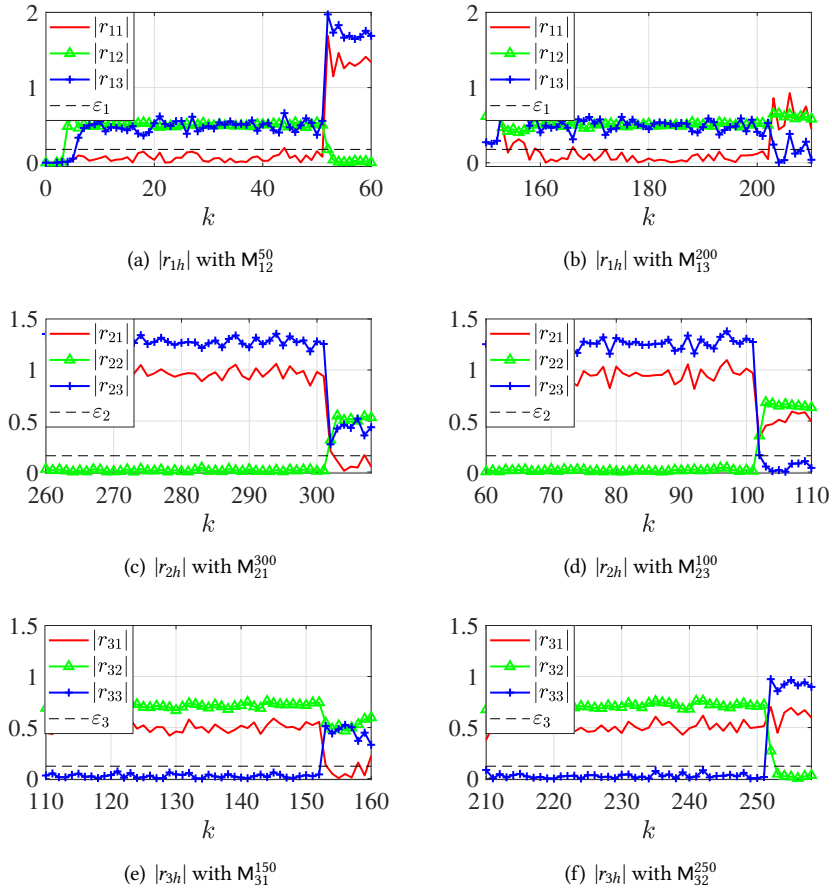

(a) $|r_{1h}|$ with M_{12}^{50} (b) $|r_{1h}|$ with M_{13}^{200}

(c) $|r_{2h}|$ with M_{21}^{300} (d) $|r_{2h}|$ with M_{23}^{100}

(e) $|r_{3h}|$ with M_{31}^{150} (f) $|r_{3h}|$ with M_{32}^{250}

Figure 2.4: Residuals behavior under different scenarios: Let M_{ij}^{k} stand for a system transition from i to j at time k.

The controller gains are

$$K_1 = [-0.0395 \ -0.0741],\ K_2 = [-0.0648\ 0.0510],\ \text{and}\ K_3 = [-0.0420\ 0.0326].$$

We set the degree of the filters $d_N = 1$, the denominator $a(\mathfrak{q}) = (\mathfrak{q}+0.1)(\mathfrak{q}+0.2)$. The reference signal is set as $\bar{d} = 0.5$. The parameter of the iid sub-Gaussian noise is 1. The filters are constructed by using the approach proposed in Theorem 2.3.1 and Proposition 2.3.2. We solve the optimization problems by YALMIP toolbox [126]. The thresholds are computed according to (2.22) where the reliability level $\beta = 0.05$ and $\mu = 0.5$. Thus, the thresholds are $\varepsilon_1 = 0.18$, $\varepsilon_2 = 0.16$, and $\varepsilon_3 = 0.12$. The waiting time τ_i for $i \in \{1,2,3\}$ computed by (2.24) are $\tau_1 = 7, \tau_2 = 6$, and $\tau_3 = 7$. To cover all the scenarios, we set the switching sequence as: $1 \to 2 \to 3 \to 1 \to 3 \to 2 \to 1$.

Figure 2.4 depicts the behavior of residuals under different scenarios. Here, we only analyze r_{1h} for $h \in \{1,2,3\}$ with the transition M_{12}^{50} shown in Figure 2.4(a), because the rest

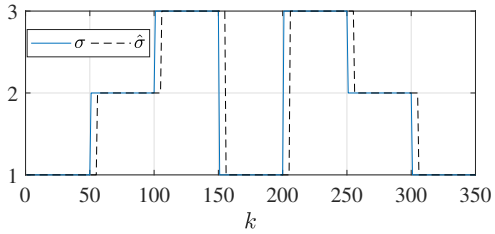

Figure 2.5: Diagnosis result of the whole process.

are similar. Since the initial status of the closed-loop system is S_{11}, the absolute value $|r_{11}(k)|$ remains below ε_1 until transition happens at $k = 50$. The other two residuals r_{12} and r_{13} first reach their corresponding steady values. Then, they oscillate around the steady values because of the noise. The matched residual r_{11} and the unmatched residuals r_{12} and r_{13} are separated. After the transition M_{12}^{50} happens at $k = 50$, $|r_{11}(k)|$ exceeds the threshold ε_1 immediately such that the switching is detected. Then, $|r_{12}(k)|$ reaches ε_1 at about $k = 53$ while the other two residuals are above ε_1. As a result, active mode 2 is determined. Figure 2.5 shows the diagnosis result of the whole process, where the switching signal is correctly estimated.

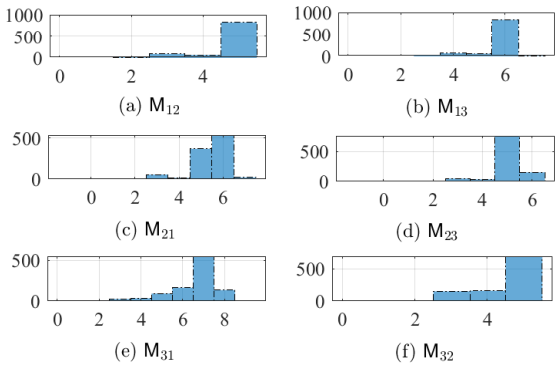

Figure 2.6: Distribution of the diagnosis time for each scenario.

We execute the experiment 1000 times for each switching scenario to obtain the distributions of the diagnosis time and the probability of wrong detection. The results are shown in Figure 2.6. The average diagnosis time (ADT) and the wrong detection probability (WDP) are presented in Table 2.1. We compute the estimated matched time T_{ij} based on (2.23). From Table 2.1, the estimated matched time estimates the average diagnosis time well, and the wrong detection probability is low.

Table 2.1: Average diagnosis time and wrong detection probability when $\mu = 0.5$ and $\beta = 0.05$.

Transition	M_{12}	M_{13}	M_{21}	M_{23}	M_{31}	M_{32}
ADT	5	6	6	6	7	5
T_{ij}	5	7	7	7	7	5
WDP	0	0	0.002	0.003	0	0

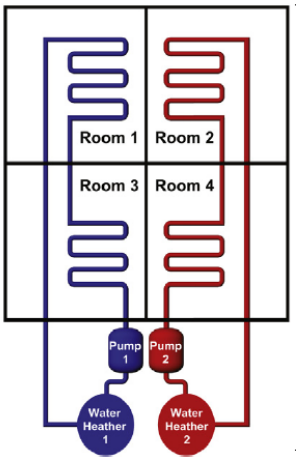

Figure 2.7: Illustration of the building radiant system [116].

2.5.2 Building Radiant Systems

In this section, a building radiant system is considered. We adopt the example from [116], where the building with four rooms of the same size is equipped with a radiant system with two pumps. Moreover, we compare the model invalidation approach proposed in [116] with our approach.

System model description. The radiant system can be modeled by the following equations

$$
\begin{aligned}
C_{c,1}\dot{T}_{c,1} &= K_{c,1}(T_1 - T_{c,1}) + K_{c,3}(T_3 - T_{c,1}) + K_{w,1}(T_{w,1} - T_{c,1}),\\
C_{c,2}\dot{T}_{c,2} &= K_{c,2}(T_2 - T_{c,2}) + K_{c,4}(T_4 - T_{c,2}) + K_{w,2}(T_{w,2} - T_{c,2}),\\
C_1\dot{T}_1 &= K_{c,1}(T_{c,1} - T_1) + K_1(T_a - T_1) + K_{12}(T_2 - T_1) + K_{13}(T_3 - T_1),\\
C_2\dot{T}_2 &= K_{c,2}(T_{c,2} - T_2) + K_2(T_a - T_2) + K_{12}(T_1 - T_2) + K_{24}(T_4 - T_2),\\
C_3\dot{T}_3 &= K_{c,1}(T_{c,1} - T_3) + K_3(T_a - T_3) + K_{13}(T_1 - T_3) + K_{34}(T_4 - T_3),\\
C_2\dot{T}_4 &= K_{c,2}(T_{c,2} - T_4) + K_4(T_a - T_4) + K_{24}(T_2 - T_4) + K_{34}(T_3 - T_4),
\end{aligned}
$$

where the temperatures of two cores in the radiant system are denoted by $T_{c,i}$ for $i \in \{1,2\}$. The temperature of the supply water is denoted by $T_{w,i}$. The ambient air temperature is denoted by T_a. The air temperature of room i for $i \in \{1,2,3,4\}$ is denoted by T_i. The thermal

conductance between T_i and T_a is denoted by K_i. The thermal conductance between $T_{c,i}$ and T_i is denoted by $K_{c,i}$. The thermal conductance between room i and j is denoted by K_{ij}. The piping thermal conductance between $T_{c,i}$ and $T_{w,i}$ is denoted by $K_{w,i}$. The thermal capacitance of room i and core i is denoted by C_i and $C_{c,i}$, resp. Assume that the constant flow of pumps is known. Each pump supplies water to the water pipe and is connected to a valve to adjust the constant flow. The system state consists of the temperatures of the four rooms and the two cores. Suppose both pumps are on. The values of the parameters are the same as that in [116]. The above equations can be written into the state-space form

$$\begin{aligned} \dot{x}_T &= A_{rad,1}x_T + E_{rad,1}T_d, \\ y &= C_{rad,1}x_T + \omega, \end{aligned} \tag{2.38}$$

where $x_T = [T_{c,1}, T_{c,2}, T_1, T_2, T_3, T_4]^\top$, $T_d = [T_{w,1}, T_{w,2}, T_a]^\top$ is the constant input (or reference signal). Matrices $A_{rad,1}$ and $E_{rad,1}$ are obtained from the above equations. The matrix $C_{rad,1} = \mathrm{diag}([0,0,1,1,1,1])$ indicates the measured temperatures. Assume that there is an uncertainty ν in T_a due to small changes (i.e., $T_a = 10 + \nu$ where ν is Gaussian noise with mean 0 and variance 0.1). The measurement noise denoted by ω is Gaussian noise with mean 0 and variance 0.01. The discrete-time model of the radiant system (2.38) is obtained with a sampling time of 5 min. Let $(A^d_{rad,1}, E^d_{rad,1}, C_{rad,1})$ represents the fault-free discrete-time model of the system.

Faulty modes. The normal functions of the valves and temperature measurement sensors are impaired in the faulty modes. Specifically, when there is a fault in the valve, we assume that the valve is stuck in the middle and does not respond to commands. Since the fault cuts the heat transfer in half, the fault is modeled with a change in the heat conductance parameter, i.e., $K_{w,1} \to K_{w,1}/2$ in $A_{rad,1}$ and $E_{rad,1}$. The sensor failures result in inaccurate measurements of the temperature. We change the corresponding entry in $C_{rad,1}$ to model the sensor fault, i.e., $1 \to 0.9$. Here, two faulty modes are considered. The first faulty mode is denoted by $(A^d_{rad,2}, E^d_{rad,2}, C_{rad,2})$, where faults occur in the second pump and the sensor measuring T_1. As a result, $K_{w,2}$ decreases to $K_{w,2}/2$ and $C_{rad,2} = \mathrm{diag}([0,0,0.9,1,1,1])$. The second faulty mode is denoted by $(A^d_{rad,3}, E^d_{rad,3}, C_{rad,3})$, where just one fault occurs in the first pump. Note that the second faulty mode is more incipient than the first one because the outputs do not change dramatically. The matched residual of $(A^d_{rad,i}, E^d_{rad,i}, C_{rad,i})$ is defined as r_i for $i \in \{1,2,3\}$.

Filter design and model invalidation approach. Note that there is no control signal in the radiant system (2.38). Thus, we only need to design three filters corresponding to the three modes. The degree of the filters is set as $d_N = 3$. The filters are then constructed based on Theorem 2.3.1 and Proposition 2.3.2. The idea of the model invalidation approach proposed in [116] is that, given the input and output data, detect the transitions by checking the feasibility of a mixed-integer linear programming problem. Since the example we adopt here has only one healthy mode, the mixed-integer linear programming problem

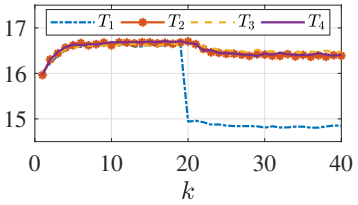

(a) Faulty mode 1: Temperatures

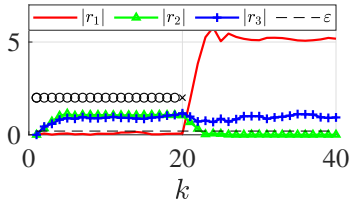

(b) Faulty mode 1: Residuals

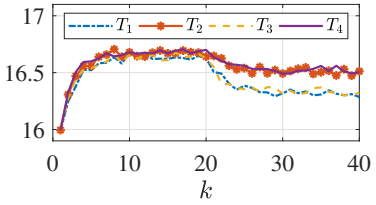

(c) Faulty mode 2: Temperatures

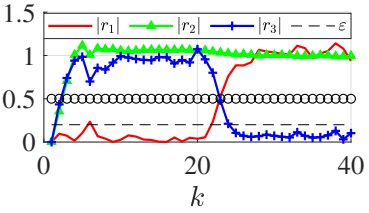

(d) Faulty mode 2: Residuals

Figure 2.8: Simulation results with faulty modes happen at $k = 20$. The symbols ◦ and × indicate the feasible and infeasible status of (2.39).

degenerates into the following linear programming problem.

$$\text{Find } \mathbf{x}(k),\ \boldsymbol{\nu}(k),\ \boldsymbol{\omega}(k),\ \forall k \in \{0,1,\ldots,T-1\}$$
$$\text{s.t.} \begin{cases} \mathbf{x}(k+1) - A_{rad,1}\mathbf{x}(k) - E_{rad,1}(T_d + [0,0,\boldsymbol{\nu}(k)]^\top) = 0, \\ y(k) - C_{rad,1}\mathbf{x}(k) - \boldsymbol{\omega}(k) = 0, \\ X_l \le \mathbf{x}(k) \le X_u,\ V_l \le \boldsymbol{\nu}(k) \le V_u, \\ W_l \le \boldsymbol{\omega}(k) \le W_u, \end{cases} \tag{2.39}$$

where the ranges of $\mathbf{x}(k)$, $\nu(k)$ and $\omega(k)$ are set as $15 \le \|\mathbf{x}\|_\infty \le 19$, $-0.3 \le \|\boldsymbol{\nu}\|_\infty \le 0.3$ and $-0.03 \le \|\boldsymbol{\omega}\|_\infty \le 0.03$, resp. The positive integer T is derived from the definition *T-Detectability* in [116]. It represents the number of steps that a faulty model needs to generate an abnormal trajectory. We refer readers to [116] for more details about the computation method of T.

Results. In the first case, we suppose the first faulty mode occurs at $k = 20$. The diagnosis results are presented in Figure 2.8. Figure 2.8(a) shows the changes in the measured temperatures. The temperature T_1 drops significantly due to sensor failure, and other measured temperatures also change slightly because of the fault in pump 2. Figure 2.8(b) shows the changes in the residuals and the feasibility of the invalidation problem (2.39). One can see that r_1 crosses the threshold at $k = 21$, and thus the fault is detected immediately after the faults happen. At $k = 23$, the matched residual r_2 reaches the threshold. Thus, the faulty mode is determined.

Meanwhile, the problem (2.39) becomes infeasible at $k = 21$, which means the faults are detected by the model invalidation method as well. In the second case, we suppose the second faulty mode happens at $k = 20$. One can see from Figure 2.8(c) that the changes in the measured temperatures are slight. This poses a challenge to the diagnosis task. Figure 2.8(d) shows the changes in the residuals and the feasibility of (2.39). Note that r_1 crosses the threshold at $k = 22$. Hence, the fault is detected. Then, the matched residual r_3 reaches the threshold at $k = 24$ such that the second faulty mode is determined. As a comparison, the invalidation problem is always feasible during the whole process, which means that the invalidation approach fails to detect the fault in the second case.

2.6 Conclusions

In this chapter, we propose a diagnosis scheme to detect the active mode of discrete-time, switched affine systems in the presence of measurement noise and asynchronous switching. Based on an integration of residual generation and $\mathcal{H}_2$ norm approaches, the design of an optimal bank of filters is formulated into a tractable optimization problem in which the noise contribution to the residuals is minimized. With the filters designed by the optimization problem, the diagnosis thresholds are determined which provide probabilistic false-alarm guarantees on the mode detection performance. Simulation results of a numerical example and a building radiant system show the effectiveness of the proposed approach. As future work, the first research direction is to combine the proposed approach with the active fault diagnosis method to deal with the unknown disturbance. One can design certain input sequences such that the unmatched residuals are separated from the matched residual with guaranteed probability. Note that the switching delay between the active mode and its corresponding controller is stochastic because of the stochastic noise. As a result, the second research direction would be focused on the impacts of the stochastic delay on the stability of asynchronously switched systems.

3

Multivariate Fault Detection and Estimation in the Finite Frequency Domain

This chapter is based on *J. Dong, K. Pan, S. Pequito, P. Mohajerin Esfahani. Multivariate fault detection and estimation in the finite frequency domain. [to be submitted to Automatica]*

3.1 Introduction

Fault diagnosis has been the focus of research in the past decades due to its critical importance in ensuring the safety and reliability of various engineering systems, such as power networks, vehicle dynamics, and aircraft systems [2, 11]. Timely and accurate FDE of faults while a system is still operating in a controllable condition, can help prevent further damage and reduce losses. However, fault detection and estimation (FDE) performance is inevitably affected in practice by model uncertainties, unknown inputs, and stochastic noise. These disturbing factors can result in false fault alarms, missing detection, and incorrect fault estimates. Hence, it is essential to consider the disruptive signals when designing FDE methods.

In recent years, there also has been a growing recognition of the need to address faults in the finite frequency domain. This stems from the fact that many practical faults (or cyber-attack signals [119]) are in the finite frequency domain, e.g., incipient faults in a low-frequency range and actuator's stuck faults with zero frequency [127]. Unfortunately, FDE methods developed for the entire frequency domain can cause conservatism when dealing with these faults. Motivated by the above issues, we study the FDE problem in the finite frequency domain, taking into account both unknown inputs and stochastic noise.

Fault detection: A number of model-based fault detection methods have been developed for linear systems with unknown inputs and stochastic noise. The basic idea is to design a residual generator using observer-based or parity-space approaches [1, 2]. The output of the residual generator (called residual) is used to indicate the occurrence of faults. Performance indices, such as $\mathcal{H}_2$ and $\mathcal{H}_\infty$ norms, are often adopted to measure the robustness against disturbances and noise [46]. The residual generator design is usually formulated as a multi-objective optimization problem in the framework of the robust control theory, see [1, Chapter 7] for more details about the residual generator design with $\mathcal{H}_2$ and $\mathcal{H}_\infty$ norms.

We would like to point out that residual generators constructed by using observer-based and parity-space approaches generally have the same order as the system. However, reduced-order residual generators are more desirable for online implementation and large-scale systems. Nyberg [45] proposes a parity-space-like design method in the differential-algebraic equation (DAE) framework, which finds residual generators of the possibly lowest order. Moreover, this method offers more design freedom due to its characterization of all possible residual generators for systems in the form of DAE. Based on the parity-space-like design method, several fault detection methods have been developed in the DAE framework to deal with nonlinear terms[53] and modeling uncertainties [107].

Note that the methods mentioned above are all for the entire frequency domain. In order to characterize the fault sensitivity in the finite frequency domain, Liu [128] introduces the $\mathcal{H}_-$ index, which is the minimum singular value of the transfer function matrix, to represent the worst-case fault sensitivity. The $\mathcal{H}_-$ index can then be augmented in a specific frequency range by incorporating weighting functions. In contrast to the approximation through weighting functions, the generalized Kalman-Yakubovich-Popov (GKYP) lemma proposed by Iwasaki [129] enables the direct design of fault detection observers in the finite frequency domain. They converted transfer function inequalities to matrix inequalities.

Based on the GKYP lemma, most results are focused on mixed indices such as $\mathcal{H}_\infty/\mathcal{H}_-$ or $l_\infty/\mathcal{H}_-$ [127, 130–132], where unknown inputs with deterministic bounds are considered,

and $\mathcal{H}_\infty$ and l_∞ are adopted to characterize the energy and peak value of unknown inputs, respectively. However, the deterministic bounds can be difficult to obtain and may cause conservative diagnosis results [117]. Besides, results that consider the effects of stochastic noise and unknown inputs simultaneously when designing residual generators for fault detection in the finite frequency domain are quite limited. This is more demanding and, therefore, more challenging for the residual generator design.

Fault estimation: Accurate fault estimation that provides the size and shape of faults is a fundamental task in the fault diagnosis area and has been widely studied as well. Many model-based methods based on various observers, such as sliding mode observers [133], adaptive observers [134], and unknown input observers [31], are developed to address this problem. When applying these observer-based fault estimation methods, one requires an assumption on the derivatives of fault signals. To further achieve reliable fault estimation results, optimization methods or high-gain design approaches are usually employed to attenuate the effects of unknown inputs [31, 133, 134].

In contrast to observer-based methods, the use of fault estimation filters, as another widely-used approach, does not require an estimate of system states and the assumption regarding the derivatives of fault signals. A fault estimation filter is driven by system measurements and control inputs, whose output is an estimate of fault signals. There are two main ways to construct a fault estimation filter. The first approach involves utilizing the inverse of the fault subsystem, as described in [1, Theorem 14.2]. The second approach aims to minimize the difference between the transfer function of the fault subsystem and the identity matrix in the $\mathcal{H}_\infty$ optimization framework [135]. Recently, authors in [59, 136] construct system-inversion-based fault estimation filters with Markov parameters identified from the input-output data and obtain the estimated fault signals by solving a least-square problem. However, the existence of a stable system-inversion-based fault estimation filter cannot be ensured when there are unstable zeros in the fault subsystem (i.e., non-minimum-phase system) [137]. This also relates to input observability conditions explored in [138].

Once again, it is worth emphasizing that the aforementioned estimation methods are for the entire frequency domain. The available methods for fault estimation in the finite frequency domain are primarily built on observer-based methods and the GKYP lemma, see for example [139–141]. However, fault estimation filter design in the finite frequency domain received much less attention. Designing a fault estimation filter in the finite frequency domain is advantageous in the sense that: (i) it does not require the assumption about the derivatives of fault signals as observer-based methods; (ii) it provides more accurate estimation results for faults in a specific frequency range; and (iii) it can circumvent unstable zeros by properly choosing the frequency range. To our knowledge, only [1, Theorem 14.6] integrates weighting functions in the $\mathcal{H}_\infty$ optimization framework to design the fault estimation filter in the finite frequency domain, where the selection of weighting functions is critical to the estimation performance. Moreover, the design of a fault estimation filter in the finite frequency domain while considering both stochastic noise and unknown inputs has not been reported in the literature.

Main contributions: In view of the existing methods mentioned above, we consider FDE for linear discrete-time systems in the finite frequency domain, taking into account both the presence of stochastic noise and unknown inputs. The contributions of this

chapter are summarized as follows:

- **Multivariate FDE in the finite frequency domain:** For the first time, we exploit the prior information about the frequency domain of fault signals when designing FDE filters in the DAE framework. The design of FDE filters is formulated into a unified optimization framework that provides design freedom and (possibly) low-order filters with residuals of arbitrary dimension. The derived optimization problems for filter design are non-convex but can be solved effectively through the alternating optimization approach.

  (*i*) *Optimal fault detection filter design*: By utilizing mixed $\mathcal{H}_2/\mathcal{H}_-$ indices, we formulate the optimal design of the fault detection filter in the DAE framework as a finite optimization problem (Theorem 3.3.1) to address unknown inputs, stochastic noise, and improve fault sensitivity in the finite frequency domain.

  (*ii*) *Optimal fault estimation filter design*: By replacing the $\mathcal{H}_-$ index in the fault detection filter design with the finite-frequency $\mathcal{H}_\infty$ norm to characterize fault estimation performance, we formulate the optimal design of the fault estimation filter in the DAE framework as a finite optimization problem (Theorem 3.3.6).

- **Probabilistic guarantee for fault detection:** We propose a method to determine the fault detection threshold that provides probabilistic guarantees on false alarms (Theorem 3.3.5). The bound exhibits a logarithmic dependence on the reliability level, improving the polynomial dependence obtained in [117]. We further obtain fault detection rates with the derived threshold, which is a particularly difficult task when dealing with multivariate fault signals. The result is also an improvement of our previous work [96] which solely focuses on one-dimensional residuals and has no guarantees on fault detection rates.

- **Relaxed design and optimality gap for fault estimation:** To reduce computational complexity, we relax the conditions in the fault estimation filter design and reformulate it as a quadratic programming problem (Theorem 3.3.7), which has an analytical solution (Corollary 3.3.8). Additionally, we obtain an optimality gap (Proposition 3.3.9) for the original fault estimation filter design problem by solving its exact and relaxed reformulations.

The rest of the chapter is organized as follows. The problem formulation is introduced in Section 3.2. In Section 3.3, we present the design methods of the FDE filters with some performance analysis. To improve the flow of the chapter and its accessibility, we relegate some of the technical proofs to Section 3.4. The proposed approaches are applied to a synthetic non-minimum phase system and a multi-area power system in Section 3.5 to provide evidence of their effectiveness. Finally, Section 3.6 concludes the chapter with some remarks and future directions.

3.2 Model Description and Problem Statement

Consider the following linear discrete-time system

$$\begin{cases} x(k+1) = Ax(k) + Bu(k) + B_d d(k) + B_\omega \omega(k) + B_f f_a(k) \\ y(k) = Cx(k) + Du(k) + D_\omega \omega(k) + D_f f_s(k), \end{cases} \tag{3.1}$$

where $x(k) \in \mathbb{R}^{n_x}$, $u(k) \in \mathbb{R}^{n_u}$, $d(k) \in \mathbb{R}^{n_d}$, and $y(k) \in \mathbb{R}^{n_y}$ are the state, the control input, the unknown input, and the measurement output, respectively. The signal $\omega(k) \in \mathbb{R}^{n_\omega}$ denotes the independent and identically distributed (iid) white noise with zero mean and known variance. The signals $f_a(k) \in \mathbb{R}^{n_{fa}}$ and $f_s(k) \in \mathbb{R}^{n_{fs}}$ denote the process and measurement faults, respectively. System matrices in (3.1) are all assumed to be known and with appropriate dimensions. We introduce the following assumption on fault signals.

Assumption 3.2.1 (Fault regularity)**.** *The faults f_a and f_s are deterministic and the frequency θ_f is in the finite frequency domain $\Theta := \{\theta_f : \underline{\theta} \le \theta_f \le \overline{\theta}\}$, with $\underline{\theta}$, $\overline{\theta} \in \{0, \mathbb{R}_+\}$ denote known lower and upper bounds, respectively.*

Note that Assumption 3.2.1 reflects many practical scenarios where faults have finite frequencies, such as incipient faults and stuck faults of actuators [127, 139].

The objective of this work is to design filters that can detect and estimate faults in the finite frequency domain Θ through the control input u and the measurement y. To this end, we consider filters in the DAE framework and introduce the time-shift operator $\mathfrak{q}$, i.e., $x(k+1) = \mathfrak{q}x(k)$. Then, we transform the state-space model (3.1) into the DAE format

$$H(\mathfrak{q}) \begin{bmatrix} x \\ d \end{bmatrix} + L \begin{bmatrix} y \\ u \end{bmatrix} + W[\omega] + G \begin{bmatrix} f_a \\ f_s \end{bmatrix} + \begin{bmatrix} x_0 \\ 0 \end{bmatrix} = 0, \tag{3.2}$$

where $x(0) = x_0$ is the unknown initial condition, the polynomial matrices $H(\mathfrak{q})$, L, W and G are given by

$$H(\mathfrak{q}) = H_1\mathfrak{q} + H_0 = \begin{bmatrix} -\mathfrak{q}I + A & B_d \\ C & 0 \end{bmatrix}, \; H_0 = \begin{bmatrix} A & B_d \\ C & 0 \end{bmatrix}, \; H_1 = \begin{bmatrix} -I & 0 \\ 0 & 0 \end{bmatrix},$$

$$L = \begin{bmatrix} 0 & B \\ -I & D \end{bmatrix}, \; W = \begin{bmatrix} B_\omega \\ D_\omega \end{bmatrix}, \text{ and } G = \begin{bmatrix} B_f & 0 \\ 0 & D_f \end{bmatrix}.$$

To design the filters, we further introduce a transfer function

$$\mathbb{F}(\mathfrak{q}) = \frac{\mathcal{N}(\mathfrak{q})}{a(\mathfrak{q})}, \tag{3.3}$$

where the polynomial matrix $\mathcal{N}(\mathfrak{q}) = \sum_{i=0}^{d_N} N_i \mathfrak{q}^i$, $N_i \in \mathbb{R}^{n_r \times (n_x + n_y)}$, and d_N denotes the degree of $\mathcal{N}(\mathfrak{q})$. The denominator $a(\mathfrak{q}) = \sum_{i=0}^{d_a} a_i \mathfrak{q}^i + \mathfrak{q}^{d_a+1}$, $a_i \in \mathbb{R}$, and $d_a + 1$ is the degree of $a(\mathfrak{q})$. For simplicity, we set $d_a \ge d_N$ to ensure that $\mathbb{F}(\mathfrak{q})$ is strictly proper.

By multiplying the left-hand side of (3.2) by $\mathbb{F}(\mathfrak{q})$, we can re-arrange the terms to obtain the residual $r \in \mathbb{R}^{n_r}$ as follows

$$r = \mathbb{F}(\mathfrak{q})L\begin{bmatrix} y \\ u \end{bmatrix} = -\mathbb{F}(\mathfrak{q})H(\mathfrak{q})[X] - \mathbb{F}(\mathfrak{q})W[\omega] - \mathbb{F}(\mathfrak{q})G[f] - \mathbb{F}(\mathfrak{q})\begin{bmatrix} x_0 \\ 0 \end{bmatrix}, \tag{3.4}$$

where $X = [x^\top \ d^\top]^\top$, $f = [f_a^\top \ f_s^\top]^\top$ with dimension $n_f = n_{f_a} + n_{f_s}$. Note that $\mathbb{F}(q)L$ is called the implementation form of the filter because all the entities are known to us. The right-hand side of (3.4) indicates the input-output relations from X, ω, and f to r, based on which we can design $\mathbb{F}(\mathfrak{q})$ such that desired mapping relations are satisfied for different diagnosis purposes. Subsequently, we denote the mapping relations from X to r, from ω to r, and from f to r by

$$\mathbb{T}_{Xr}(\mathfrak{q}) = -\mathbb{F}(\mathfrak{q})H(\mathfrak{q}),\ \mathbb{T}_{\omega r}(\mathfrak{q}) = -\mathbb{F}(\mathfrak{q})W, \text{ and } \mathbb{T}_{fr}(\mathfrak{q}) = -\mathbb{F}(\mathfrak{q})G. \tag{3.5}$$

Assumption 3.2.2 (Initial condition dependency)**.** *The contribution of the initial condition, i.e., the last term in* (3.4)*, vanishes exponentially fast under appropriate stability conditions.*

Assumption 3.2.2 is commonly adopted in fault detection literature to simplify the analysis [59, 142].

Next, we present the formulation of the two problems studied in this work: (i) fault detection (Section 3.2.1), and (ii) fault estimation (Section 3.2.2).

3.2.1 Problem 1: Fault Detection

In order to formally introduce the fault detection problem statement, we start by introducing the $\mathcal{H}_2$ norm and $\mathcal{H}_-$ index of a transfer function, e.g., $y = \mathbb{T}(\mathfrak{q})[u]$, $\mathbb{T}(\mathfrak{q}) = C(\mathfrak{q}I - \mathcal{A})^{-1}\mathcal{B}$.

Definition 3.2.3 ($\mathcal{H}_2$ norm [46])**.** *Assume $\mathcal{A}$ is stable. The $\mathcal{H}_2$ norm of $\mathbb{T}(\mathfrak{q})$ is defined as*

$$\|\mathbb{T}(\mathfrak{q})\|_{\mathcal{H}_2} = \left(\frac{1}{2\pi}\int_{-\pi}^{\pi} \text{Trace}\left(\mathbb{T}^*(e^{j\theta})\mathbb{T}(e^{j\theta})\right) \mathrm{d}\theta\right)^{1/2},$$

and corresponds to the asymptotic variance of the output when the system is driven by the white noise with zero mean, i.e., $\lim_{T\to\infty} \frac{1}{T}\sum_{k=0}^{T} \mathbf{E}\left[y(k)^\top y(k)\right]$.

Definition 3.2.4 ($\mathcal{H}_-$ index [128])**.** *The $\mathcal{H}_-$ index of $\mathbb{T}(\mathfrak{q})$ in a frequency domain Θ is defined as*

$$\|\mathbb{T}(\mathfrak{q})\|_{\mathcal{H}_-(\Theta)} = \inf_{\theta\in\Theta, u\neq 0} \frac{\left\|\mathbb{T}(e^{j\theta})u\right\|_{\mathcal{L}_2}}{\|u\|_{\mathcal{L}_2}}.$$

The definition can also be rewritten as $\|\mathbb{T}(\mathfrak{q})\|_{\mathcal{H}_-(\Theta)} = \inf_{\theta\in\Theta} \underline{\sigma}\left(\mathbb{T}(e^{j\theta})\right)$, where $\underline{\sigma}(\cdot)$ denotes the minimum singular value.

Let us look into the right-hand side of (3.4). We expect the residual r to be insensitive to d, robust to ω, and sensitive to f in Θ. First, to decouple d from r, we need to guarantee that

$$\mathbb{T}_{Xr}(\mathfrak{q}) = -\mathbb{F}(\mathfrak{q})H(\mathfrak{q}) = 0. \tag{3.6a}$$

Second, we set an upper bound $\eta_1 \in \mathbb{R}_+$ on the $\mathcal{H}_2$ norm of $\mathbb{T}_{\omega r}(\mathfrak{q})$, to suppress the contribution of ω to r, as

$$\|\mathbb{T}_{\omega r}(\mathfrak{q})\|_{\mathcal{H}_2}^2 = \|-\mathbb{F}(\mathfrak{q})W\|_{\mathcal{H}_2}^2 \leq \eta_1. \tag{3.6b}$$

Finally, we let the $\mathcal{H}_-$ index of $\mathbb{T}_{fr}(\mathfrak{q})$ in Θ be larger than some positive value $\eta_2 \in \mathbb{R}_+$ to guarantee the worst-case fault sensitivity, which is

$$\|\mathbb{T}_{fr}(\mathfrak{q})\|_{\mathcal{H}_-(\Theta)}^2 = \|-\mathbb{F}(\mathfrak{q})G\|_{\mathcal{H}_-(\Theta)}^2 \geq \eta_2. \tag{3.6c}$$

In view of the desired mapping conditions (3.6), the design of the fault detection filter is formulated as the following optimization problem.

Problem 1a. (Fault detection filter design) *Consider the system* (3.1)*, the structure of* $\mathbb{F}(\mathfrak{q})$ *in* (3.3)*, and the residual* (3.4)*. Given a scalar* $\alpha \in [0,1]$*, find* $\mathbb{F}(\mathfrak{q})$ *via the minimization program:*

$$\min_{\eta_1,\eta_2\in\mathbb{R}_+,\ \mathbb{F}(\mathfrak{q})} \quad \{\alpha\eta_1 - (1-\alpha)\eta_2 \ :\ \text{(3.6a), (3.6b), (3.6c)}\}. \tag{3.7}$$

We emphasize that the following assumption is required for the feasibility of Problem 1a.

Assumption 3.2.5 (Feasibility condition)**.** *The pair* (A,C) *is observable. For* $\mathfrak{q} = \varphi e^{j\theta}$ *with* $|\varphi| > 1$ *and* $\theta \in \Theta$*, the following rank condition holds*

$$n_x + n_y \geq \operatorname{Rank}\left(\begin{bmatrix} -\mathfrak{q}I + A & B_d & B_f & 0 \\ C & 0 & 0 & D_f \end{bmatrix}\right) = n_x + \operatorname{Rank}\left(\begin{bmatrix} B_d \\ 0 \end{bmatrix}\right) + n_f.$$

Denote the transfer functions from d and f_a to y by $\mathbb{T}_{dy}(\mathfrak{q}) = C(\mathfrak{q}I - A)^{-1}B_d$ and $\mathbb{T}_{f_a y}(\mathfrak{q}) = C(\mathfrak{q}I - A)^{-1}B_f$, respectively. We can show that

$$n_y \geq \operatorname{Rank}[\mathbb{T}_{dy}(\mathfrak{q}) \quad [\mathbb{T}_{f_a y}(\mathfrak{q})\ D_f]] = \operatorname{Rank}\left(\begin{bmatrix} B_d \\ 0 \end{bmatrix}\right) + n_f,$$

if Assumption 3.2.5 holds [1, Theorem 6.2]. Therefore, Assumption 3.2.5 ensures simultaneously the following: (i) the unknown input d can be decoupled, and (ii) the faults f satisfy input observability condition in the frequency domain Θ, which also indicates that there are no unstable invariant zeros in Θ. The second term is necessary for a nonzero $\mathcal{H}_-$ index [128, Lemma 5]. Moreover, we incorporate the frequency domain into the analysis, which is different from the classical result on the input observability condition in [138, Theorem 3] and [1, Corollary 14.1].

Additionally, notice that a solution to Problem 1a ensures that the residual r can be written as

$$r = \mathbb{T}_{\omega r}(\mathfrak{q})[\omega] + \mathbb{T}_{fr}(\mathfrak{q})[f],$$

where no dependency on X is present, i.e., it is decoupled. In practice, the residual r will oscillate around zero as a response to the noise ω in the absence of f. In contrast, the

residual will ideally be away from zero when a fault happens. Subsequently, let us take the average 2-norm of r over a time interval $\mathcal{T} \in \mathbb{N}$ as the evaluation function, i.e.,

$$J(r) = \frac{1}{\mathcal{T}} \sum_{k=k_1}^{k_1+\mathcal{T}} \|r(k)\|_2,\ k_1 \in \mathbb{N}. \tag{3.8}$$

Given a threshold $J_{th} \in \mathbb{R}_+$, we can consider the following fault detection logic:

$$\begin{cases} J(r) \le J_{th} & \Rightarrow \quad \text{no fault alarm,} \\ J(r) > J_{th} & \Rightarrow \quad \text{fault alarm.} \end{cases}$$

Note that false alarms and missing detection of faults are inevitable due to the random nature of noise ω. In order to mitigate these issues, we consider determining a threshold J_{th} that can provide guarantees on the false alarm rate (FAR) and fault detection rate (FDR) in the following problem.

Problem 1b. (Threshold setting with probabilistic guarantees) *Given* $\mathbb{F}(\mathfrak{q})$ *constructed from Problem 1a, an acceptable false alarm rate* $\varepsilon_1 \in (0, 1]$*, and a set of fault signals of interest* $\Omega_f := \{f : \|f(k)\|_2 \ge \underline{f},\ \underline{f} \in \mathbb{R}_+,\ \theta_f \in \Theta\}$*, determine the threshold* J_{th} *such that:*

$$\text{FAR: } \mathbf{Pr}\left\{ J(r) > J_{th} \middle| f = 0 \right\} \le \varepsilon_1, \tag{3.9a}$$

$$\text{FDR: } \mathbf{Pr}\left\{ J(r) > J_{th} \middle| f \in \Omega_f \right\} \ge \varepsilon_2, \tag{3.9b}$$

where ε_2 *is the lower bound on FDR to be computed.*

3.2.2 Problem 2: Fault Estimation

In some cases, we need not only to detect the occurrence of faults but also to estimate them accurately. For instance, incorporating fault estimates into fault-tolerant controllers is a common practice to counteract the effects of faults [43]. To quantify the estimation performance, we introduce the finite-frequency $\mathcal{H}_\infty$ norm.

Definition 3.2.6 (Finite-frequency $\mathcal{H}_\infty$ norm [143])**.** *The finite-frequency* $\mathcal{H}_\infty$ *norm of* $\mathbb{T}(\mathfrak{q})$ *over some frequency range* Θ *is defined as*

$$\|\mathbb{T}(\mathfrak{q})\|_{\mathcal{H}_\infty(\Theta)} = \sup_{\theta\in\Theta, u\neq 0} \frac{\left\|\mathbb{T}(e^{j\theta})u\right\|_{\mathcal{L}_2}}{\|u\|_{\mathcal{L}_2}}.$$

The definition can also be rewritten as $\|\mathbb{T}(\mathfrak{q})\|_{\mathcal{H}_\infty(\Theta)} = \sup_{\theta\in\Theta} \overline{\sigma}\left(\mathbb{T}(e^{j\theta})\right)$*, where* $\overline{\sigma}(\cdot)$ *denotes the maximum singular value.*

Recall the design form in (3.4). To estimate the faults, a possible solution consists in finding a stable transfer function $\mathbb{F}(\mathfrak{q})$ such that $\mathbb{T}_{fr}(e^{j\theta}) = -\mathbb{F}(e^{j\theta})G \equiv I$ in Θ. However, this condition is too demanding and generally impossible to achieve because it contains an infinite number of equality constraints, especially in the presence of unknown inputs

and noise. Therefore, we opt to let $\mathbb{T}_{fr}(\mathfrak{q})$ approximate the identity matrix I over Θ by setting $n_r = n_f$ and, instead of considering (3.6c), we consider the following condition

$$\left\|\mathbb{T}_{fr}(\mathfrak{q}) - I\right\|^2_{\mathcal{H}_\infty(\Theta)} \leq \eta_2. \tag{3.6c'}$$

Hence, the generated residual r can be viewed as an estimate of f if $\mathbb{T}_{fr}(\mathfrak{q})$ is sufficiently close to I over Θ. We maintain conditions (3.6a) and (3.6b) to suppress the influence of d and ω on the residual r. As a result, our second problem is to design the fault estimation filter through the following optimization problem.

Problem 2. (Fault estimation filter design) *Consider the system* (3.1)*, the structure of* $\mathbb{F}(\mathfrak{q})$ *in* (3.3)*, and the residual* (3.4)*. Given a scalar* $\beta \in [0,1]$*, find* $\mathbb{F}(\mathfrak{q})$ *via the minimization program*

$$\min_{\eta_1,\eta_2\in\mathbb{R}_+,\ \mathbb{F}(\mathfrak{q})} \quad \{\beta\eta_1 + (1-\beta)\eta_2 \ :\ \text{(3.6a), (3.6b), (3.6c')}\}. \tag{3.10}$$

Remark 3.2.7 (Difference between Problem 1a and 2)**.** *The condition* (3.6c') *for fault estimation is more stringent compared to the condition* (3.6c) *used for fault detection. In particular, it suffices to have the minimum singular value of* $\mathbb{T}_{fr}(\mathfrak{q})$ *be positive for fault detection, whereas* $\mathbb{T}_{fr}(\mathfrak{q})$ *needs to be as close to* I *as possible to obtain a decent estimation performance. Additionally, filters that satisfy condition* (3.6c') *with a sufficiently small finite-frequency* $\mathcal{H}_\infty$ *norm can provide a positive* $\mathcal{H}_-$ *index over* Θ*, but the opposite is not true.*

3.3 Main Results

In this section, we first present the design method of the fault detection filter (Theorem 3.3.1) and the computation of thresholds that provide probabilistic guarantees on the FAR and FDR (Theorem 3.3.5). We then proceed to show the design method of the fault estimation filter, both under exact estimation conditions (Theorem 3.3.6) and under relaxed conditions (Theorem 3.3.7). To improve the clarity of the presentation, some proofs are relegated to Section 3.4.

3.3.1 Fault Detection Filter Design

Let us start by considering the transfer function $\mathbb{F}(\mathfrak{q})$ in (3.3). First, notice that the degrees d_N, d_a, the residual dimension n_r, and coefficients of $\mathcal{N}(\mathfrak{q})$ and $a(\mathfrak{q})$ are all design parameters. For simplicity, we fix n_r, d_N, and set $d_N = d_a$ in what follows. To compute the $\mathcal{H}_2$ norm and $\mathcal{H}_-$ index, we convert $\mathbb{T}_{\omega r}(\mathfrak{q}) = -\mathbb{F}(\mathfrak{q})W$ and $\mathbb{T}_{fr}(\mathfrak{q}) = -\mathbb{F}(\mathfrak{q})G$ into the observable canonical forms denoted by $(\mathcal{A}_r, \mathcal{B}_{\omega r}, \mathcal{C}_r)$ and $(\mathcal{A}_r, \mathcal{B}_{fr}, \mathcal{C}_r)$, respectively. Let $N_{i,j}$ denote the j-th row of N_i for $i \in \{0,1,\dots,d_N\}$ and $j \in \{1,\dots,n_r\}$. Then, the matrices $\mathcal{A}_r$, $\mathcal{B}_{\omega r}$, $\mathcal{B}_{fr}$, and $\mathcal{C}_r$ are given by

$$\mathcal{A}_r = \operatorname{diag}(\underbrace{A_r,\dots,A_r}_{n_r}),\ \mathcal{B}_{\omega r} = [B_{\omega r,1}^\top,\dots,B_{\omega r,n_r}^\top]^\top,\ \mathcal{B}_{fr} = [B_{fr,1}^\top,\dots,B_{fr,n_r}^\top]^\top, \text{ and}$$

$$\mathcal{C}_r = \operatorname{diag}(\underbrace{C_r,\dots,C_r}_{n_r}),$$

where

$$A_r = \begin{bmatrix} 0 & \dots & 0 & -a_0 \\ 1 & \dots & 0 & -a_1 \\ \vdots & \ddots & \vdots & \vdots \\ 0 & \dots & 1 & -a_{d_N} \end{bmatrix},\ B_{\omega r,j} = \begin{bmatrix} N_{0,j} \\ N_{1,j} \\ \vdots \\ N_{d_N,j} \end{bmatrix} W,\ B_{fr,j} = \begin{bmatrix} N_{0,j} \\ N_{1,j} \\ \vdots \\ N_{d_N,j} \end{bmatrix} G,\ C_r = \begin{bmatrix} 0 \dots 0 & 1 \end{bmatrix}.$$

The dimension of the filter states is $n_{x_r} = n_r(d_N+1)$. Note that the parameters a_i and $N_{i,j}$ to be determined are reformulated into $\mathcal{A}_r$, $\mathcal{B}_{\omega r}$, and $\mathcal{B}_{fr}$. An advantage of such a transformation is that all the design parameters are decoupled from each other. This allows us to exactly formulate the design of the fault detection filter into a bilinear optimization problem as stated in the following theorem.

Theorem 3.3.1 (Optimal fault detection filter design: exact finite reformulation)**.** *Consider the system* (3.1)*, the structure of* $\mathbb{F}(\mathfrak{q})$ *in* (3.3)*, and the state-space realizations* $(\mathcal{A}_r, \mathcal{B}_{\omega r}, C_r)$ *and* $(\mathcal{A}_r, \mathcal{B}_{fr}, C_r)$*. Given the degree* d_N*,* $d_a = d_N$*, the dimension of the residual* n_r*, a scalar* $\alpha \in [0,1]$*, a sufficiently small* $\vartheta \in \mathbb{R}_+$*, and the frequency domain* Θ*, the minimization program in Problem 1a can be equivalently stated as follows*

$$\begin{aligned} &\min\ \alpha\eta_1 - (1-\alpha)\eta_2 \\ &\text{s.t. } \eta_1,\ \eta_2 \in \mathbb{R}_+,\ a_i \in \mathbb{R},\ N_i \in \mathbb{R}^{n_r \times (n_x+n_y)},\ i \in \{0,1,\dots,d_N\}, \\ &\quad P_1 \in \mathcal{S}^{n_{x_r}},\ Q_1 \in \mathcal{S}^{n_r},\ P_2 \in \mathbb{H}^{n_{x_r}},\ Q_2 \in \mathbb{H}^{n_{x_r}},\ V \in \mathbb{R}^{n_{x_r} \times (2n_{x_r}+n_f)}, \\ &\quad \bar{\mathcal{N}}\bar{H} = 0, \end{aligned} \tag{3.11a}$$

$$\begin{bmatrix} P_1 & \mathcal{A}_r P_1 & \mathcal{B}_{\omega r} \\ * & P_1 & 0 \\ * & * & I \end{bmatrix} \succeq \vartheta I,\ \begin{bmatrix} Q_1 & C_r P_1 \\ * & P_1 \end{bmatrix} \succeq \vartheta I,\ \mathrm{Trace}(Q_1) \le \eta_1 - \vartheta, \tag{3.11b}$$

$$\begin{bmatrix} -P_2 & \delta Q_2 & 0 \\ * & \Xi & 0 \\ * & * & \eta_2 I \end{bmatrix} + \begin{bmatrix} -I \\ \mathcal{A}_r^\top \\ \mathcal{B}_{fr}^\top \end{bmatrix} V + V^\top \begin{bmatrix} -I & \mathcal{A}_r & \mathcal{B}_{fr} \end{bmatrix} \preceq -\vartheta I,\ Q_2 \succeq \vartheta I, \tag{3.11c}$$

where the following conditions hold for different frequency ranges:

(i) $\delta = 1$, $\Xi = P_2 - 2\cos(\theta_l)Q_2 - C_r^\top C_r$*, for the low frequency range* $\Theta = \{\theta_f : 0 \le \theta_f \le \theta_l\}$*;*

(ii) $\delta = \mathrm{e}^{j\theta_c}$, $\Xi = P_2 - 2\cos(\theta_d)Q_2 - C_r^\top C_r$*, for the middle frequency range* $\Theta = \{\theta_f : \theta_1 \le \theta_f \le \theta_2\}$ *with* $\theta_c = (\theta_1+\theta_2)/2$, $\theta_d = (\theta_2-\theta_1)/2$*;*

(iii) $\delta = -1$, $\Xi = P_2 + 2\cos(\theta_h)Q_2 - C_r^\top C_r$*, for the high frequency range* $\Theta = \{\theta_f : \theta_f \ge \theta_h\}$*.*

Additionally, the matrices $\bar{\mathcal{N}}$ *and* $\bar{H}$ *are given by*

$$\bar{\mathcal{N}} = [N_0\ N_1\ \dots\ N_{d_N}] \text{ and } \bar{H} = \begin{bmatrix} H_0 & H_1 & \dots & 0 \\ \vdots & \ddots & \ddots & \vdots \\ 0 & \dots & H_0 & H_1 \end{bmatrix}.$$

Proof. The proof is relegated to Section 3.4.1. □

Note that the optimization problem (3.11) is nonlinear because of the bilinear terms $\mathcal{A}_r P_1$ in (3.11b), and $\mathcal{A}_r^\top V$ and $\mathcal{B}_{fr}^\top V$ in (3.11c). To tackle the optimization problem (3.11), we employ the alternating optimization (AO) method, which divides the decision variables into two sets and optimizes over the two sets of variables alternatively. One way of division is

$$\mathcal{G}_1^k := \{\eta_1^k, \eta_2^k, \bar{\mathcal{N}}^k, a_0^k, \dots, a_{d_N}^k\} \text{ and } \mathcal{G}_2^k := \{P_1^k, P_2^k, Q_1^k, Q_2^k, \eta_1^k, \eta_2^k, V^k\}, \tag{3.12}$$

where $k \in N$ serves as the iteration indicator.

The initial values for the optimization process are obtained as follows. First, we select a stable denominator, denoted by $a^0(\mathfrak{q})$ with coefficients a_i^0. The coefficients of $\mathcal{N}^0(\mathfrak{q})$, i.e., $\bar{\mathcal{N}}^0$, are then determined by solving equation (3.11a) subject to the constraint $\|\bar{\mathcal{N}}^0\|_\infty \geq 1$ to avoid the trivial solution $\bar{\mathcal{N}}^0 = 0$. The initial values of η_1^0 and η_2^0 are found via equations (3.11b) and (3.11c), respectively. The AO process can then be initiated. The procedure is summarized in Algorithm 1. Additionally, we highlight that the stability of the filter is guaranteed as (3.11b) is satisfied [123, Lemma 1].

The proposed approach in (3.11) introduces an auxiliary matrix V in (3.11c) when dealing with the $\mathcal{H}_-$ index of $\mathbb{T}_{fr}(\mathfrak{q})$. Different from the existing results [127, 131, 132], where V is given, we treat V as a decision variable. The reason is that the number of parameters to be determined in V will be large for large-scale or high-dimensional systems. If the parameters are not chosen properly, it can lead to a poor $\mathcal{H}_-$ index or even an infeasible constraint. By optimizing over V, with the AO method, we can obtain better fault sensitivity. Moreover, we find that using relaxation techniques, e.g., [118, Lemma 1], to transform (3.11c) into linear matrix inequality easily makes the problem infeasible. This is because other constraints restrict the set of feasible solutions.

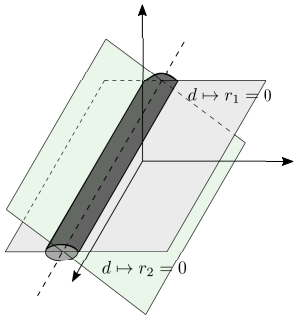

Figure 3.1: Geometric illustration of the multi-dimensional residual.

Remark 3.3.2 (Residuals with arbitrary dimensions)**.** *The proposed design approach enables the fault detection filter to have residuals of arbitrary dimension n_r. Compared to the results in [53, 107, 119], where only one-dimensional residuals are generated, our approach improves two deficiencies:*

(i) Consider a two-dimensional residual depicted in Figure 3.1 as an example. The filters in [53, 107, 119] cannot detect the faults that lie on the same hyperplane as the unknown

input d, i.e., $d \mapsto r = 0$. By considering the two-dimensional residual, faults that can bypass detection exists at the intersection of two hyperplanes. This means that our approach greatly reduces the size of the set containing undetectable faults.

(ii) As indicated in [119], different elements of the fault signals may cancel out each other's contributions to the one-dimensional residual. In our method, we guarantee the fault sensitivity by letting the $\mathcal{H}_-$ index be positive in Θ.

Algorithm 1 Solution to optimization problem stated in (3.11)

Step 1. **Initialization of Filter Parameters**

(a) Set d_N, n_r, the frequency domain Θ, the iteration indicator $k = 0$, and select a stable denominator $a^0(\mathfrak{q})$

(b) Compute the numerator $\mathcal{N}^0(\mathfrak{q})$ via (3.11a) with $\|\bar{\mathcal{N}}^0\|_\infty \geq 1$

(c) Compute η_1^0 and η_2^0 via (3.11b) and (3.11c), respectively

Step 2. **Optimization of Filter Parameters**

(a) Select $\alpha \in [0, 1]$, a sufficiently small $\vartheta > 0$

(b) While $|(\alpha\eta_1^{k+1} - (1-\alpha)\eta_2^{k+1}) - (\alpha\eta_1^k - (1-\alpha)\eta_2^k)| > \vartheta$, do

With $a^k(\mathfrak{q})$ and $\mathcal{N}^k(\mathfrak{q})$, compute P_1^k, and V^k by solving (3.11) over $\mathcal{G}_1^k$

With P_1^k and V^k, compute $a^{k+1}(\mathfrak{q})$, and $\mathcal{N}^{k+1}(\mathfrak{q})$ by solving (3.11) over $\mathcal{G}_2^k$

Set $k = k + 1$

(c) Return $a^\star(\mathfrak{q})$ and $\mathcal{N}^\star(\mathfrak{q})$

3.3.2 Fault Detection Performance Certificates

With the transfer function $\mathbb{F}(\mathfrak{q})$ constructed by solving the optimization problem (3.11) and the residual evaluation function $J(r) = \frac{1}{\mathcal{T}} \sum_{k=k_1}^{k_1+\mathcal{T}} \|r(k)\|_2$, $k_1 \in \mathbb{N}$, we can determine the threshold J_{th} which provides probabilistic guarantees on FAR and FDR as outlined in Problem 1b. To proceed with this, let us first introduce the following lemma and assumption to be used hereafter.

Lemma 3.3.3 (Sub-Gaussian concentration [120, Proposition 2.5.2])**.** *Let a random vector $\omega \in \mathbb{R}^{n_\omega}$ be subject to a sub-Gaussian distribution with mean $\mathbf{E}[\omega]$ and parameter $\lambda_\omega \in \mathbb{R}_+$, i.e., $\mathbf{E}\left[e^{\phi v^\top(\omega - \mathbf{E}[\omega])}\right] \leq e^{\lambda_\omega^2 \phi^2/2}$, $\forall \phi \in \mathbb{R}$ and $v \in \mathbb{R}^{n_\omega}$ with $\|v\|_2 = 1$. Then, the following inequality holds*

$$\mathbf{Pr}[\|\omega - \mathbf{E}[\omega]\|_\infty \leq \epsilon] \geq 1 - 2n_\omega e^{-\frac{\epsilon^2}{2\lambda_\omega^2}}, \quad \forall \epsilon \in \mathbb{R}_+. \tag{3.13}$$

Assumption 3.3.4 (Sub-Gaussian noise)**.** *The measurement noise ω follows an iid sub-Gaussian distribution with zero mean and a time-invariant parameter $\lambda_\omega \in \mathbb{R}_+$.*

The class of sub-Gaussian distributions is board, containing Gaussian, Bernoulli, and all bounded distributions. Also, the tails of sub-Gaussian distributions decrease exponentially

fast from (3.13), which is expected in many applications. Given an acceptable FAR, the following theorem provides the determination method of the threshold J_{th} and a lower bound on FDR.

Theorem 3.3.5 (Probabilistic performance certificates)**.** *Suppose Assumption 3.3.4 holds. Consider the system* (3.1)*, the evaluation function* (3.8)*, the filter* $\mathbb{F}(\mathfrak{q})$ *obtained by solving* (3.11) *with the corresponding optimal values* $\eta_1^\star$ *and* $\eta_2^\star$*, and faults of interest* $f \in \Omega_f$*. Given an acceptable FAR* $\varepsilon_1 \in (0,1]$*, the probabilistic performance* (3.9a) *in Problem 1b is achieved if the threshold* J_{th} *is set as*

$$J_{th} = \lambda_\omega \sqrt{2 n_r \eta_1^\star \ln(2\mathcal{T} n_r/\varepsilon_1)}, \tag{3.14}$$

and the FDR in (3.9b) *satisfies*

$$\mathbf{Pr}\left\{J(r) > J_{th} | f \in \Omega_f\right\} > \max\left\{0, 1 - 2\mathcal{T} n_r \mathrm{e}^{-\frac{\left(\underline{f}\sqrt{\eta_2^*/n_r} - J_{th}\right)^2}{2\eta_1^* \lambda_\omega^2}}\right\}, \quad \text{when } \underline{f} > J_{th}\sqrt{n_r/\eta_2^\star}. \tag{3.15}$$

Proof. The proof is relegated to Section 3.4.1. □

From the concentration property of sub-Gaussian distributions, the derived threshold J_{th} in (3.14) depends logarithmically on FAR, i.e., $\sqrt{\ln(1/\varepsilon_1)}$. This improves the state-of-the-art results (e.g., [117] and [1, Section 10.2.1]), which rely on Chebyshev's inequality and result in thresholds that scale polynomially with $\sqrt{1/\varepsilon_1}$. Moreover, the threshold (3.14) extends our previous work [96, Theorem 3.8] where the one-dimensional residual is considered. In addition, a lower bound for $\underline{f}$ is derived in (3.15) to ensure that FDR can be achieved.

3.3.3 Fault Estimation Filter Design

When designing the fault estimation filter, we choose $\mathbb{F}(\mathfrak{q})$ of the same form as (3.3). Then, considering the desired mapping relations presented in Problem 2, we formulate the design of the fault estimation filter into a bilinear optimization problem in the following theorem.

Theorem 3.3.6 (Optimal fault estimation filter design: exact finite reformulation)**.** *Consider the system* (3.1)*, the structure of* $\mathbb{F}(\mathfrak{q})$ *in* (3.3)*, and the state-space realizations* $(\mathcal{A}_r, \mathcal{B}_{\omega r}, \mathcal{C}_r)$ *and* $(\mathcal{A}_r, \mathcal{B}_{fr}, \mathcal{C}_r)$*. Given the filter order* d_N*,* $d_a = d_N$*, the dimension of residual* $n_r = n_f$*, a scalar* $\beta \in [0,1]$*, a sufficiently small* $\vartheta \in \mathbb{R}_+$*, and the frequency domain* Θ*, the minimization program in Problem 2 can be equivalently stated as follows*

$$\begin{aligned}
&\min\ \beta\eta_1 + (1-\beta)\eta_2 \\
&\text{s.t. } \eta_1,\ \eta_2 \in \mathbb{R}_+,\ a_i \in \mathbb{R},\ N_i \in \mathbb{R}^{n_r \times (n_x + n_y)},\ i \in \{0,1,\ldots,d_N\}, \\
&\quad P_1 \in \mathcal{S}^{n_{x_r}},\ Q_1 \in \mathcal{S}^{n_r},\ P_2 \in \mathbb{H}^{n_{x_r}},\ Q_2 \in \mathbb{H}^{n_{x_r}},\ V \in \mathbb{R}^{n_{x_r} \times (2n_{x_r} + n_f)}, \\
&\quad \text{(3.11a), (3.11b)}, \\
&\quad \begin{bmatrix} -P_2 & \delta Q_2 & 0 \\ * & \Xi & -\mathcal{C}_r^\top \\ * & * & I - \eta_2 I \end{bmatrix} + \begin{bmatrix} -I \\ \mathcal{A}_r^\top \\ \mathcal{B}_{fr}^\top \end{bmatrix} V + V^\top \begin{bmatrix} -I & \mathcal{A}_r & \mathcal{B}_{fr} \end{bmatrix} \preceq -\vartheta I,\ Q_2 \succeq \vartheta I,
\end{aligned} \tag{3.16}$$

where the following conditions hold for different frequency ranges:

(i) $\delta = 1$, $\Xi = P_2 - 2\cos(\theta_l)Q_2 + C_r^\top C_r$, *for the low frequency range* $\Theta = \{\theta_f : \theta_f \le \theta_l\}$;

(ii) $\delta = \mathrm{e}^{j\theta_c}$, $\Xi = P_2 - 2\cos(\theta_d)Q_2 + C_r^\top C_r$, *for the middle frequency range* $\Theta = \{\theta_f : \theta_1 \le \theta_f \le \theta_2\}$ *with* $\theta_c = (\theta_1+\theta_2)/2$, $\theta_d = (\theta_2-\theta_1)/2$;

(iii) $\delta = -1$, $\Xi = P_2 + 2\cos(\theta_h)Q_2 + C_r^\top C_r$, *for the high frequency range* $\Theta = \{\theta_f : \theta_f \ge \theta_h\}$.

Proof. It is proved in Theorem 3.3.1 that (3.11a) and (3.11b) are equivalent to conditions (3.6a) and (3.6b), respectively. To demonstrate that (3.16) is equivalent to the condition (3.6c'), we derive the state-space realization of $\mathbb{T}_{fr}(\mathfrak{q}) - I$ through $(\mathcal{A}_r, \mathcal{B}_{fr}, \mathcal{C}_r, -I)$. Then, by setting the matrix $\Pi = \mathrm{diag}(I, -\eta_2 I)$ and using the state-space realization in Lemma 3.4.1, we obtain the equivalence between (3.16) and (3.6c'). The procedure is similar to the derivation of (3.11c) in the proof of Theorem 3.3.1. This completes the proof. □

The optimization problem in Theorem 3.3.6 can be solved by Algorithm 1. However, the key to achieving satisfactory estimation results is to ensure that $\|\mathbb{T}_{fr}(\mathfrak{q}) - I\|_{\mathcal{H}_\infty(\Theta)}$ is sufficiently small. This usually requires several iteration steps by Algorithm 1 and results in heavy computational loads when dealing with large-scale systems.

To reduce the computational complexity, we relax the estimation condition (3.6c') by letting $\mathbb{T}_{fr}(\mathfrak{q})$ approximate the identity matrix at $\kappa \in \mathbb{N}$ selected frequency points $\theta_i \in \Theta$ instead of the whole frequency domain Θ, i.e.,

$$\left\| \mathrm{Real}\left(\mathbb{T}_{fr}(\mathrm{e}^{j\theta_i}) - I\right) \right\|_2^2 \le \bar{\eta}_{2i}, \text{ and } \left\| \mathrm{Imag}\left(\mathbb{T}_{fr}(\mathrm{e}^{j\theta_i})\right) \right\|_2^2 \le \bar{\eta}_{3i},\ i \in \{1, \dots, \kappa\}, \tag{3.17}$$

where $\bar{\eta}_{2i},\ \bar{\eta}_{3i} \in \mathbb{R}_+$, $\mathrm{Real}(\cdot)$ and $\mathrm{Imag}(\cdot)$ denote the real and imaginary parts of the transfer function, respectively. By replacing (3.6c') in Problem 2 with the relaxed condition (3.17), we obtain the following relaxed version of Problem 2.

Problem 2r. (Fault estimation filter design with relaxed conditions) *Consider the system* (3.1)*, the structure of* $\mathbb{F}(\mathfrak{q})$ *in* (3.3)*, and the residual* (3.4)*. Given a scalar* $\beta \in [0,1]$*, find* $\mathbb{F}(\mathfrak{q})$ *via the minimization program*

$$\min_{\eta_1, \bar{\eta}_{2i}, \bar{\eta}_{3i} \in \mathbb{R}_+,\ \mathbb{F}(\mathfrak{q})} \left\{ \beta\eta_1 + \frac{1-\beta}{\kappa} \sum_{i=1}^{\kappa} (\bar{\eta}_{2i} + \bar{\eta}_{3i}) : \text{(3.6a), (3.6b), (3.17)} \right\}. \tag{3.18}$$

Before presenting the solution to (3.18), let us make some clarifications on the filter $\mathbb{F}(\mathfrak{q})$. To simplify the design, we fix the denominator $a(\mathfrak{q})$ in the following design. We select roots of $a(\mathfrak{q})$ inside the unit disk and set $d_a = d_N$ so that the fault estimation filter is stable and strictly proper. Subsequently, the coefficient matrices N_i for $i \in \{0, 1, \dots, d_N\}$ are the only parameters to be designed.

Recall the mapping relations presented in (3.4). For the sake of clarity, we further write the transfer functions $\mathbb{T}_{fr}(\mathfrak{q})$ and $\mathbb{T}_{\omega r}(\mathfrak{q})$ into

$$\mathbb{T}_{fr}(\mathfrak{q}) = -\frac{\mathcal{N}(\mathfrak{q})G}{a(\mathfrak{q})} = \bar{\mathcal{N}}\Psi_G(\mathfrak{q}) \text{ and } \mathbb{T}_{\omega r}(\mathfrak{q}) = -\frac{\mathcal{N}(\mathfrak{q})W}{a(\mathfrak{q})} = \bar{\mathcal{N}}\Psi_W(\mathfrak{q}), \tag{3.19}$$

where

$$\Psi_G(\mathfrak{q}) = -a^{-1}(\mathfrak{q})\text{diag}(G,\dots,G)[I,\mathfrak{q}I,\dots,\mathfrak{q}^{d_N}I]^\top,$$
$$\Psi_W(\mathfrak{q}) = -a^{-1}(\mathfrak{q})\text{diag}(W,\dots,W)[I,\mathfrak{q}I,\dots,\mathfrak{q}^{d_N}I]^\top.$$

By utilizing the multiplication rule of polynomial matrices [53, Lemma 4.2] in (3.19), we obtain the polynomial matrices $\Psi_G(\mathfrak{q})$ and $\Psi_W(\mathfrak{q})$ that contain all known elements in $\mathbb{T}_{fr}(\mathfrak{q})$ and $\mathbb{T}_{\omega r}(\mathfrak{q})$, respectively. Now, we can present the design method of $\mathbb{F}(\mathfrak{q})$ depicted in Problem 2r in the following theorem.

Theorem 3.3.7 (Optimal fault estimation filter design: relaxed requirements)**.** *Consider the system* (3.1)*, the structure of* $\mathbb{F}(\mathfrak{q})$ *in* (3.3)*, and the reformulations of* $\mathbb{T}_{fr}(\mathfrak{q})$ *and* $\mathbb{T}_{\omega r}(\mathfrak{q})$ *in* (3.19)*. Given the order* d_N*, the dimension* $n_r = n_f$*, the stable denominator* $a(\mathfrak{q})$ *with* $d_a = d_N$*,* κ *frequency points* $\theta_i \in \Theta$*, and the weight* $\beta \in [0,1]$*, the optimization problem* (3.18) *can be stated as the following quadratic programming problem:*

$$\begin{aligned}
&\min\ \beta\eta_1 + \frac{1-\beta}{\kappa}\sum_{i=1}^{\kappa}(\bar{\eta}_{2i}+\bar{\eta}_{3i})\\
&\text{s.t. } \bar{\mathcal{N}} \in \mathbb{R}^{n_r\times(d_N+1)(n_x+n_y)},\ \eta_1,\ \bar{\eta}_{2i},\ \bar{\eta}_{3i} \in \mathbb{R}_+,\ i\in\{1,\dots,\kappa\},\\
&\quad \bar{\mathcal{N}}\bar{H} = 0, && \text{(3.20a)}\\
&\quad \text{Trace}\left[\bar{\mathcal{N}}\Phi\bar{\mathcal{N}}^\top\right] \le \eta_1, && \text{(3.20b)}\\
&\quad \left\|\bar{\mathcal{N}}\mathcal{R}_i - I\right\|_2^2 \le \bar{\eta}_{2i},\ i\in\{1,\dots,\kappa\}, && \text{(3.20c)}\\
&\quad \left\|\bar{\mathcal{N}}\mathcal{I}_i\right\|_2^2 \le \bar{\eta}_{3i},\ i\in\{1,\dots,\kappa\}, && \text{(3.20d)}
\end{aligned}$$

where $\mathcal{R}_i = \text{Real}\left(\Psi_G(e^{j\theta_i})\right)$*,* $\mathcal{I}_i = \text{Imag}\left(\Psi_G(e^{j\theta_i})\right)$*, and* $\Phi = \frac{1}{2\pi}\int_{-\pi}^{\pi}\Psi_W(e^{j\theta})\Psi_W^*(e^{j\theta})d\theta$*.*

Proof. The proof is relegated to Section 3.4.2. □

In comparison to (3.16), the design of the fault estimation filter outlined in (3.18) which incorporates relaxed conditions described in (3.20), is computationally tractable as it is a quadratic programming problem. Furthermore, if we use the Frobenius norm instead of the 2 norm in (3.20), we can obtain an approximate analytical solution to it by leveraging the idea from [144]. The result is presented in the following corollary.

Corollary 3.3.8 (Approximate analytical solution)**.** *Consider the convex quadratic programming problem in* (3.20) *with the* 2 *norm replaced by the Frobenius norm. An approximate analytical solution to* (3.20) *is given by:*

$$\bar{\mathcal{N}}^\star_{App}(\gamma) = \frac{1-\beta}{\gamma\kappa}\sum_{i=1}^{\kappa}\mathcal{R}_i^\top\left[\gamma^{-1}\left(\beta\Phi + \frac{1-\beta}{\kappa}\sum_{i=1}^{\kappa}(\mathcal{R}_i\mathcal{R}_i^\top + \mathcal{I}_i\mathcal{I}_i^\top)\right) + \bar{H}\bar{H}^\top\right]^\dagger,$$

where $(\cdot)^\dagger$ *denotes the pseudo-inverse and* $\gamma \ge 0$ *is the Lagrange multiplier. The approximate solution converges to the optimal solution to* (3.20) *as* γ *tends to* ∞*.*

Proof. We first obtain the dual program of (3.20) by penalizing the equality constraint (3.20a), which is

$$\begin{aligned} g(\gamma) &= \inf_{\bar{\mathcal{N}}} \mathcal{L}(\bar{\mathcal{N}}, \gamma) \\ &= \inf_{\bar{\mathcal{N}}} \beta \mathrm{Trace}\left[\bar{\mathcal{N}}\Phi\bar{\mathcal{N}}^\top\right] + \frac{1-\beta}{\kappa}\sum_{i=1}^{\kappa}\left(\left\|\bar{\mathcal{N}}\mathcal{R}_i - I\right\|_F^2 + \left\|\bar{\mathcal{N}}\mathcal{I}_i\right\|_F^2\right) + \gamma\|\bar{\mathcal{N}}\bar{H}\|_F^2, \end{aligned}$$

where $\mathcal{L}(\bar{\mathcal{N}}, \gamma)$ is the Lagrange function of (3.20) and $\|\cdot\|_F$ denotes the Frobenius norm of a matrix. It holds that $\sup_{\gamma\geq 0} g(\gamma) = \lim_{\gamma\to\infty} g(\gamma)$.

By taking the partial derivative of the above Lagrange function, we have

$$\frac{\partial\mathcal{L}(\bar{\mathcal{N}}, \gamma)}{\partial\bar{\mathcal{N}}} = 2\beta\bar{\mathcal{N}}\Phi + \frac{2(1-\beta)}{\kappa}\sum_{i=1}^{\kappa}\left(\bar{\mathcal{N}}\mathcal{R}_i\mathcal{R}_i^\top - \mathcal{R}_i^\top + \bar{\mathcal{N}}\mathcal{I}_i\mathcal{I}_i^\top\right) + 2\gamma\bar{\mathcal{N}}\bar{H}\bar{H}^\top.$$

Setting the partial derivative to zero, we obtain

$$\bar{\mathcal{N}}^\star_{App}(\gamma) = \frac{1-\beta}{\gamma\kappa}\sum_{i=1}^{\kappa}\mathcal{R}_i^\top\left[\gamma^{-1}\left(\beta\Phi + \frac{1-\beta}{\kappa}\sum_{i=1}^{\kappa}(\mathcal{R}_i\mathcal{R}_i^\top + \mathcal{I}_i\mathcal{I}_i^\top)\right) + \bar{H}\bar{H}^\top\right]^\dagger.$$

This completes the proof. □

It is worth mentioning that, for a fixed denominator $a(\mathfrak{q})$, we can obtain an optimality gap for the optimization problem of the fault estimation filter design stated in Problem 2 by solving its exact and relaxed reformulations presented in Theorem 3.3.6 and Theorem 3.3.7. We present this result in the following proposition. To enhance readability, let us introduce several notations first. Recall the structure of $\mathbb{F}(\mathfrak{q})$ in (3.3). Given a stable numerator $a(\mathfrak{q})$, we define the optimal value of the objective function in Problem 2 as

$$\mathcal{J}^* = \min_{\mathcal{N}(\mathfrak{q})}\left\{\beta\|\mathbb{T}_{\omega r}(\mathfrak{q})\|_{\mathcal{H}_2}^2 + (1-\beta)\|\mathbb{T}_{fr}(\mathfrak{q}) - I\|_{\mathcal{H}_\infty(\Theta)}^2 \,:\, \mathbb{T}_{Xr}(\mathfrak{q}) = 0\right\}.$$

Furthermore, we use $\eta^*_{1,AO}$ and $\eta^*_{2,AO}$ to represent the values obtained by solving the optimization problem (3.16) using the AO approach, and use $\eta^*_{1,RR}$, $\bar{\eta}^*_{2i,RR}$, and $\bar{\eta}^*_{3i,RR}$ to denote the optimal values obtained by solving the optimization problem (3.20). The following proposition outlines the method to derive the optimality gap for Problem 2.

Proposition 3.3.9 (Optimality gap with a fixed denominator)**.** *Given a stable denominator $a(\mathfrak{q})$, the optimal value of the objective function in Problem 2 is bounded by*

$$\beta\eta^*_{1,RR} + \frac{(1-\beta)}{\kappa}\sum_{i=1}^{\kappa}(\bar{\eta}^*_{2i,RR} + \bar{\eta}^*_{3i,RR}) \leq \mathcal{J}^* \leq \beta\eta^*_{1,AO} + (1-\beta)\eta^*_{2,AO}. \tag{3.21}$$

Proof. The proof is relegated to Section 3.4.2. □

Different from the lower bound in (3.21) which is directly obtained by solving the optimization problem (3.20), the upper bound derived using the AO approach typically requires several iteration steps. This process will result in heavy computational loads if

Algorithm 2 Computing the optimality gap in (3.21)

Setp 1. **Initialization**

(a) Select d_N, $n_r = n_f$, and a stable denominator $a(\mathfrak{q})$

(b) Select κ frequency points uniformly from the frequency domain Θ and the weight β

Step 2. **Derivation of the lower bound**

(a) Compute the matrix $\mathcal{R}_i$, $\mathcal{I}_i$, and Φ for $i \in \{1, \dots, \kappa\}$

(b) Solve the numerator $\mathcal{N}^*_{RR}(\mathfrak{q})$ and the bounds $\eta^*_{1,RR}$, $\bar{\eta}^*_{2i,RR}$, and $\bar{\eta}^*_{3i,RR}$ by solving (3.20)

(c) Output the lower bound: $\beta\eta^*_{1,RR} + \frac{(1-\beta)}{\kappa}\sum_{i=1}^{\kappa}(\bar{\eta}^*_{2i,RR} + \bar{\eta}^*_{3i,RR})$

Step 3. **Derivation of the upper bound**

(a) Set $\mathcal{N}^*_{RR}(\mathfrak{q})$ as the initial condition and fix $a(\mathfrak{q})$ for (3.16)

(b) Optimize the numerator by solving (3.16) with the AO approach, and obtain $\eta^*_{1,AO}$ and $\eta^*_{2,AO}$

(c) Output the upper bound: $\beta\eta^*_{1,AO} + (1-\beta)\eta^*_{2,AO}$

the initial value is not appropriately chosen. Fortunately, we can utilize the solution of the relaxed design problem in Theorem 3.3.7 as the initial value. We then further optimize the upper bound (3.16) by solving the optimization problem using the AO approach. The procedure is summarized in Algorithm 2.

Suppose the fault signal f can be represented by the combination of components with different frequency $\theta_i \in \Theta$, i.e., $f(k) = \sum_{i=1}^{\kappa} f_i(k) = \sum_{i=1}^{\kappa} \mu_i \sin(\theta_i k)$, where each $\mu_i \in \mathbb{R}^{n_f}$ for $\{1, \dots, \kappa\}$ denotes the unknown weight of each component. Then, the estimation error of the method in Theorem (3.3.7) satisfies $\|r - f\|^2_{\mathcal{L}_2} \leq \sum_{i=0}^{\kappa}(\bar{\eta}^*_{2i,RR} + \bar{\eta}^*_{3i,RR})\|f_i\|^2_{\mathcal{L}_2}$ in the absence of the noise because of

$$
\begin{aligned}
\|r - f\|^2_{\mathcal{L}_2} &= \left\| \mathbb{T}_{fr}(\mathfrak{q}) \sum_{i=1}^{\kappa}[f_i] - \sum_{i=1}^{\kappa} f_i \right\|^2_{\mathcal{L}_2} \leq \sum_{i=1}^{\kappa} \|\mathbb{T}_{fr}(\mathrm{e}^{j\theta_i})[f_i] - f_i\|^2_{\mathcal{L}_2} \leq \sum_{i=1}^{\kappa} \|\mathbb{T}_{fr}(\mathrm{e}^{j\theta_i}) - I\|_2^2 \|f_i\|^2_{\mathcal{L}_2} \\
&= \sum_{i=1}^{\kappa} \|\mathrm{Real}(\mathbb{T}_{fr}(\mathrm{e}^{j\theta_i})) + j\mathrm{Imag}(\mathbb{T}_{fr}(\mathrm{e}^{j\theta_i})) - I\|_2^2 \|f_i\|^2_{\mathcal{L}_2} \\
&\leq \sum_{i=1}^{\kappa} \left(\|\mathrm{Real}(\mathbb{T}_{fr}(\mathrm{e}^{j\theta_i})) - I\|_2^2 + \|j\mathrm{Imag}(\mathbb{T}_{fr}(\mathrm{e}^{j\theta_i}))\|_2^2 \right) \|f_i\|^2_{\mathcal{L}_2} \\
&\leq \sum_{i=1}^{\kappa} (\bar{\eta}^{\star}_{2i,RR} + \bar{\eta}^{\star}_{3i,RR}) \|f_i\|^2_{\mathcal{L}_2},
\end{aligned}
$$

where $\|\mathrm{Real}(\mathbb{T}_{fr}(\mathrm{e}^{j\theta_i})) - I\|_2^2 \leq \bar{\eta}^*_{2i,RR}$ and $\|\mathrm{Imag}(\mathbb{T}_{fr}(\mathrm{e}^{j\theta_i}))\|_2^2 \leq \bar{\eta}^*_{3i,RR}$ from (3.20a) and (3.20b).

We close this section with the following remarks on the trade-off and conservatism analysis of the proposed design approach to fault estimation filters.

Remark 3.3.10 (Trade-off analysis)**.** *There is a trade-off between decoupling the unknown signals X, suppressing the noise ω, and estimating the fault f in* (3.16) *and* (3.20)*. First, the*

feasible solutions to (3.16) *and* (3.20) *lie in the left null space of* $\bar{H}$*, which restricts the choice of* $\bar{\mathcal{N}}$*. Second, increasing* β *improves the noise suppression capability of the filter. However, it reduces the estimation performance and vice versa. The trade-offs can, therefore, be used as a guide for selecting appropriate weights.*

Remark 3.3.11 (Selection of decision variable sets)**.** *When using the AO approach to solve the bilinear optimization problems stated in Theorem 3.3.1 and Theorem 3.3.6, it is essential to partition the decision variables in the bilinear terms into two sets, namely* $\mathcal{G}_1^k$ *and* $\mathcal{G}_2^k$*. We observe that, for different optimization problems, the choice of decision variable sets greatly influences the convergence speed of the AO approach. In particular, when solving the optimization problem* (3.16)*, if we select the decision variable sets without overlap, i.e.,* $\{\bar{\mathcal{N}}^k, a_0^k, \ldots, a_{d_N}^k\}$ *and* $\{P_1^k, P_2^k, Q_1^k, Q_2^k, V^k\}$*, it leads to a more efficient solution compared to the selection approach in* (3.12)*.*

Remark 3.3.12 (Extension to nonlinear systems)**.** *There are several ways to extend the proposed FDE filter design methods to nonlinear systems.*

(i) The most straightforward way is to linearize the nonlinear systems, while the linearization approach has poor diagnosis performance when handling systems with wide frequency ranges because of large model mismatches.

(ii) We leverage the idea form [53] by extracting the features of stochastic disturbances. Then, We can construct the nonlinear signatures with the mapping relations and the extracted features and robustify the filter to the nonlinearity signatures by design.

(iii) We can approximate the nonlinear terms with polynomials [122] and incorporate the approximation into the proposed optimization framework used for FDE filter design to minimize the effects of the nonlinear terms.

(iv) It is also possible to approximate the nonlinear systems with fuzzy Markov jump systems [145]. By doing so, we are able to design FDE filters for each linear subsystem with the proposed methods. When conducting diagnosis tasks, we switch the filters according to the rules.

Remark 3.3.13 (Fault estimation for non-minimal phase systems)**.** *For a non-minimal phase system, it is reported in the literature [1, Theorem 14.5] that the optimal distance between* $\mathbb{T}_{fr}$ *and* I *in the* $\mathcal{H}_\infty$ *framework is* 1*, i.e.,* $\min_{\bar{\mathcal{N}}} \|\mathbb{T}_{fr}(\mathfrak{q}) - I\|_{\mathcal{H}_\infty} = 1$*, which indicates that a satisfactory fault estimation over the whole frequency domain is not achievable. Our methods proposed in Theorem 3.3.6 and Theorem 3.3.7 can improve the estimation performance by limiting the frequency range interested for the fault estimation purpose. We will demonstrate this through simulation results.*

Remark 3.3.14 (Conservatism analysis)**.** *The conservatism of the fault estimation filter design method is summarized as follows:*

(i) In order to reduce computational complexity, we adopt a selective approach for the design of fault estimation filters in (3.20)*. Specifically, we only impose constraints on a subset of frequency points in* Θ*, instead of all the frequency points. As a result, the estimation performance at the other frequency points in* Θ *may not be guaranteed. However, as demonstrated by simulation results, the degradation of estimation performance at those points is minor.*

(ii) For simplicity, the denominator of the transfer function $a(\mathfrak{q})$ is fixed in the optimization problem (3.20), which restricts the design freedom. However, including the simultaneous design of both $a(\mathfrak{q})$ and $\mathcal{N}(\mathfrak{q})$ would result in a much more complex optimization problem, which might not be computationally tractable.

3.4 Technical Proofs of Main Results

3.4.1 Proofs of Results in Fault Detection

The following two lemmas are required for the proof of Theorem 3.3.1.

Lemma 3.4.1. *(GKYP lemma [129]) Consider a transfer function defined by $\mathbb{T}(\mathfrak{q}) = C(\mathfrak{q}I - \mathcal{A})^{-1}\mathcal{B} + \mathcal{D}$. Given a symmetric matrix Π and a finite frequency domain Θ, the following statements are equivalent:*

(i) The inequality holds in the finite-frequency domain $\theta \in \Theta$

$$\begin{bmatrix} \mathbb{T}(e^{j\theta}) \\ I \end{bmatrix}^* \Pi \begin{bmatrix} \mathbb{T}(e^{j\theta}) \\ I \end{bmatrix} \prec 0. \tag{3.22}$$

(ii) There exists Hermitian matrices $\mathcal{P}$ and $\mathcal{Q}$ with appropriate dimensions and $\mathcal{Q} \succ 0$ such that

$$\begin{bmatrix} \mathcal{A} & \mathcal{B} \\ I & 0 \end{bmatrix}^\top \Lambda \begin{bmatrix} \mathcal{A} & \mathcal{B} \\ I & 0 \end{bmatrix} + \begin{bmatrix} \mathcal{C} & \mathcal{D} \\ 0 & I \end{bmatrix}^\top \Pi \begin{bmatrix} \mathcal{C} & \mathcal{D} \\ 0 & I \end{bmatrix} \prec 0, \tag{3.23}$$

where the following holds:

a. For the low frequency range $\Theta = \{\theta : |\theta| \le \theta_l\}$, $\Lambda = \begin{bmatrix} -\mathcal{P} & \mathcal{Q} \\ \mathcal{Q} & \mathcal{P} - 2\cos(\theta_l)\mathcal{Q} \end{bmatrix}$;

b. For the middle frequency range $\Theta = \{\theta : \theta_1 \le \theta \le \theta_2\}$, $\Lambda = \begin{bmatrix} -\mathcal{P} & e^{j\theta_c}\mathcal{Q} \\ e^{-j\theta_c}\mathcal{Q} & \mathcal{P} - 2\cos(\theta_d)\mathcal{Q} \end{bmatrix}$, where $\theta_c = (\theta_1 + \theta_2)/2$, $\theta_d = (\theta_2 - \theta_1)/2$;

c. For the high frequency range $\Theta = \{\theta : |\theta| \ge \theta_h\}$, $\Lambda = \begin{bmatrix} -\mathcal{P} & -\mathcal{Q} \\ -\mathcal{Q} & \mathcal{P} + 2\cos(\theta_h)\mathcal{Q} \end{bmatrix}$.

Lemma 3.4.2. *(Finsler's lemma [146]) For matrices $\mathcal{V} \in \mathbb{R}^{n\times n}$ and $\mathcal{Y} \in \mathbb{R}^{n\times m}$, the following statements are equivalent:*

(i) $\mathcal{Y}^\perp \mathcal{V} \left(\mathcal{Y}^\perp\right)^\top \prec 0$, where $\mathcal{Y}^\perp$ denotes matrices satisfying $\mathcal{Y}^\perp \mathcal{Y} = 0$;

(ii) There exists a matrix $\mathcal{U} \in \mathbb{R}^{m\times n}$ such that $\mathcal{V} + \mathcal{Y}\mathcal{U} + \mathcal{U}^\top \mathcal{Y}^\top \prec 0$.

Proof of Theorem 3.3.1. First, the constraint (3.11a) implies $\mathcal{N}(\mathfrak{q})H(\mathfrak{q}) = 0$ according to multiplication rule of polynomial matrices [53, Lemma 4.2], which means that X is completely decoupled from the residual r. Thus, the condition (3.6a) is satisfied.

Second, the transfer function from ω to r is $-a^{-1}(\mathfrak{q})\mathcal{N}(\mathfrak{q})W$ when (3.11a) is satisfied, and its state-space realization is denoted by $(\mathcal{A}_r, \mathcal{B}_{\omega r}, \mathcal{C}_r)$. According to the classical result on $\mathcal{H}_2$

norm [123, Lemma 1], we can directly obtain the equivalence between the constraint (3.11b) and condition (3.6b).

In the last part of the proof, we demonstrate that the constraints (3.11c) are equivalent to the mapping requirement on the $\mathcal{H}_-$ performance (3.6c). We only present the result for the low-frequency scenario, as the proofs for the mid-frequency and high-frequency cases follow similar logic. According to Lemma 3.4.2, the first matrix inequality in (3.11c) is equivalent to

$$\begin{bmatrix}\begin{bmatrix}\mathcal{A}_r^\top\\ \mathcal{B}_{fr}^\top\end{bmatrix} & I\end{bmatrix}\left[\begin{array}{c|cc} -P_2 & \delta Q_2 & 0\\ \hline * & \Xi & 0\\ * & * & \eta_2 I\end{array}\right]\begin{bmatrix}\begin{bmatrix}\mathcal{A}_r & \mathcal{B}_{fr}\end{bmatrix}\\ I\end{bmatrix} \preceq -\vartheta I, \tag{3.24}$$

where $\delta = 1$ and $\Xi = P_2 - 2\cos(\theta_l)Q_2 - \mathcal{C}_r^\top \mathcal{C}_r$ for the low-frequency case. Expanding (3.24) leads to

$$\begin{aligned}
&\begin{bmatrix}\Xi & 0\\ * & \eta_2 I\end{bmatrix} - \begin{bmatrix}\mathcal{A}_r^\top\\ \mathcal{B}_{fr}^\top\end{bmatrix} P_2 \begin{bmatrix}\mathcal{A}_r & \mathcal{B}_{fr}\end{bmatrix} + \begin{bmatrix}\mathcal{A}_r^\top\\ \mathcal{B}_{fr}^\top\end{bmatrix}\begin{bmatrix}Q_2 & 0\end{bmatrix} + \begin{bmatrix}Q_2^\top\\ 0\end{bmatrix}\begin{bmatrix}\mathcal{A}_r & \mathcal{B}_{fr}\end{bmatrix}\\
=&\begin{bmatrix}\Xi - \mathcal{A}_r^\top P_2 \mathcal{A}_r + \mathcal{A}_r^\top Q_2 + Q_2^\top \mathcal{A}_r & -\mathcal{A}_r^\top P_2 \mathcal{B}_{fr} + Q_2^\top \mathcal{B}_{fr}\\ * & -\mathcal{B}_{fr}^\top P_2 \mathcal{B}_{fr} + \eta_2 I\end{bmatrix}\\
=&\begin{bmatrix}\mathcal{A}_r & \mathcal{B}_{fr}\\ I & 0\end{bmatrix}^\top \begin{bmatrix}-P_2 & Q_2\\ * & P_2 - (2\cos(\theta_l))Q_2\end{bmatrix}\begin{bmatrix}\mathcal{A}_r & \mathcal{B}_{fr}\\ I & 0\end{bmatrix}\\
&+\begin{bmatrix}\mathcal{C}_r & 0\\ 0 & I\end{bmatrix}^\top \begin{bmatrix}-I & 0\\ 0 & \eta_2 I\end{bmatrix}\begin{bmatrix}\mathcal{C}_r & 0\\ 0 & I\end{bmatrix} \preceq -\vartheta I.
\end{aligned} \tag{3.25}$$

Recall that the transfer function from f to r, denoted by $\mathbb{T}_{rf}(\mathfrak{q})$, has a state-space realization given by $(\mathcal{A}_r, \mathcal{B}_{fr}, \mathcal{C}_r)$. From Lemma 3.4.1, the last line of (3.25) is equivalent to

$$\begin{bmatrix}\mathbb{T}_{rf}(\mathrm{e}^{j\theta})\\ I\end{bmatrix}^*\begin{bmatrix}-I & 0\\ 0 & \eta_2 I\end{bmatrix}\begin{bmatrix}\mathbb{T}_{rf}(\mathrm{e}^{j\theta})\\ I\end{bmatrix} = -\mathbb{T}_{rf}^*(\mathrm{e}^{j\theta})\mathbb{T}_{rf}(\mathrm{e}^{j\theta}) + \eta_2 I \preceq -\vartheta I. \tag{3.26}$$

Thus, it holds that $\|\mathbb{T}_{rf}(\mathrm{e}^{j\theta})\|^2_{\mathcal{H}_-(\Theta)} \geq \eta_2$ for $\theta \in \Theta$. This completes the proof. □

To prove Theorem 3.3.5, we first introduce the following lemma.

Lemma 3.4.3. *(Linear transformation of sub-Gaussian signals [96, Lemma 4.3]) Let $\mathbb{T}_{\omega r}$ be the transfer function from ω to r. If ω follows iid sub-Gaussian distribution with zero mean and parameter λ_ω, the signal r is sub-Gaussian with zero mean and respective parameter $\lambda_r = \|\mathbb{T}_{\omega r}\|_{\mathcal{H}_2}\lambda_\omega$.*

Proof of Theorem 3.3.5. We first show that the FAR, i.e., ε_1, is guaranteed if J_{th} is determined by (3.14) in the absence of faults. From (3.4), the residual $r = \mathbb{T}_{\omega r}(\mathfrak{q})[\omega]$ since X is decoupled and $f = 0$. According to Lemma 3.4.3, r is sub-Gaussian with zero mean and the parameter λ_r satisfies

$$\lambda_r = \|\mathbb{T}_{\omega r}(\mathfrak{q})\|_{\mathcal{H}_2}\lambda_\omega \leq \sqrt{\eta_1^*}\lambda_\omega, \tag{3.27}$$

where the inequality holds by invoking Theorem 3.3.1. Then, we have

$$\begin{aligned}
\mathbf{Pr}[J(r) > J_{th} | f = 0] &= \mathbf{Pr}\left[\frac{1}{\mathcal{T}}\sum_{k=k_1}^{k_1+\mathcal{T}} \|r(k)\|_2 > J_{th} \middle| f = 0\right] \\
&\overset{(a)}{\leq} \mathbf{Pr}\left[\sum_{k=k_1}^{k_1+\mathcal{T}} \sqrt{n_r}\|r(k)\|_\infty > \mathcal{T} J_{th} \middle| f = 0\right] \\
&\overset{(b)}{\leq} \sum_{k=k_1}^{k_1+\mathcal{T}} \mathbf{Pr}\left[\|r(k)\|_\infty > \frac{J_{th}}{\sqrt{n_r}} \middle| f = 0\right] \\
&\overset{(c)}{\leq} 2\mathcal{T} n_r \mathrm{e}^{-\frac{(J_{th}/\sqrt{n_r})^2}{2\lambda_r^2}} \overset{(d)}{\leq} 2\mathcal{T} n_r \mathrm{e}^{-\frac{J_{th}^2}{2n_r\eta_1^*\lambda_\omega^2}}.
\end{aligned} \tag{3.28}$$

The inequality (a) holds as a result of the equivalence of vector norms, i.e., $\|r(k)\|_2 \leq \sqrt{n_r}\|r(k)\|_\infty$. The inequality (b) holds due to the fact that

$$\mathbf{Pr}[v_1 + v_2 > v_3] \leq \mathbf{Pr}[v_1 > v_3/2] + \mathbf{Pr}[v_2 > v_3/2],$$

where $v_1, v_2, v_3 \in \mathbb{R}_+$. The inequality (c) is derived from the concentration inequality in Lemma 3.3.3. And the inequality (d) is established according to (3.27). By substituting (3.14) into the last inequality, we arrive at $\mathbf{Pr}[J(r) > J_{th} | f = 0] \leq \varepsilon_1$. This completes the first part of the proof.

Second, we demonstrate that (3.15) holds when faults $f \in \Omega_f$ happen. To do so, we start by considering the residual, which is given by $r = \mathbb{T}_{fr}[f] + \mathbb{T}_{\omega r}[\omega]$ and has an expectation of $\mathbf{E}[r] = \mathbb{T}_{fr}[f]$. Note that $r - \mathbf{E}[r] = \mathbb{T}_{\omega r}[\omega]$ is sub-Gaussian with the parameter $\sqrt{\eta_1^*}\lambda_\omega$ as stated before. Thus, for a positive scalar $\epsilon \in \mathbb{R}_+$, we have

$$\mathbf{Pr}\left\{\sum_{k=k_1}^{k_1+\mathcal{T}} \|r(k) - \mathbf{E}[r(k)]\|_\infty > \mathcal{T}\epsilon \middle| f \in \Omega_f\right\} \leq 2\mathcal{T} n_r \mathrm{e}^{-\frac{\epsilon^2}{2\eta_1^*\lambda_\omega^2}},$$

which is equivalent to

$$\mathbf{Pr}\left\{\sum_{k=k_1}^{k_1+\mathcal{T}} \|r(k) - \mathbf{E}[r(k)]\|_\infty \leq \mathcal{T}\epsilon \middle| f \in \Omega_f\right\} \geq 1 - 2\mathcal{T} n_r \mathrm{e}^{-\frac{\epsilon^2}{2\eta_1^*\lambda_\omega^2}}.$$

Since it holds that $\sum_{k=k_1}^{k_1+\mathcal{T}} (\|\mathbf{E}[r(k)]\|_\infty - \|r(k)\|_\infty) \leq \sum_{k=k_1}^{k_1+\mathcal{T}} \|r(k) - \mathbf{E}[r(k)]\|_\infty$, we have

$$\mathbf{Pr}\left\{\sum_{k=k_1}^{k_1+\mathcal{T}} (\|\mathbf{E}[r(k)]\|_\infty - \|r(k)\|_\infty) \leq \mathcal{T}\epsilon \middle| f \in \Omega_f\right\} \geq 1 - 2\mathcal{T} n_r \mathrm{e}^{-\frac{\epsilon^2}{2\eta_1^*\lambda_\omega^2}}.$$

Let $\mathcal{T}\epsilon = \sum_{k=k_1}^{k_1+\mathcal{T}} \|\mathbf{E}[r(k)]\|_\infty - \mathcal{T} J_{th} > 0$. The above inequality becomes

$$\mathbf{Pr}\left\{ \sum_{k=k_1}^{k_1+\mathcal{T}} \|r(k)\|_\infty \geq \mathcal{T} J_{th} \middle| f \in \Omega_f \right\} \geq 1 - 2\mathcal{T} n_r \, \mathrm{e}^{-\frac{\epsilon^2}{2\eta_1^* \lambda_\omega^2}}. \tag{3.29}$$

Besides, we have the following inequalities

$$\sum_{k=k_1}^{k_1+\mathcal{T}} \|\mathbf{E}[r(k)]\|_\infty \geq \frac{1}{\sqrt{n_r}} \sum_{k=k_1}^{k_1+\mathcal{T}} \|\mathbf{E}[r(k)]\|_2 = \frac{1}{\sqrt{n_r}} \sum_{k=k_1}^{k_1+\mathcal{T}} \left\|\mathbb{T}_{fr}[f(k)]\right\|_2 \geq \frac{\sqrt{\eta_2^*}}{\sqrt{n_r}} \mathcal{T} \underline{f},$$

where the first inequality holds because of the equivalence of vector norms and the second inequality follows from the result in Theorem 3.3.1, i.e., $\|\mathbb{T}_{fr}\|^2_{\mathcal{H}_-(\Theta)} \geq \eta_2^*$, and $\|f(k)\|_2 \geq \underline{f}$ for $f \in \Omega_f$. To make sure that ϵ is positive, we let

$$\epsilon = \frac{1}{\mathcal{T}} \sum_{k=k_1}^{k_1+\mathcal{T}} \|\mathbf{E}[r(k)]\|_\infty - J_{th} > \sqrt{\eta_2^*/n_r}\,\underline{f} - J_{th} > 0.$$

Thus, the lower bounds of f should satisfy $\underline{f} > J_{th}\sqrt{n_r/\eta_2^*}$.

From the inequalities (3.29), we obtain

$$\begin{aligned}
\mathbf{Pr}\left\{ J(r) > J_{th} \middle| f \in \Omega_f \right\} &= \mathbf{Pr}\left\{ \frac{1}{\mathcal{T}} \sum_{k=k_1}^{k_1+\mathcal{T}} \|r(k)\|_2 > J_{th} \middle| f \in \Omega_f \right\} \\
&\geq \mathbf{Pr}\left\{ \frac{1}{\mathcal{T}} \sum_{k=k_1}^{k_1+\mathcal{T}} \|r(k)\|_\infty > J_{th} \middle| f \in \Omega_f \right\} \\
&\geq 1 - 2\mathcal{T} n_r \, \mathrm{e}^{-\frac{\epsilon^2}{2\eta_1^* \lambda_\omega^2}} \geq 1 - 2\mathcal{T} n_r \, \mathrm{e}^{-\frac{\left(\underline{f}\sqrt{\eta_2^*/n_r} - J_{th}\right)^2}{2\eta_1^* \lambda_\omega^2}}.
\end{aligned}$$

This completes the proof. □

3.4.2 Proofs of Results in Fault Estimation

To prove Theorem 3.3.7, we compute the covariance of the output when a linear time-invariant system is driven by the white noise signal through the following lemma.

Lemma 3.4.4. *(Covariance of the estimate of the fault) Consider the design form of the filter in* (3.4) *with the unknown signal X decoupled. The noise ω is assumed to be an iid white noise and faults f are considered to be deterministic. The covariance matrix of r is given by*

$$\mathbf{E}\left[(r(k) - \mathbf{E}[r(k)])(r(k) - \mathbf{E}[r(k)])^*\right] = \frac{1}{2\pi} \int_{-\pi}^{\pi} \mathbb{T}_{\omega r}(\mathrm{e}^{j\theta}) \mathbf{E}\left[\omega(k)\omega^*(k)\right] \mathbb{T}_{\omega r}^*(\mathrm{e}^{j\theta}) d\theta.$$

Proof. Let $h_{\omega r}(k)$ be the impulse response of $\mathbb{T}_{\omega r}(\mathfrak{q})$. The covariance function of $r(k)$ denoted by $\mathcal{V}_r(\tau)$ for $\tau \in \mathbb{N}$ can be written as

$$\begin{aligned}
\mathcal{V}_r(\tau) &= \mathbf{E}\left[(r(k+\tau)-\mathbf{E}[r(k+\tau)])(r(k)-\mathbf{E}[r(k)])^*\right] \\
&= \mathbf{E}\left[\left(\sum_{m=0}^{\infty} h_{\omega r}(m)\omega(k+\tau-m)\right)\left(\sum_{l=0}^{\infty} h_{\omega r}(l)\omega(k-l)\right)^*\right] \\
&= \sum_{m=0}^{\infty}\sum_{l=0}^{\infty} h_{\omega r}(m)\mathbf{E}\left[\omega(k+\tau-m)\omega^*(k-l)\right]h_{\omega r}^*(l) \\
&= \sum_{m=0}^{\infty}\sum_{l=0}^{\infty} h_{\omega r}(m)\mathcal{V}_{\omega}(\tau-m+l)h_{\omega r}^*(l),
\end{aligned}$$

where $\mathcal{V}_{\omega}(\tau-m+l)$ is the covariance function of ω. Now, we proceed to derive the spectrum of $r(k)$ denoted by $\Gamma_r(\mathfrak{q})$ via applying the Z-transform on $\mathcal{V}_r(\tau)$, which is

$$\begin{aligned}
\Gamma_r(\mathfrak{q}) &= \sum_{k=-\infty}^{\infty} \mathcal{V}_r(k)\mathfrak{q}^{-k} = \sum_{k=-\infty}^{\infty}\sum_{m=0}^{\infty}\sum_{l=0}^{\infty} h_{\omega r}(m)\mathcal{V}_{\omega}(k-m+l)h_{\omega r}^*(l)\mathfrak{q}^{-(k-m+l)}\mathfrak{q}^{-m}\mathfrak{q}^{l} \\
&= \sum_{m=0}^{\infty} h_{\omega r}(m)\mathfrak{q}^{-m}\sum_{k=-\infty}^{\infty}\mathcal{V}_{\omega}(k-m+l)\mathfrak{q}^{-(k-m+l)}\sum_{l=0}^{\infty} h_{\omega r}^*(l)\mathfrak{q}^{l} \\
&= \mathbb{T}_{\omega r}(\mathfrak{q})\Gamma_{\omega}(\mathfrak{q})\mathbb{T}_{\omega r}^*(\mathfrak{q}^{-*}),
\end{aligned}$$

where $\Gamma_{\omega}(\mathfrak{q})$ is the spectrum of ω. When $\tau = 0$, since ω is an uncorrelated sequence, we have

$$\begin{aligned}
\mathcal{V}_r(0) &= \mathbf{E}\left[(r(k)-\mathbf{E}[r(k)])(r(k)-\mathbf{E}[r(k)])^*\right] \\
&= \sum_{m=0}^{\infty}\sum_{l=0}^{\infty} h_{\omega r}(m)\mathbf{E}\left[\omega(k-m)\omega^*(k-l)\right]h_{\omega r}^*(l) \\
&= \sum_{m=0}^{\infty} h_{\omega r}(m)\mathbf{E}\left[\omega(k)\omega^*(k)\right]h_{\omega r}^*(m) \\
&= \frac{1}{2\pi j}\int_{-\pi}^{\pi}\Gamma_r(\mathfrak{q})\mathfrak{q}^{-1}d\mathfrak{q} \\
&= \frac{1}{2\pi j}\int_{-\pi}^{\pi}\mathbb{T}_{\omega r}(\mathfrak{q})\mathbf{E}\left[\omega(k)\omega^*(k)\right]\mathbb{T}_{\omega r}^*(\mathfrak{q})\mathfrak{q}^{-1}d\mathfrak{q},
\end{aligned}$$

where the inverse Z-transform and the fact that $\mathfrak{q}^{-*} = \mathfrak{q}$ on the unit circle are used in the last two equations. Also, due to the derivative $d\mathfrak{q}/d\theta = j\mathrm{e}^{j\theta}$, we arrive at

$$\mathbf{E}\left[(r(k)-\mathbf{E}[r(k)])(r(k)-\mathbf{E}[r(k)])^*\right] = \frac{1}{2\pi}\int_{-\pi}^{\pi}\mathbb{T}_{\omega r}(\mathrm{e}^{j\theta})\mathbf{E}\left[\omega(k)\omega^*(k)\right]\mathbb{T}_{\omega r}^*(\mathrm{e}^{j\theta})d\theta.$$

This completes the proof. □

Proof of Theorem 3.3.7. First, Theorem 3.3.1 demonstrates that (3.20a) is equivalent to conditions (3.6a). Second, we establish that (3.20b) implies the satisfaction of (3.6b). Recall

that $r = \mathbb{T}_{fr}(\mathfrak{q})[f] + \mathbb{T}_{\omega r}(\mathfrak{q})[\omega]$ where $\mathbb{T}_{\omega r}(\mathfrak{q}) = \bar{\mathcal{N}}\Psi_W(\mathfrak{q})$ and the fault signal is assumed to be deterministic. According to Lemma 3.4.4, the covariance of r satisfies

$$\begin{aligned}\mathbf{E}[(r(k)-\mathbf{E}[r(k)])(r(k)-\mathbf{E}[r(k)])^*] &= \frac{1}{2\pi}\int_{-\pi}^{\pi}\mathbb{T}_{\omega r}(\mathrm{e}^{j\theta})\mathbf{E}[\omega(k)\omega^*(k)]\mathbb{T}^*_{\omega r}(\mathrm{e}^{j\theta})d\theta \\ &\preceq \frac{\lambda_\omega^2}{2\pi}\int_{-\pi}^{\pi}\mathbb{T}_{\omega r}(\mathrm{e}^{j\theta})\mathbb{T}^*_{\omega r}(\mathrm{e}^{j\theta})d\theta \\ &= \bar{\mathcal{N}}\frac{\lambda_\omega^2}{2\pi}\int_{-\pi}^{\pi}\Psi_W(\mathrm{e}^{j\theta})\Psi^*_W(\mathrm{e}^{j\theta})d\theta\bar{\mathcal{N}}^\top \\ &= \bar{\mathcal{N}}\Phi\bar{\mathcal{N}}^\top\lambda_\omega^2, \end{aligned} \tag{3.30}$$

where the aforementioned inequality holds due to its demonstration through Taylor series expansion and comparison of terms of the same power for ϕ (defined in Lemma 3.3.3). It can be shown that for sub-Gaussian random variables, $\mathbf{E}[\omega(k)\omega^*(k)] \preceq \lambda_\omega^2 I$. As a result, the condition (3.6b) which is introduced to suppress the effect of the noise on r can be achieved by bounding the trace of $\bar{\mathcal{N}}\Phi\bar{\mathcal{N}}^\top$. This also coincides with the definition of the $\mathcal{H}_2$ norm.

In the last part of the proof, we show that (3.20c) and (3.20d) enforce the relaxed estimation condition (3.17). The transfer function $\mathbb{T}_{fr}(\mathfrak{q}) = \bar{\mathcal{N}}\Psi_G(\mathfrak{q})$ according to (3.19). Substituting $\bar{\mathcal{N}}\Psi_G(\mathfrak{q})$ into (3.17) directly leads to (3.20a) and (3.20b), respectively. This completes the proof. □

Proof of Proposition 3.3.9. We first show that the upper bound holds. Since the optimization problem (3.16) is an exact reformulation of Problem 2, applying the AO approach to solve (3.16) leads to the convergence of the objective function value to the optimal value $\mathcal{J}^*$ of Problem 2. Thus, the derived objective function value, i.e., $\eta^*_{1,AO} + (1-\beta)\eta^*_{2,AO}$, is an upper bound on $\mathcal{J}^*$.

In the second part of the proof, we demonstrate the satisfaction of the lower bound by contradiction. Suppose that

$$\min_{\mathcal{N}(\mathfrak{q})}\frac{1}{\kappa}\sum_{i=1}^{\kappa}\|\mathbb{T}_{fr}(\mathrm{e}^{j\theta_i}) - I\|_2^2 \geq \min_{\mathcal{N}(\mathfrak{q})}\|\mathbb{T}_{fr}(\mathrm{e}^{j\theta}) - I\|^2_{\mathcal{H}_\infty(\Theta)}.$$

Let $\mathcal{N}^*(\mathfrak{q})$ and $\mathcal{N}^*_{RR}(\mathfrak{q})$ denote the optimal solutions to

$$\min_{\mathcal{N}(\mathfrak{q})}\|\mathbb{T}_{fr}(\mathrm{e}^{j\theta}) - I\|^2_{\mathcal{H}_\infty(\Theta)} \text{ and } \min_{\mathcal{N}(\mathfrak{q})}\frac{1}{\kappa}\sum_{i=1}^{\kappa}\|\mathbb{T}_{fr}(\mathrm{e}^{j\theta_i}) - I\|_2^2,$$

respectively. Recall the definition of the finite-frequency $\mathcal{H}_\infty$ norm. Then, the following inequalities hold

$$\begin{aligned}\frac{1}{\kappa}\sum_{i=1}^{\kappa}\|\mathbb{T}_{fr}(\mathrm{e}^{j\theta_i}, \mathcal{N}^*_{RR}(\mathfrak{q})) - I\|_2^2 &\geq \sup_{\theta\in\Theta}\|\mathbb{T}_{fr}(\mathrm{e}^{j\theta}, \mathcal{N}^*(\mathfrak{q})) - I\|_2^2 \\ &\geq \frac{1}{\kappa}\sum_{i=1}^{\kappa}\|\mathbb{T}_{fr}(\mathrm{e}^{j\theta_i}, \mathcal{N}^*(\mathfrak{q})) - I\|_2^2,\end{aligned}$$

where $\mathbb{T}_{fr}(e^{j\theta_i}, \mathcal{N}^*_{RR}(q))$ indicates the usage of $\mathcal{N}^*_{RR}(q)$ in $\mathbb{T}_{fr}$, and the rest are similar. The above inequality contradicts the fact that $\mathcal{N}^*_{RR}(q)$ is the optimal solution to $\min_{\mathcal{N}(q)} \frac{1}{\kappa}\sum_{i=1}^{\kappa} \|\mathbb{T}_{fr}(e^{j\theta_i}) - I\|_2^2$. Thus, we have

$$\min_{\mathcal{N}(q)} \frac{1}{\kappa}\sum_{i=1}^{\kappa} \|\mathbb{T}_{fr}(e^{j\theta_i}) - I\|_2^2 \leq \min_{\mathcal{N}(q)} \|\mathbb{T}_{fr}(e^{j\theta}) - I\|^2_{\mathcal{H}_\infty(\Theta)}.$$

Additionally, the constraints (3.6a) and (3.6b) on noise suppression and disturbance decoupling are identical in both Problems 2 and 2r. As a result, the optimal objective value of Problem 2r, obtained by solving (3.20), serves as a lower bound for $\mathcal{J}^*$. This completes the proof. □

3.5 Simulation Results

In this section, we validate the effectiveness of the proposed fault detection and estimation methods on a synthetic non-minimum phase system and a multi-area power system.

3.5.1 Non-minimum Phase Systems

Consider a synthetic non-minimum phase system

$$\mathbb{T}(s) = \frac{(s-2)(s+0.1)}{(s+0.1)(s+0.5)(s+0.8)}.$$

The state-space realization is

$$A = \begin{bmatrix} -1.4 & -0.53 & -0.04 \\ 1 & 0 & 0 \\ 0 & 1 & 0 \end{bmatrix}, \; B_f = \begin{bmatrix} 1 \\ 0 \\ 0 \end{bmatrix}, \text{ and } C = \begin{bmatrix} 1 & -1.9 & -0.2 \end{bmatrix}.$$

We discretize the model with the sampling period 0.1s. Note that the inverse system of a non-minimum phase system is unstable because of the zeros located at the right-half complex plane (or outside of the unit disk for discrete-time cases). This makes the fault estimation problem of non-minimum phase systems quite challenging [147]. In this part, we use the methods developed in Theorem 3.3.6 (ER, exact reformulation) and Theorem 3.3.7 (RR, relaxed requirement) to estimate the fault signal that occurs in the above non-minimum phase system without considering disturbances and noise. We also compare the two methods with the UIO (unknown input observer) method [43], the LS (least square) method [59], and the IUIE (inversion-based unknown input estimation) method [60]. Both the UIO, LS, and IUIE methods are proven to be asymptotically unbiased estimation methods under certain conditions.

The frequency domain of interest is $\Theta = [0, 0.3]$ and the fault signal is

$$f(k) = 0.05\sin(0.18k) + 0.06\sin(0.25k).$$

We first design a fault estimation filter with the RR method in Theorem 3.3.7, where the parameters are set as $d_N = 4$, $\beta = 0$. We choose a stable denominator $a(q) = (q-0.1)^5$ and 7

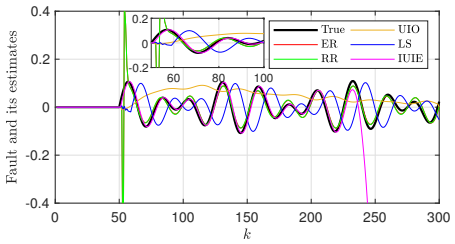

Figure 3.2: Fault estimates.

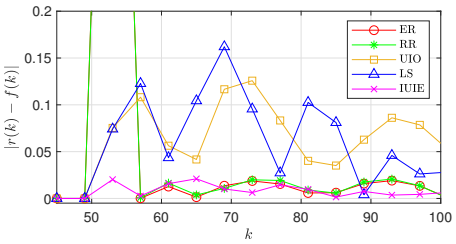

Figure 3.3: Error of fault estimates.

3

frequency points $\{0, 0.05, 0.1, \ldots, 0.3\}$. By solving the optimization problem (3.20), we obtain the numerator $\mathcal{N}^*_{RR}(\mathfrak{q})$ and the optimal values $\sum_{i=1}^{\kappa} \bar{\eta}^*_{2i,RR} = 1.42$ and $\sum_{i=1}^{\kappa} \bar{\eta}^*_{3i,RR} = 0.06$. Then, we fix the denominator $a(\mathfrak{q})$ and take $\mathcal{N}^*_{RR}(\mathfrak{q})$ as the initial condition when using the ER method in Theorem 3.3.6 and Algorithm 1 to design the fault estimation filter. We have $\eta^*_{2,AO} = 0.29$ after 50 iteration steps. According to (3.21), the optimality gap is $0.21 \leq \mathcal{J}^* \leq 0.29$.

The fault signal and its estimates obtained by different methods are presented in Figure 3.2, while errors of fault estimates are shown in Figure 3.3. As seen in Figure 3.2, the IUIE method performs well initially but experiences divergence at around $k = 230$. This is because the inversion-based estimation filter is unstable. Both the LS and UIO methods produce high estimation errors as shown in Figure 3.3. In comparison with the above methods, the proposed ER and RR methods offer better estimation performance. In Figure 3.4, we further demonstrate that increasing the degree of the RR filter leads to a reduction in the estimation error.

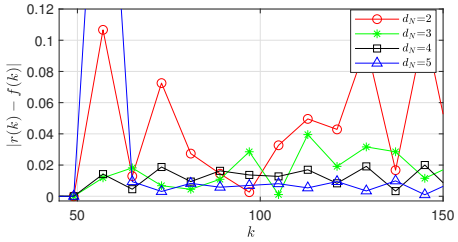

Figure 3.4: Error of fault estimates with different degrees.

3.5.2 Multi-area Power Systems

Consider a three-area power system described in [119]. Suppose each area of the power system can be represented by a model with equivalent governors, turbines, and generators.

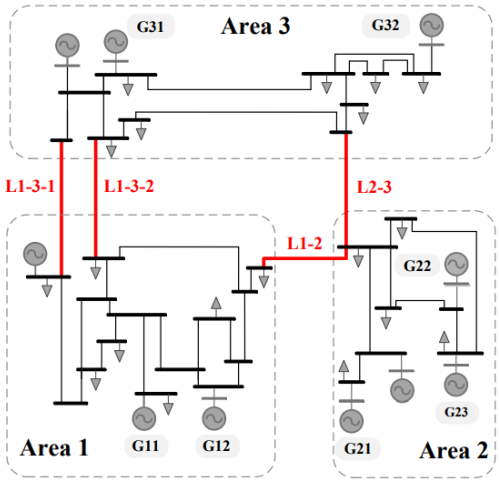

Figure 3.5: Illustration of the 3-area power system [107]

Then, in area i for $i \in \{1,2,3\}$, the dynamics of frequency $\Delta \boldsymbol{w}_i$ can be written as

$$\begin{cases} \Delta \dot{\boldsymbol{w}}_i &= \frac{\boldsymbol{w}_0}{2h_i S_{B_i}}(\Delta p_{m_i} - \Delta p_{tie_i} - \Delta p_{d_i} - \frac{1}{D_{li}}\Delta \boldsymbol{w}_i), \\ \Delta p_{m_i} &= \sum_{g=1}^{Gen_i} \Delta p_{m_{ig}},\ \Delta p_{tie_i} = \sum_{j \in Nbr_i} \Delta p_{tie_{ij}}, \\ \Delta \dot{p}_{m_{ig}} &= -\frac{1}{T_{ch_{ig}}}(\Delta p_{m_{ig}} + \frac{1}{S_i}\Delta \boldsymbol{w}_i - \rho_{ig}\Delta p_{agc_i}), \\ \Delta \dot{p}_{tie_{ij}} &= 2\pi P_{T_{ij}}(\Delta \boldsymbol{w}_i - \Delta \boldsymbol{w}_j), \\ ACE_i &= \zeta_i \Delta \boldsymbol{w}_i + \Delta p_{tie_i}, \\ \Delta \dot{p}_{agc_i} &= -K_{I_i} ACE_i, \end{cases} \tag{3.31}$$

where h_i represents the equivalent inertia constant, f_0 denotes the nominal frequency, S_{B_i} is the power base, Δp_{m_i} denotes the total generated power, $\Delta p_{tie,i}$ denotes the total tie-line power exchanges from area i, Δp_{d_i} denotes the deviation caused by the load, and $1/D_{li}\Delta \boldsymbol{w}_i$ is the deviation caused by the frequency dependency of the load. Let G_{en_i} and N_{br_i} be the number of generators and the set of areas that connect to area i, respectively. The term $\Delta p_{m_{ig}}$ denotes the power generated by the gth generator, $\Delta p_{tie_{ij}}$ is the power exchanges between area i and j, and $P_{T_{ij}}$ is the maximum transfer power on the line, which is assumed to be constant. It holds that $\Delta p_{tie_{ij}} = -\Delta p_{tie_{ji}}$. For the dynamics of $\Delta p_{m_{ig}}$, $T_{ch_{ig}}$ is the governor turbine's time constant, and S_i is the drop coefficient. The term Δp_{agc_i} is the Automatic Generation Control (AGC) signal and ρ_{ig} is the participating factor, i.e., $\sum_{g=1}^{Gen_i} \rho_{ig} = 1$. The area control error signal is denoted by ACE_i and ζ_i is the frequency bias factor. The AGC signal Δp_{agc_i} in the last line of (3.31) is in integration of ACE_i with the integral gain K_{I_i}.

Note that different faults may happen due to the vulnerabilities of multi-area systems. Here, we consider the following fault scenarios:

(i) faults on the tie line between areas that cause deviation in frequency, i.e., $\Delta\dot{p}_{tie_{ij}} = 2\pi P_{T_{ij}}(\Delta \boldsymbol{w}_i - \Delta \boldsymbol{w}_j + f_{tie_{ij}})$;

(ii) faults on the AGC part of area i, i.e., $\Delta\dot{p}_{agc_i} = -K_{I_i}(ACE_i + f_{agc_i})$;

(iii) faults on the sensors of area i, i.e., $y_i(t) = C_i x_i(t) + D_{f,i} f_{y_i}$, where y_i, C_i and x_i are the output, the output matrix, and states of area i, respectively. The matrix $D_{f,i}$ characterizes the sensors that are vulnerable.

Based on the dynamics (3.31) and descriptions of the faults, we get the following state-space model of area i with faults

$$\begin{cases} \dot{x}_i(t) = A_{ii}x_i(t) + B_{d,i}\Delta p_{d_i}(t) + B_{\omega,i}\omega_i(t) + \sum_{j\in N_{br_i}} A_{ij}x_j(t) + B_{f,i}f_i(t) \\ y_i(t) = C_i x_i(t) + D_{\omega,i}\omega_i(t) + D_{f,i}f_{y_i}(t), \end{cases} \tag{3.32}$$

where the state $x_i = \left[\Delta p_{tie_i}\ \Delta \boldsymbol{w}_i\ \{\Delta p_{m_{ig}}\}_{1:Gen_i}\ \Delta p_{agc_i}\right]^\top$, $f_i = [\{f_{tie_{ij}}\}_{j\in N_{br_i}}\ f_{agc_i}]^\top$ is the fault signal. We introduce a noise signal ω in the system. The matrices A_{ii}, $B_{d,i}$, A_{ij}, $B_{f,i}, D_{f,i}$ can be derived based on the dynamics (3.31) and the vulnerable parts of area i. The output matrix C_i is a tall or square matrix with the full column rank, i.e., $C_i = I$. The matrices $B_{\omega,i}$ and $D_{\omega,i}$ indicate which signal is affected by the noise. By stacking the state of each area, i.e., $x = [x_1^\top,\ x_2^\top,\ x_3^\top]^\top$ and discretizing the system with sampling period 0.1s, we obtain the discrete-time state-space model for the whole three-area power system in the form of (3.1). The system matrices are given by

$$A = \begin{bmatrix} A_{11} & A_{12} & A_{13} \\ A_{21} & A_{22} & A_{23} \\ A_{31} & A_{32} & A_{33} \end{bmatrix},\ B_d = \mathrm{diag}(B_{d,1}, B_{d,2}, B_{d,3}),\ B_f = \mathrm{diag}(B_{f,1}, B_{f,2}, B_{f,3}),\ B = D = 0,$$

$$B_\omega = \mathrm{diag}(B_{\omega,1}, B_{\omega,2}, B_{\omega,3}),\ D_\omega = \mathrm{diag}(D_{\omega,1}, D_{\omega,2}, D_{\omega,3}),\ \text{and}\ D_f = \mathrm{diag}(D_{f,1}, D_{f,2}, D_{f,3}).$$

The parameters of the system are given as follows: (1) The nominal frequency (Hz), $\boldsymbol{w}_0 = 60$; (2) The inertia time constant (MW/MVA), $h_1 = 4.41,\ h_2 = 4.15,\ h_3 = 3.46$; (3) The power base (MVA), $S_{B_1} = 1500,\ S_{B_2} = 2100,\ S_{B_3} = 1700$; (4) The damping coefficient (Hz/MW), $D_{l1} = 0.0064,\ D_{l2} = 0.0045,\ D_{l3} = 0.0056$; (5) The number of generators, $Gen_1 = 2,\ Gen_2 = 3, Gen_3 = 2$; (6) The time constant of governor-turbine: $T_{ch_{ig}} = 1.4950$ for all $i \in \{1,2,3\}$ and $g \in \{1,\ldots,Gen_i\}$; (7) The drop control coefficient (MW/Hz), $S_1 = 0.002,\ S_2 = 0.0014,\ S_3 = 0.0018$; (8) The participation factor, $\rho_{11} = \rho_{12} = \rho_{31} = \rho_{32} = 1/2,\ \rho_{21} = \rho_{22} = \rho_{23} = 1/3$; (9) The maximum transfer power (MW), $P_{T_{12}} = P_{T_{13}} = P_{T_{23}} = 2100$; (10) The frequency bias factor (Hz/MW), $\zeta_1 = 500.0064,\ \zeta_2 = 700.0045,\ \zeta_3 = 566.6723$; (11) The AGC integral gain, $K_{I_1} = K_{I_2} = K_{I_3} = 0.65$.

We consider faults in the tie-line of area 1, AGC part of area 2, and the measurement of area 1. The frequency range $\Theta = [0, 0.3]$. The faulty matrices are

$$B_{f,1} = [2\pi P_{T_{12}}\ 0\ 0\ 0\ 0]^\top,\ B_{f,2} = [0\ 0\ 0\ 0\ 0\ -K_{I_2}]^\top,\ D_{f,1} = [0\ 1\ 0\ 0\ 0]^\top, \text{and}$$
$$B_{f,3} = D_{f,2} = D_{f,3} = 0.$$

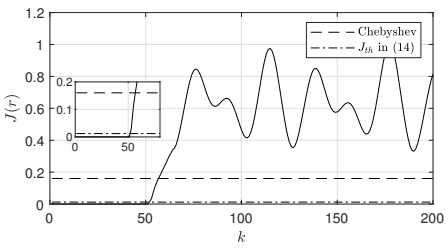

Figure 3.6: The value of the evaluation function and the diagnosis threshold.

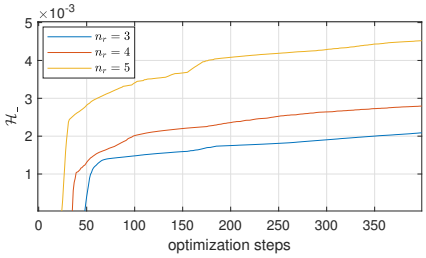

Figure 3.7: The $\mathcal{H}_-$ indices for residuals with different dimensions.

The fault signals are

$$f_{tie_{12}}(k) = 0.05\sin(0.2k) + 0.06\sin(0.3k),$$
$$f_{agc_2}(k) = 0.08\sin(0.15k) + 0.03\sin(0.25k), \text{ and } f_{y_1}(k) = 0.1.$$

The unknown loads are $\Delta p_{d_1}(k) = \Delta p_{d_2}(k) = \Delta p_{d_3}(k) = 1 + v(k)$ with uncertain value $v(k)$. The signal ω is a white noise with zero mean and variance 0.01. The matrices $B_\omega = 0$ and $D_\omega = \mathbf{1}$, where $\mathbf{1}$ represents a column vector with all elements 1. With the above settings, we now present the simulation results in the following parts.

Fault detection results: For the design of the fault detection filter, we set the dimension of the residual $n_r = 3$, the degree $d_N = 2$, and the weight $\alpha = 0.5$ by using Theorem 3.3.1 and Algorithm 1. Note that the dimension of the filter is $n_r(d_N + 1) = 9$, which is smaller than that of the power system $n_x = 16$. The obtained $\mathcal{H}_2$ norm value $\|\mathbb{T}_{\omega r}\|_{\mathcal{H}_2} = 0.0053$ and the $\mathcal{H}_-$ index $\|\mathbb{T}_{fr}\|_{\mathcal{H}_-(\Theta)} = 0.0254$ after 15 iteration steps by Algorithm 1. We determine the threshold $J_{th} = 0.0122$ according to Theorem 3.3.5 with the acceptable FAR $\varepsilon_1 = 0.001$ and time interval $\mathcal{T} = 10$. Then, we compute FDR $\varepsilon_2 = 0.9909$ for $\underline{f} > 0.17$.

Figure 3.6 presents the changes in the evaluation function's value. One can see that the value of $J(r(k))$ remains below the threshold J_{th} for $k \leq 50$ and exceeds J_{th} immediately after faults happen at $k = 50$, thus indicating the detection of faults. Moreover, the threshold derived using (3.14) is found to be less conservative than the threshold derived using Chebyshev's inequality, i.e., $\lambda_\omega \sqrt{\mathcal{T} n_r \eta_1^\star / \epsilon_1} = 0.1603$. Finally, let us consider a more stringent situation, e.g., $D_\omega = 0.1I$. We show in Figure 3.7 that increasing the dimension of the residual can lead to better $\mathcal{H}_-$ indices.

Fault estimation results: When using the proposed ER and RR methods to design fault estimation filters, we choose the degree of the numerator $d_N = 4$ and the dimension of the residual $n_r = n_f$. For the RR method, we select a stable denominator $a(\mathfrak{q})$ and some frequency points between $[0, 0.3]$, which are $\{0, 0.1, 0.2, 0.3\}$. To validate the performance of ER and RR methods, we compare them with the UIO, LS, and IUIE methods in the two cases of no noise and considering noise. Note that we revised the LS method in [59] by decoupling the unknown input, which is not considered in the original work. When using the IUIE method, we simultaneously estimate the disturbance and fault signals.

In the noise-free situation, we choose the weight $\beta = 0$ in the optimization problems (3.16) and (3.20). We first design a fault estimation filter with the ER method. By solving (3.16) with AO approach, we obtain $\eta_{2,AO}^* = 0.0172$ after 50 iteration steps. When using

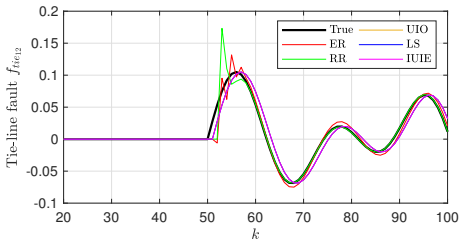

Figure 3.8: Estimates of f_{tie12} without noise.

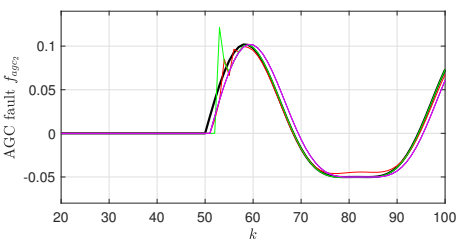

Figure 3.9: Estimates of f_{agc_2} without noise.

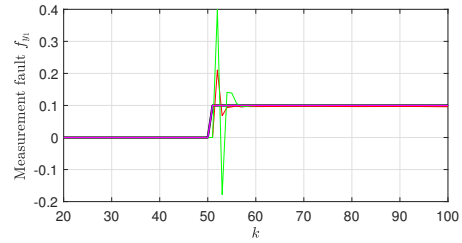

Figure 3.10: Estimates of f_{y_1} without noise.

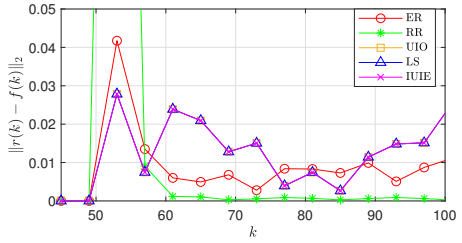

Figure 3.11: The estimation error.

the RR method to design the filter, we have $\sum_{i=1}^{\kappa} \bar{\eta}^*_{2i,RR} = 2.1\times10^{-4}$ and $\sum_{i=1}^{\kappa} \bar{\eta}^*_{3i,RR} = 1.1\times10^{-4}$. The estimation results are presented in Figures 3.8-3.11. Figures 3.8-3.10 show the estimates of the tie-line fault $f_{tie_{12}}$, the AGC fault f_{agc_2}, and the sensor fault f_{y_1} by different methods. Since the UIO, LS, and IUIE methods both obtain unbiased estimation results with a one-step delay, estimation errors of the three methods are the same as shown in Figure 3.11. Incorporating the frequency information of faults can reduce the conservatism of designing fault estimation filters in the entire frequency domain. Thus, one can see from Figure 3.11 that the proposed ER and RR methods lead to smaller errors than the other three methods.

In the case of considering noise, we set the weight $\beta = 0.1$. We design a fault estimation filter with the ER method. It takes 50 iteration steps to achieve $\eta^*_{1,AO} = 6.6\times10^{-5}$ and $\eta^*_{2,AO} = 0.0217$ by using Algorithm 1. For the RR method, we have $\eta^*_{1,RR} = 1\times10^{-7}$, $\sum_{i=0}^{\kappa} \bar{\eta}^*_{2i,RR} = 4.2\times10^{-6}$, and $\sum_{i=0}^{\kappa} \bar{\eta}^*_{3i,RR} = 3.2\times10^{-4}$ by solving (3.20). Since we ignore the effects of noises in the design of the UIO, LS, and IUIE methods, we consider a much smaller noise whose variance is 2.5×10^{-5} for these three methods. Figures 3.12-3.14 depict the estimates of the fault signals in the presence of noise by different methods. One can see from Figure 3.13 that the estimates of the AGC fault signal obtained by the UIO, LS, and IUIE methods are corrupted by noise seriously, which is the main source of the estimation error. In contrast, thanks to the noise suppression and finite frequency design, the ER and RR methods achieve smaller estimation errors than the other three methods under the effects of noise as illustrated in Figure 3.15.

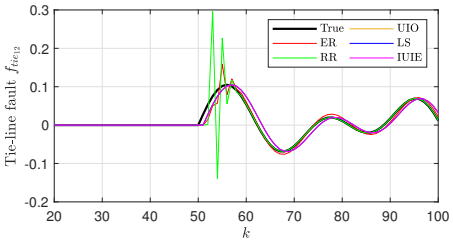

Figure 3.12: Estimates of $f_{tie_{12}}$ with noise.

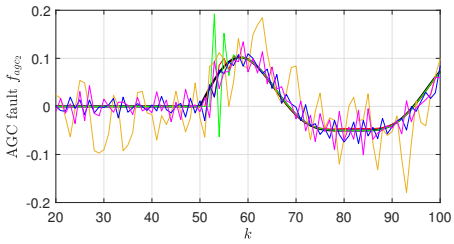

Figure 3.13: Estimates of f_{agc_2} with noise.

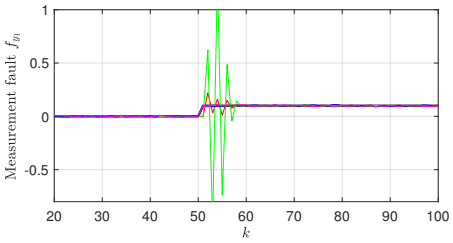

Figure 3.14: Estimates of f_{y_1} with noise.

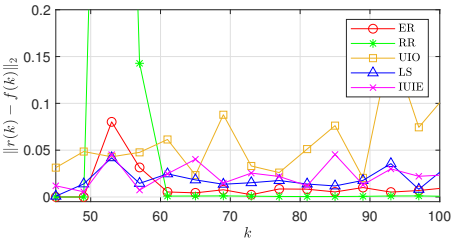

Figure 3.15: The estimation error.

3.6 Conclusions

In this chapter, we propose design methods for FDE filters in a finite-frequency domain for linear time-invariant discrete-time systems with unknown inputs and stochastic noise. Based on an integration of residual generation and norm approaches, the optimal design of fault detection filters that simultaneously decouple the unknown input, suppress noise, and enhance fault sensitivity is formulated into an optimization problem. Considering the random nature of the residual, we design detection thresholds that provide probabilistic guarantees on false alarm and fault detection rates. We further propose the design method of fault estimation filters by changing constraints in the same optimization framework of the fault detection filter design. To reduce computational complexity, we relax the fault estimation conditions and obtain a quadratic programming problem to solve the desired fault estimation filters. Simulation results of a synthetic non-minimum phase system and a multi-area power system show the effectiveness of the proposed approaches. In future work, the first research direction is to develop fault-tolerant control schemes by using estimation to compensate for the effect of faults. Since nonlinearity exists widely in practical systems, our second research direction would be focused on extending the derived optimization framework to nonlinear systems.

4

Real-time Ground Fault Detection for Inverter-based Microgrid Systems

This chapter is based on *J. Dong, Y. Liao, P. Mohajerin Esfahani. Real-time ground fault detection for inverter-based microgrid systems. [submitted to IEEE Transactions on Control Systems Technology]*

4.1 Introduction

In the past decade, inverter-based microgrid systems have gained popularity as power systems become increasingly complex and rely more on renewable energy sources [148]. These microgrid systems help integrate renewable energy sources into power systems and regulate the amount of power supplied to customers to provide high-quality power and reduce energy costs. They can also operate independently and allow for local control of distributed generation, for example, when the main grid is unavailable due to blackouts or storms [149]. This greatly increases the reliability of power systems.

Although inverter-based microgrid systems offer many benefits, they are susceptible to faults that can pose safety risks and damage equipment. Therefore, it is crucial to promptly and accurately detect faults to ensure the safe operation of inverter-based microgrid systems. However, the conventional protection strategy for power systems, such as overcurrent detection, is inefficient in detecting faults in inverter-based microgrid systems [150]. This is because the fault current only slightly deviates from the nominal value due to a current limiter embedded in the inverter controller [151]. According to IEEE Std. 1547.2 [152], the inverter current when the microgrid systems work in the islanded mode is restricted to 1-2 times the rated current during short-circuit faults.

The fault detection problem is more difficult when considering disturbances that have similar effects on the output current as faults. Therefore, developing an effective fault detection scheme for inverter-based microgrid systems in the presence of disturbances remains a challenge, particularly when only the output current is available as a measurement. In this chapter, we focus on the detection of ground faults as they are the most common and problematic type of faults in inverter-based microgrid systems [152, 153].

To tackle the fault detection problem for microgrid systems, researchers have developed several differential methods that rely on communication infrastructures between relays. These methods measure the difference in the current symmetrical components [154], the energy content of current [155], instantaneous current with comparative voltage [156], and traveling wave polarities [157] to detect faults. Some advanced signal processing techniques, such as sequence components [154, 158] and wavelet analysis [159], are usually combined with differential methods to detect faults in microgrid systems as well. Though these methods show effectiveness in detecting faults in microgrid systems, dependence on communication devices can degrade the reliability of systems, as these devices are vulnerable to faults and cyber attacks. Additionally, most differential methods require the installation of new equipment, sensors, and communication infrastructure, which can be expensive and time-consuming to implement and maintain [160].

In addition to differential methods, active fault detection methods have emerged as another popular solution to fault detection for microgrid systems in recent years. By introducing carefully designed input signals into the system, active fault detection methods can enhance the detectability of faults. In [161], the authors inject a small negative-sequence current ($< 3\%$) into the microgrid system and detect faults by using a signal processing technique to quantify the resulting negative-sequence voltage. Most recently, the authors in [162] provide an optimal input design method ensuring that the output sets of healthy and faulty modes of an inverter-based microgrid system are separated with a probabilistic guarantee. Then, it compares the output of the real-time process with the output sets to generate diagnosis results. However, the injected input signals can degrade the system

performance to some extent. Additionally, to obtain optimal input sequences as described in [162], an optimization problem must be solved each time, which can be computationally intensive and is unsuitable for online monitoring.

In contrast to differential methods, fault detection methods based on residual generation can be less dependent on the communication infrastructure and additional sensors, as these methods make full use of modeling information of systems. Moreover, residual generation-based methods are more suitable for online monitoring than active fault detection methods since they do not require continuous updates and have no impact on system performance. Let us briefly review several approaches to designing a residual generator. In the field of fault detection, the residual generator is generally constructed using observer-based or parity-space methods [2]. To handle disturbances, optimization techniques can be employed to determine the parameters of the residual generator, ensuring that the residual is sensitive to faults while being robust against disturbances [31, 163].

Alternatively, decomposition techniques such as the unknown input observer (UIO) [30] can be utilized to decouple disturbances from the residual. However, we found that the UIO approach could fail to satisfy the detectability condition when applied to inverter-based microgrid systems with a limited number of measurements, even when disturbances can be fully decoupled. In [45], the authors propose a parity-space-like approach for designing residual generators in the framework of the linear differential-algebraic equation (DAE). The derived residual generator can have lower order than that of the system, which reduces computational complexity when dealing with large-scale systems. Additionally, this framework provides design freedom. In specific, one is able to transform the design of the residual generator into various optimization problems to obtain desired solutions based on different requirements, such as disturbance decoupling [45], nonlinear suppression [53], and model mismatch handling [107] in fault detection tasks, as well as multiple fault estimation [125].

Main contributions: In this chapter, we leverage the advantages of the DAE framework to design fault detection filters for inverter-based microgrid systems. To the best of our knowledge, this is the first attempt to design fault detection filters using the DAE framework that enables real-time monitoring of ground faults in inverter-based microgrid systems. It is worth noting that disturbances may not be completely decoupled in some scenarios because of the limited number of sensors in the systems. The contributions of this chapter are summarized as follows:

- **Dynamic system modeling:** We develop a unified state-space model for the inverter-based microgrid system in both healthy mode and the presence of ground faults (Sections 4.2.2, 4.2.3). This model is further formulated in the DAE framework, which facilitates the design of robust fault detection filters.
- **Linear programming design for perfect setting:** We formulate the design of fault detection filters into a linear programming (LP) problem (Proposition 4.3.1), which achieves disturbance decoupling and ensures fault sensitivity simultaneously.
- **Data-assisted disturbance rejection:** To deal with non-decoupled disturbances, we borrow ideas from [53, Approach (II)] to extend the design to a quadratic programming (QP) problem, wherein the average effects of available disturbance patterns on the residual are minimized (Theorem 4.3.3). Inspiring from [144, Corollary 1], we

also obtain an approximate analytical solution to this QP problem with arbitrary accuracy (Corollary 4.3.4), allowing for online updates of filter parameters.

- **Probabilistic false alarm certificate:** Leveraging the classical Markov inequality, we further propose a threshold determination method along with probabilistic false-alarm guarantees (Proposition 4.3.8).

The rest of the chapter is organized as follows. The modeling of an inverter-based microgrid system and the problem formulation are presented in Section 4.2. In Section 4.3, we provide the design methods of the fault detection filters. In Section 4.4, we evaluate the effectiveness of the proposed approaches with numerical simulation. Finally, Section 4.5 concludes the chapter with some remarks and future directions.

Notation. For two discrete-time signals σ_1 and σ_2 taking values in $\mathbb{R}^n$ with length T, the $\mathcal{L}_2$ inner product is represented as $\langle \sigma_1, \sigma_2 \rangle := \sum_{k=1}^{T} \sigma_1^\top(k)\sigma_2(k)$, and the corresponding norm $\|\sigma_1\|_{\mathcal{L}_2} := \sqrt{\langle \sigma_1, \sigma_1 \rangle}$.

4.2 Model Description and Problem Statement

In this section, we first present the state-space model of an inverter-based microgrid system and consider three-phase symmetrical ground faults. Then, we formulate the two problems addressed in this work.

4.2.1 System Description

An inverter-based microgrid generally consists of four components: the power supplier, the LCL filter, the controller, and the load, see Figure 4.1. Let us elaborate on the functions of each component.

- **Power supplier**: The power supply part provides power to the microgrid by following a reference voltage v_i^* from the current controller. It contains a distributed generator (DG) source and an inverter. Here, we make two assumptions: (1) an ideal DG source is available, and (2) the inverter switching process can be neglected due to its high switching frequency. Therefore, instead of modeling the generator and inverter, we can set the inverter's output voltage directly to $v_i = v_i^*$. The real-time output current of the inverter is denoted by i_l. As the single DG source supplies all power to the load, droop control is unnecessary, and the microgrid frequency ω is constant. This differs from [164], where multiple DG sources operate simultaneously.

- **LCL filter**: The LCL filter is used to filter the harmonics produced by the inverter. It consists of two resistors R_f and R_c, two inductors L_f and L_c, and a capacitor C_f. The signals v_o and i_o denote the grid-side voltage and the output current, respectively.

- **Controller**: The control part keeps the voltage of the supply at some reference voltage v_o^*. This can be achieved through an inner current controller and an outer voltage controller, which are all PI controllers [165]. The outer voltage controller sets reference i_l^* for the inner current controller. The fault current limiter (FCL) is a saturation block that protects the microgrid from large fault currents.

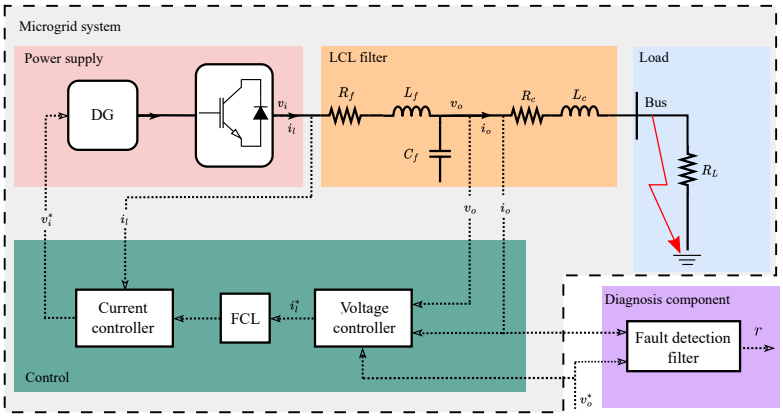

Figure 4.1: Architecture of an inverter-based microgrid with a diagnosis component.

- **Load**: We assume the load denoted by R_L is purely resistive. Note that the unknown part of the load is the main source of disturbances.

The mentioned voltage and current are based on a three-phase system. We introduce the direct-quadrature (dq) transform to simplify the analysis. Specifically, for a three-phase system with current $i = [i_a\ i_b\ i_c]^\top$ and voltage $v = [v_a\ v_b\ v_c]^\top$, the dq transform projects i and v onto d-axis and q-axis, i.e.,

$$i_{dq} = \mathbf{P}i, \quad v_{dq} = \mathbf{P}v,$$

where $i_{dq} = \left[i_d\ i_q\right]^\top$, $v_{dq} = \left[v_d\ v_q\right]^\top$, and the projection matrix $\mathbf{P}$ is given by

$$\mathbf{P} = \frac{2}{3}\begin{bmatrix} \cos(\theta) & \cos\left(\theta - \frac{2\pi}{3}\right) & \cos\left(\theta + \frac{2\pi}{3}\right) \\ \sin(\theta) & \sin\left(\theta - \frac{2\pi}{3}\right) & \sin\left(\theta + \frac{2\pi}{3}\right) \end{bmatrix},$$

in which $\theta = \omega t$ is a constantly changing angle between the d axis and the chosen reference phase. We refer interested readers to [166] for more details about the dq transformation. For simplicity of expression, we add subscripts to indicate the variables after dq transformation throughout the chapter, e.g., $v \xrightarrow{dq} v_{dq} = [v_d\ v_q]^\top$, $i \xrightarrow{dq} i_{dq} = [i_d\ i_q]^\top$, and so forth.

4.2.2 State-space Model of the Healthy Microgrid System

To obtain the state-space model of the healthy microgrid system, we first model individual components of the microgrid including the voltage controller, the current controller, and the LCL filter in this subsection.

We start with the voltage controller in the control component. Let us transform v_o, v_o^*, i_o and i_l^* into the dq framework, which are v_{odq}, v_{odq}^*, i_{odq} and i_{ldq}^*, respectively. We further define the cumulative error between v_{odq} and v_{odq}^* by $\phi_{dq} := [\phi_d\ \phi_q]^\top$, which can be written as

$$\frac{\mathrm{d}\phi_d(t)}{\mathrm{d}t} = v_{od}^*(t) - v_{od}(t), \quad \frac{\mathrm{d}\phi_q(t)}{\mathrm{d}t} = v_{oq}^*(t) - v_{oq}(t). \tag{4.1}$$

Considering that the voltage controller is a PI controller, based on Kirchhoff's laws, we obtain

$$\begin{cases} i_{ld}^*(t) = Fi_{od}(t) - \omega C_f v_{oq}(t) + K_P^v \left(v_{od}^*(t) - v_{od}(t)\right) + K_I^v \phi_d(t), \\ i_{lq}^*(t) = Fi_{oq}(t) + \omega C_f v_{od}(t) + K_P^v \left(v_{oq}^*(t) - v_{oq}(t)\right) + K_I^v \phi_q(t), \end{cases} \tag{4.2}$$

where F is the feedforward coefficient, K_P^v and K_I^v denote the proportional and integral gains of the voltage controller, respectively. From (4.1) and (4.2), we obtain the state-space model of the voltage controller

$$\begin{cases} \dot{\phi}_{dq}(t) = B_{v1} v_{odq}^*(t) + B_{v2} \begin{bmatrix} i_{ldq}(t) & v_{odq}(t) & i_{odq}(t) \end{bmatrix}^\top, \\ i_{ldq}^*(t) = C_v \phi_{dq}(t) + D_{v1} v_{odq}^*(t) + D_{v2} \begin{bmatrix} i_{ldq}(t) & v_{odq}(t) & i_{odq}(t) \end{bmatrix}^\top, \end{cases} \tag{4.3}$$

where the matrices are

$$B_{v1} = \begin{bmatrix} 1 & 0 \\ 0 & 1 \end{bmatrix}, \; B_{v2} = \begin{bmatrix} 0 & 0 & -1 & 0 & 0 & 0 \\ 0 & 0 & 0 & -1 & 0 & 0 \end{bmatrix}, \; C_v = \begin{bmatrix} K_I^v & 0 \\ 0 & K_I^v \end{bmatrix},$$
$$D_{v1} = \begin{bmatrix} K_P^v & 0 \\ 0 & K_P^v \end{bmatrix}, \text{ and } D_{v2} = \begin{bmatrix} 0 & 0 & -K_P^v & -\omega C_f & F & 0 \\ 0 & 0 & \omega C_f & -K_P^v & 0 & F \end{bmatrix}.$$

Similarly, one can obtain the state-space model of the current controller. Let us transform i_l, i_l^* and v_i^* into the dp framework, which are i_{ldq}, i_{ldq}^* and v_{idq}^*, respectively. The cumulative error between i_{ldq} and i_{ldq}^* is denoted by $\gamma_{dq} := [\gamma_d \; \gamma_q]^\top$, i.e.,

$$\frac{\mathrm{d}\gamma_d(t)}{\mathrm{d}t} = i_{ld}^*(t) - i_{ld}(t), \quad \frac{\mathrm{d}\gamma_q(t)}{\mathrm{d}t} = i_{lq}^*(t) - i_{lq}(t). \tag{4.4}$$

Then, the dynamics of the current controller follows

$$\begin{cases} v_{id}^*(t) = -\omega L_f i_{lq}(t) + K_P^c (i_{ld}^*(t) - i_{ld}(t)) + K_I^c \gamma_d(t), \\ v_{iq}^*(t) = \omega L_f i_{ld}(t) + K_P^c (i_{lq}^*(t) - i_{lq}(t)) + K_I^c \gamma_q(t), \end{cases} \tag{4.5}$$

where K_P^c and K_I^c denote the proportional and integral gains of the current controller, respectively. Based on (4.4) and (4.5), the state-space model of the current controller is given by

$$\begin{cases} \dot{\gamma}_{dq}(t) = B_{c1} i_{ldq}^*(t) + B_{c2} \begin{bmatrix} i_{ldq}(t) & v_{odq}(t) & i_{odq}(t) \end{bmatrix}^\top, \\ v_{idq}^*(t) = C_c \gamma_{dq}(t) + D_{c1} i_{ldq}^*(t) + D_{c2} \begin{bmatrix} i_{ldq}(t) & v_{odq}(t) & i_{odq}(t) \end{bmatrix}^\top, \end{cases} \tag{4.6}$$

where

$$B_{c1} = \begin{bmatrix} 1 & 0 \\ 0 & 1 \end{bmatrix},\ B_{c2} = \begin{bmatrix} -1 & 0 & \mathbf{0}_{1\times4} \\ 0 & -1 & \mathbf{0}_{1\times4} \end{bmatrix},\ C_c = \begin{bmatrix} K_I^c & 0 \\ 0 & K_I^c \end{bmatrix},$$
$$D_{c1} = \begin{bmatrix} K_P^c & 0 \\ 0 & K_P^c \end{bmatrix},\ \text{and}\ D_{c2} = \begin{bmatrix} -K_P^c & -\omega L_f & \mathbf{0}_{1\times4} \\ \omega L_f & -K_P^c & \mathbf{0}_{1\times4} \end{bmatrix}.$$

For the LCL filter modeling, we transform the output voltage of the inverter v_i and the bus voltage v_b into the dq framework, i.e., v_{idq} and v_{bdq}, respectively. By applying Kirchhoff's laws, we get the dynamics of the LCL filter as follows

$$\begin{cases} \dot{i}_{ld}(t) = \frac{-R_f}{L_f} i_{ld}(t) + \omega i_{lq}(t) + \frac{1}{L_f} v_{id}(t) - \frac{1}{L_f} v_{od}(t), \\ \dot{i}_{lq}(t) = \frac{-R_f}{L_f} i_{lq}(t) - \omega i_{ld}(t) + \frac{1}{L_f} v_{iq}(t) - \frac{1}{L_f} v_{oq}(t), \\ \dot{v}_{od}(t) = \omega v_{oq}(t) + \frac{1}{C_f} i_{ld}(t) - \frac{1}{C_f} i_{od}(t), \\ \dot{v}_{oq}(t) = -\omega v_{od}(t) + \frac{1}{C_f} i_{lq}(t) - \frac{1}{C_f} i_{oq}(t)\ , \\ \dot{i}_{od}(t) = \frac{-R_c}{L_c} i_{od}(t) + \omega i_{oq}(t) + \frac{1}{L_c} v_{od}(t) - \frac{1}{L_c} v_{bd}(t), \\ \dot{i}_{oq}(t) = \frac{-R_c}{L_c} i_{oq}(t) - \omega i_{od}(t) + \frac{1}{L_c} v_{oq}(t) - \frac{1}{L_c} v_{bq}(t). \end{cases}$$

The state-space model of the LCL filter is

$$\begin{bmatrix} \dot{i}_{ldq}(t) \\ \dot{v}_{odq}(t) \\ \dot{i}_{odq}(t) \end{bmatrix} = A_l \begin{bmatrix} i_{ldq}(t) \\ v_{odq}(t) \\ i_{odq}(t) \end{bmatrix} + \begin{bmatrix} B_{l1} & B_{l2} \end{bmatrix} \begin{bmatrix} v_{idq}(t) \\ v_{bdq}(t) \end{bmatrix}, \tag{4.7}$$

where the bus voltage $v_{bdq}(t) = \begin{bmatrix} R_L & 0 \\ 0 & R_L \end{bmatrix} i_{odq}(t)$, and the matrices are

$$A_l = \begin{bmatrix} -\frac{R_f}{L_f} & \omega & -\frac{1}{L_f} & 0 & 0 & 0 \\ -\omega & -\frac{R_f}{L_f} & 0 & -\frac{1}{L_f} & 0 & 0 \\ \frac{1}{C_f} & 0 & 0 & \omega & -\frac{1}{C_f} & 0 \\ 0 & \frac{1}{C_f} & -\omega & 0 & 0 & -\frac{1}{C_f} \\ 0 & 0 & \frac{1}{L_c} & 0 & -\frac{R_c}{L_c} & \omega \\ 0 & 0 & 0 & \frac{1}{L_c} & -\omega & -\frac{R_c}{L_c} \end{bmatrix},\ B_{l1} = \begin{bmatrix} \frac{1}{L_f} & 0 & \mathbf{0}_{1\times4} \\ 0 & \frac{1}{L_f} & \mathbf{0}_{1\times4} \end{bmatrix}^\top,\ \text{and}$$
$$B_{l2} = \begin{bmatrix} \mathbf{0}_{1\times4} & -\frac{1}{L_c} & 0 \\ \mathbf{0}_{1\times4} & 0 & -\frac{1}{L_c} \end{bmatrix}^\top.$$

Recall that $v_i = v_i^*$ and, thus, $v_{idq} = v_{idq}^*$. With the derived models (4.3), (4.6), and (4.7), we obtain the complete state-space model of the inverter-based microgrid system

$$\begin{cases} \dot{x}(t) = A_h x(t) + B_h v_{odq}^*(t) + B_d d(t), \\ i_{odq}(t) = C x(t), \end{cases} \tag{4.8}$$

where $x(t) = \begin{bmatrix} \phi_{dq}^\top(t) & \gamma_{dq}^\top(t) & i_{ldq}^\top(t) & v_{odq}^\top(t) & i_{odq}^\top(t) \end{bmatrix}^\top$ is the augmented state of the microgrid system and d denotes the disturbance. The system matrices A_h, B_h, and C are given by

$$A_h = \begin{bmatrix} \mathbf{0}_{2\times2} & \mathbf{0}_{2\times2} & B_{v2} \\ B_{c1}C_v & \mathbf{0}_{2\times2} & B_{c1}D_{v2} + B_{c2} \\ B_{l1}D_{c1}C_v & B_{l1}C_c & A_{h33} \end{bmatrix}, \; B_h = \begin{bmatrix} B_{v1} \\ B_{c1}D_{v1} \\ B_{l1}D_{c1}D_{v1} \end{bmatrix}, \text{ and } C = \begin{bmatrix} \mathbf{0}_{2\times8} & I_{2\times2} \end{bmatrix},$$

where $A_{h33} = A_l + B_{l1}(D_{c1}D_{v2} + D_{c2}) + B_{l2}\begin{bmatrix} R_L & 0 \\ 0 & R_L \end{bmatrix}\begin{bmatrix} \mathbf{0}_{2\times4} & I \end{bmatrix}$. We would like to highlight that the number of states is 10, while we only have 2 measurements.

Referring to [164, 167], we consider that changes in the load component can result in deviations from the nominal value of the output current i_{odq}. Furthermore, the following assumption on the matrix B_d is introduced to describe the impact of the disturbance d on the system.

Assumption 4.2.1 (Disturbance structure)**.** *The disturbance d directly influences the grid-side current i_{odq}, which is characterized through the matrix B_d. Here, we consider both one-dimensional and two-dimensional disturbances. The structure of B_d is: (1) $B_d = \begin{bmatrix} \mathbf{0}_{1\times8} & [\xi_1 \; \xi_2] \end{bmatrix}^\top$ for $d(t) \in \mathbb{R}$, and (2) $B_d = \begin{bmatrix} \mathbf{0}_{2\times8} & \text{diag}([\xi_1 \; \xi_2]) \end{bmatrix}^\top$ for $d(t) \in \mathbb{R}^2$, where $\xi_1, \xi_2 \in \mathbb{R}$ represent the level of disturbance in the corresponding channel.*

Remark 4.2.2 (Disturbance decoupling condition)**.** *Let $\mathbb{T}_{di_{odq}}$ denote the transfer function from the disturbance d to the measurement i_{odq}, and Rank$(\mathbb{T}_{di_{odq}})$ denotes the rank of $\mathbb{T}_{di_{odq}}$. According to the result in [1, Chapter 6], d can be decoupled from i_{odq} if the number of unknown inputs is smaller than the number of sensors, i.e., Rank$(\mathbb{T}_{di_{odq}}) < 2$. Therefore, d can be decoupled from i_{odq} when d is a one-dimensional signal but not for a two-dimensional (and higher-dimensional) disturbance.*

4.2.3 State-space Model of the Faulty Microgrid System

We consider three-phase symmetrical ground faults which can cause a short circuit and a sharp increase in the output current i_{odq}. Therefore, we know that after ground faults occur: (1) the load $R_L = 0$ because of the short circuit, leading to a zero bus voltage $v_{bdq} = 0$; and (2) the output of the voltage controller i_{ldq}^* saturates to a constant value τ_{dq} immediately, i.e., $i_{ldq}^*(t) = \tau_{dq}$ for $t \geq t_f$, where t_f denotes the time instant when the faults occur.

The state-space model of the current controller (4.6) in the fault scenario becomes

$$\begin{cases} \dot{\gamma}_{dq}(t) = B_{c1}\tau_{dq} + B_{c2}\begin{bmatrix} i_{ldq}(t) & v_{odq}(t) & i_{odq}(t) \end{bmatrix}^\top, \\ v^*_{idq}(t) = C_c\gamma_{dq}(t) + D_{c1}\tau_{dq} + D_{c2}\begin{bmatrix} i_{ldq}(t) & v_{odq}(t) & i_{odq}(t) \end{bmatrix}^\top. \end{cases} \tag{4.9}$$

Based on (4.3), (4.7), and (4.9), the state-space model of the inverter-based microgrid system with ground faults can be written as

$$\begin{cases} \dot{x}(t) = A_{uh}x(t) + B_{uh1}v^*_{odq}(t) + B_{uh2}\tau_{dq}, \\ i_{odq}(t) = Cx(t), \end{cases} \tag{4.10}$$

where the matrices A_f, B_{uh1}, and B_{uh2} are

$$A_{uh} = \begin{bmatrix} \mathbf{0}_{2\times2} & \mathbf{0}_{2\times2} & B_{v2} \\ \mathbf{0}_{2\times2} & \mathbf{0}_{2\times2} & B_{c2} \\ \mathbf{0}_{6\times2} & B_{l1}C_c & A_l + B_{l1}D_{c2} \end{bmatrix}, \; B_{uh1} = \begin{bmatrix} B_{v1} \\ \mathbf{0}_{2\times2} \\ \mathbf{0}_{6\times2} \end{bmatrix}, \text{ and } B_{uh2} = \begin{bmatrix} \mathbf{0}_{2\times2} \\ B_{c1} \\ B_{l1}D_{c1} \end{bmatrix}.$$

Note that the disturbance d has no effect on the system in the fault scenario because of the short circuit.

To write the healthy and faulty models (4.8) and (4.10) into a more compact form, we introduce a signal f to indicate the occurrence of the ground faults, i.e.,

$$\begin{cases} f = 0, & \text{no faults,} \\ f = 1, & \text{faults happen.} \end{cases}$$

With $f(t)$, we can express the healthy and faulty models in the following unified form

$$\begin{cases} \dot{x}(t) = \mathcal{A}(f(t))x(t) + \mathcal{B}_u(f(t))u(t) + \mathcal{B}_d(f(t))d(t), \\ y(t) = Cx(t), \end{cases} \tag{4.11}$$

where $u = [v^*_{odq} \; \tau_{dq}]^\top$ consists of the known input signals, $y = i_{odq}$ denotes the output current. The dimensions of x, u, d and y are denoted by n_x, n_u, n_d, and n_y, respectively. The system matrices are

$$\mathcal{A}(f(t)) = A_h + f(t)(A_{uh} - A_h), \; \mathcal{B}_u(f(t)) = [B_h + f(t)(B_{uh1} - B_h) \quad f(t)B_{uh2}], \text{ and}$$
$$\mathcal{B}_d(f(t)) = (1 - f(t))B_d.$$

Remark 4.2.3 (Discretization). *Considering that the discrete-time samplings of data are used in the realistic framework, we discretize the continuous-time state-space model* (4.11) *when designing the fault diagnosis scheme. In what follows, all signals are presented in the discrete-time form. For convenience, we use the same notation for system matrices in both the continuous and discrete representations.*

4.2.4 Problem Statement

The objective of this work is to detect the occurrence of the ground faults in the presence of the disturbance d through the input u and the measurement y. Our proposed diagnosis scheme is to design a residual generator denoted by a linear transfer function $\mathbb{F}$, whose output is a scalar-valued signal $r := \mathbb{F}[y^\top \; u^\top]^\top$ (called the residual) that only sensitive to the faulty mode. The structure is illustrated in the diagnosis component of Figure 4.1. We expect the residual r to be as close to zero as possible in the healthy mode and extremely high in the faulty mode for fault detection. Then, two questions arise naturally. How can we design $\mathbb{F}$ to achieve the following objectives:

1. *Suppress the contribution of the disturbance to the residual in the healthy mode;*
2. *Enhance the fault sensitivity of the residual in the faulty mode.*

In this work, we provide a design method of the filter $\mathbb{F}$ in the DAE framework to satisfy the above two design requirements. To this end, let us introduce the shift operator $\mathfrak{q}$, i.e., $\mathfrak{q}x(k) = x(k+1)$, and transform the discrete-time version of the unified state-space model (4.11) into

$$H(\mathfrak{q}, f)[X] + L(\mathfrak{q}, f)[Y] = 0, \tag{4.12}$$

where $X = [x^\top \; d^\top]^\top$, $Y = [y^\top \; u^\top]^\top$. The matrices $H(\mathfrak{q}, f)$ and $L(\mathfrak{q}, f)$ are polynomial functions in the operator $\mathfrak{q}$, depending on the indicator signal $f \in \{0, 1\}$, which are

$$H(\mathfrak{q}, f) = \mathfrak{q}H_1 + H_0(f) = \begin{bmatrix} -\mathfrak{q}I + \mathcal{A}(f) & \mathcal{B}_d(f) \\ C & 0 \end{bmatrix}, \; H_1 = \begin{bmatrix} -I & 0 \\ 0 & 0 \end{bmatrix}, \; H_0(f) = \begin{bmatrix} \mathcal{A}(f) & \mathcal{B}_d(f) \\ C & 0 \end{bmatrix},$$

$$\text{and } L(\mathfrak{q}, f) = \begin{bmatrix} 0 & \mathcal{B}_u(f) \\ -I & 0 \end{bmatrix}.$$

Since $L(\mathfrak{q}, f)$ is independent of $\mathfrak{q}$, we define $L(\mathfrak{q}, 0) = L_0$ and $L(\mathfrak{q}, 1) = L_1$.

The fault detection filter $\mathbb{F}$ is in the form of

$$\mathbb{F}(\mathfrak{q}) = \frac{1}{a(\mathfrak{q})} N(\mathfrak{q}) L_0, \tag{4.13}$$

where the numerator $N(\mathfrak{q})$ is a polynomial row vector $N(\mathfrak{q}) = \sum_{i=0}^{d_N} N_i \mathfrak{q}^i$, $N_i \in \mathbb{R}^{1\times(n_x+n_y)}$, d_N is the degree of $N(\mathfrak{q})$. The denominator $a(\mathfrak{q})$ is a polynomial with the degree larger than d_N and all roots inside the unit circle so that the derived filter is strictly proper and stable. For simplicity of design, we fix d_N and $a(\mathfrak{q})$, and only design the coefficients of $N(\mathfrak{q})$. It is worth pointing out that $a(\mathfrak{q})$ can be chosen up to the user and specific requirements, e.g., noise sensitivity and dynamic performance, which will be our future research.

By setting $f = 0$ and multiplying from the left-hand side of (4.12) by $a^{-1}(\mathfrak{q})N(\mathfrak{q})$, we obtain the residual r in the healthy mode, which is

$$r = \frac{1}{a(\mathfrak{q})} N(\mathfrak{q}) L_0[Y] = -\frac{1}{a(\mathfrak{q})} N(\mathfrak{q}) H(\mathfrak{q}, 0)[X]. \tag{4.14}$$

When ground faults happen, i.e., $f = 1$, DAE model (4.12) becomes $H(q,1)[X] + L_1[Y] = 0$. Thus, $Y = -L_1^{\dagger} H(q,1)[X]$, where $L_1^{\dagger}$ is the left inverse of L_1. The residual r in the faulty mode becomes

$$r = \frac{1}{a(\mathfrak{q})} N(\mathfrak{q}) L_0[Y] = -\frac{1}{a(\mathfrak{q})} N(\mathfrak{q}) L_0 L_1^{\dagger} H(q,1)[X]. \tag{4.15}$$

Note that all the entities in $a^{-1}(\mathfrak{q})N(\mathfrak{q})L_0[Y]$ are known and, thus, can be used to generate the residual. The right-hand side of (4.14) and (4.15) characterize the mapping relations between the unknown signal X and r in the healthy and faulty modes, respectively, based on which we can design $\mathbb{F}(\mathfrak{q})$ for different diagnosis purposes.

First, we consider the one-dimensional disturbance that can be fully decoupled. To ensure that the residual is zero in the healthy mode and sensitive to the faulty mode, i.e., $r = 0$ when $f = 0$ and $r \neq 0$ when $f = 1$, we introduce the following conditions:

$$N(\mathfrak{q})H(\mathfrak{q},0) = 0, \tag{4.16a}$$

$$N(\mathfrak{q})L_0 L_1^{\dagger} H(q,1) \neq 0. \tag{4.16b}$$

In view of the desired mapping relations (4.16a) and (4.16b), we proceed with the first problem.

Problem 1. (Fault detection filter design for perfect setting) *Consider the state-space model of the inverter-based microgrid system* (4.11) *with three-phase symmetrical ground faults and Assumption 4.2.1 with* $n_d = 1$. *Design a fault detection filter* $\mathbb{F}$ *in the form of* (4.13) *that satisfies* (4.16a) *and* (4.16b).

Remark 4.2.4 (Existence of $L_1^{\dagger}$)**.** *Note that the matrix* $\mathcal{B}_u(1) = [B_{uh1}\ B_{uh2}]$ *is of full column rank according to their structures in* (4.10). *Thus,* L_1 *is a full-column matrix and its left inverse exists.*

Second, when the disturbance d is a two-dimensional signal and cannot be fully decoupled, the condition (4.16a) can no longer be satisfied. A common solution is to constrain the $\mathcal{H}_\infty$ norm of the transfer function from d to r to suppress the effect of d. Here, inspired by the approach in [53, 107], we tackle the problem from a data-driven perspective. Specifically, we use the historical data of the disturbance to train the filter so that it is robust to the disturbance. To this end, let us split $H(\mathfrak{q},0)$ into two parts, i.e., $H(\mathfrak{q},0) = [E_1(\mathfrak{q},0)\ E_2]$, and matrices $E_1(\mathfrak{q},0), E_2$ are given by

$$E_1(\mathfrak{q},0) = \mathfrak{q}E_{11} + E_{10} = \begin{bmatrix} -\mathfrak{q}I + \mathcal{A}(0) \\ C \end{bmatrix},\ E_{11} = \begin{bmatrix} -I \\ 0 \end{bmatrix},\ E_{10} = \begin{bmatrix} \mathcal{A}(0) \\ C \end{bmatrix},\ \text{and } E_2 = \begin{bmatrix} \mathcal{B}_d(0) \\ 0 \end{bmatrix},$$

where $E_1(\mathfrak{q},0)$ corresponds to the unknown internal state x that can be decoupled and E_2 corresponds to the non-decoupled disturbance d. We obtain

$$\begin{aligned} r = \frac{1}{a(\mathfrak{q})} N(\mathfrak{q}) L_0[Y] &= -\frac{1}{a(\mathfrak{q})} N(\mathfrak{q}) H(\mathfrak{q},0)[X] \\ &= -\frac{1}{a(\mathfrak{q})} N(\mathfrak{q}) E_1(\mathfrak{q},0)[x] - \frac{1}{a(\mathfrak{q})} N(\mathfrak{q}) E_2[d]. \end{aligned} \tag{4.17}$$

To make the residual as small as possible in the healthy mode, we opt to decouple x from r, i.e.,

$$N(\mathfrak{q})E_1(\mathfrak{q},0) = 0. \tag{4.18}$$

We further suppose that the disturbance d comes from a prescribed probability space, and we have access to m independent identically distributed (iid) disturbance patterns d_i for $i \in \{1,\dots,m\}$. For each d_i, we define its contribution to the residual as

$$r_{d_i} = -\frac{1}{a(\mathfrak{q})}N(\mathfrak{q})E_2[d_i].$$

Therefore, we can mitigate the effects of the disturbance by constraining the $\mathcal{L}_2$ norm of r_{d_i} for all $i \in \{1,\dots,m\}$ in the healthy mode, i.e.,

$$\frac{1}{m}\sum_{i=1}^{m}\|r_{d_i}\|_{\mathcal{L}_2}^2 = \frac{1}{m}\sum_{i=1}^{m}\left\|\frac{1}{a(\mathfrak{q})}N(\mathfrak{q})E_2[d_i]\right\|_{\mathcal{L}_2}^2 \le \beta, \tag{4.19}$$

where $\beta \in \mathbb{R}_+$. We show later the approach to constructing $\|r_{d_i}\|_{\mathcal{L}_2}$ with a combination of the system model and the data d_i. The condition (4.16b) is adopted again to ensure the sensitivity of the residual to the faulty mode. Based on the above discussion, we formulate the second problem.

Problem 2. (Data-assisted robust fault detection filter design) *Consider the state-space model of the inverter-based microgrid system* (4.11) *with three-phase symmetrical ground faults and Assumption 4.2.1 with* $n_d = 2$. *Given multiple instances of the disturbance* d_i *for* $i \in \{1,\dots,m\}$, *find a fault detection filter* $\mathbb{F}$ *in the form of* (4.13) *that satisfies the conditions* (4.18), (4.19), *and* (4.16b).

4.3 Main Results

In this section, we present two design methods of fault detection filters in two scenarios: (i) the disturbance can be fully decoupled (i.e., perfect setting), and (ii) the disturbance cannot be fully decoupled.

4.3.1 Filter Design: Perfect Setting

We first consider the one-dimensional disturbance that can be fully decoupled. In order to find a feasible $N(\mathfrak{q})$ satisfying the conditions in Problem 1, we formulate the design of the fault detection filter as a linear programming problem in the following proposition.

Proposition 4.3.1 (Filter design: LP)**.** *Suppose that Assumption* (4.2.1) *holds and the dimension of the disturbance* $n_d = 1$. *Consider the unified state-space model of the inverter-based microgrid system* (4.11), *and the structure of the fault detection filter in* (4.13). *Given the degree* d_N, *a stable* $a(\mathfrak{q})$, *and a scalar* $\gamma \in \mathbb{R}_+$, *the detection conditions* (4.16a) *and* (4.16b) *in Problem 1 are satisfied if*

$$\bar{N}\bar{H}(0) = 0, \tag{4.20a}$$
$$\|\bar{N}\bar{L}\bar{H}(1)\|_\infty \ge \gamma, \tag{4.20b}$$

where $\bar{N} = [N_0,\ N_1,\ \ldots,\ N_{d_N}]$, $\bar{L} = diag\underbrace{[L_0 L_1^{\dagger},\ \ldots,\ L_0 L_1^{\dagger}]}_{d_N+1}$,

$$\bar{H}(f) = \begin{bmatrix} H_0(f) & H_1 & 0 & \ldots & 0 \\ 0 & H_0(f) & H_1 & 0 & \vdots \\ \vdots & 0 & \ddots & \ddots & 0 \\ 0 & \ldots & 0 & H_0(f) & H_1 \end{bmatrix}, \text{ and } f \in \{0,1\}.$$

Proof. According to the multiplication rule of polynomial matrices [53, Lemma 4.2], (4.16) can be written as

$$N(\mathfrak{q})H(\mathfrak{q},0) = \bar{N}\bar{H}(0)[I,\ \mathfrak{q}I,\ \ldots,\ \mathfrak{q}^{d_N+1}I]^{\top}, \tag{4.21a}$$

$$N(\mathfrak{q})L_0 L_1^{\dagger} H(q,1) = \bar{N}\bar{L}\bar{H}(1)[I,\ \mathfrak{q}I,\ \ldots,\ \mathfrak{q}^{d_N+1}I]^{\top}. \tag{4.21b}$$

First, one can see from (4.21a) that $\bar{N}\bar{H}(0) = 0$ is equivalent to condition (4.16a), i.e., $N(\mathfrak{q})H(\mathfrak{q},0) = 0$. Therefore, the residual in the healthy mode $r = N(\mathfrak{q})H(\mathfrak{q},0)[X] = 0$ and (4.16a) is satisfied. Second, we let the coefficients of $N(\mathfrak{q})L_0 L_1^{\dagger} H(q,1)$ be nonzero through (4.20b). Thus, (4.16b) is satisfied, which ensures the fault sensitivity. This completes the proof. □

Note that $\bar{N}\bar{L}\bar{H}(1)$ is a row vector with $(d_N+2)(n_x+n_d)$ columns. For a positive scalar γ, $\|\bar{N}\bar{L}\bar{H}(1)\|_{\infty} \geq \gamma$ holds if and only if $\bar{N}\bar{L}\bar{H}(1)v_i \geq \gamma$ or $\bar{N}\bar{L}\bar{H}(1)v_i \leq -\gamma$, where v_i is a $(d_N+2)(n_x+n_d)$-dimensional column vector with only the i-th element be 1 and the rest are zero, i.e., $v_i = [0,\ldots,1,\ldots,0]^{\top}$. Moreover, it is easy to check that if $\bar{N}^*$ is a solution to (4.20), so is $-\bar{N}^*$. Therefore, one can replace the constraint (4.20b) with $\bar{N}\bar{L}\bar{H}(1)v_i$ (or $-\bar{N}\bar{L}\bar{H}(1)v_i$) and view (4.20) as a set of $(d_N+2)(n_x+n_d)$ LP problems.

Remark 4.3.2 (Feasibility analysis)**.** *According to the well-known rank plus nullity theorem, we have* $(d_N+1)(n_x+n_y) = \mathrm{Rank}(\bar{H}(0)) + \mathrm{Null}(\bar{H}(0))$*, where* $\mathrm{Rank}(\bar{H}(0))$ *and* $\mathrm{Null}(\bar{H}(0))$ *denote the rank and the left null space dimension of* $\bar{H}(0)$*, respectively. Thus, the constraint* (4.20) *is feasible when* $\mathrm{Null}(\bar{H}(0)) \neq 0$*, i.e.,* $(d_N+1)(n_x+n_y) > \mathrm{Rank}(\bar{H}(0))$*. For the constraint* $\|\bar{N}\bar{L}\bar{H}(1)\|_{\infty} \geq \gamma$*, it is required that* $\bar{L}\bar{H}(1)$ *does not belong to the column range space of* $\bar{H}(0)$*, i.e.,* $\mathrm{Rank}([\bar{H}(0)\ \bar{L}\bar{H}(1)]) > \mathrm{Rank}(\bar{L}\bar{H}(1))$*. Otherwise, a feasible* $\bar{N}$ *to* (4.20a) *leads to* $\bar{N}\bar{L}\bar{H}(1) = 0$*.*

4.3.2 Filter Design: Non-decoupled Disturbance

In this subsection, we consider the disturbance d that cannot be fully decoupled. Recall that the residual r in the healthy mode depends on the decoupled internal state x and the non-decoupled disturbance d from the right-hand side of (4.17). For one instance of disturbances $d_i = [d_i(1),\ldots,d_i(T)]$ with a time horizon $T \in \mathbb{N}$, recall that its contribution to the residual is $r_{d_i} = -a^{-1}(\mathfrak{q})N(\mathfrak{q})E_2[d_i]$. Then, the response of the j-th element of d_i, i.e., $d_i(j)$, can be computed by

$$\left[r_{d_i(j)}(1),\ r_{d_i(j)}(2),\ \ldots,\ r_{d_i(j)}(T)\right] = -N(\mathfrak{q})E_2 d_i(j)\ell_j,$$

where $\ell_j = [\overbrace{0,\dots,0}^{j-1}, \bar{\ell}(1), \bar{\ell}(2), \dots, \bar{\ell}(T-j+1)]$ and $\bar{\ell}(k)$ for $k \in \mathbb{N}$ is the value of the discrete-time unit impulse response of $a^{-1}(\mathfrak{q})$ at time instance k. By summing up the response of $d_i(j)$ for $j \in \{1,\dots,T-d_N-1\}$, we obtain

$$\begin{aligned}\left[r_{d_i}(1),\, r_{d_i}(2),\, \dots,\, r_{d_i}(T)\right] &= -N(\mathfrak{q})E_2 \sum_{j=1}^{T-d_N-1} d_i(j)\ell_j \\ &= -\bar{N}\bar{E}_2 \begin{bmatrix} I \\ \mathfrak{q}I \\ \vdots \\ \mathfrak{q}^{d_N+1}I \end{bmatrix} [d_i(1),\, \dots,\, d_i(T-d_N-1)] \begin{bmatrix} \ell_1 \\ \vdots \\ \ell_{T-d_N-1} \end{bmatrix}, \end{aligned} \tag{4.22}$$

where $\bar{E}_2 = \mathrm{diag}(E_2,\dots,E_2)$ according to the multiplication rule of polynomial matrices. Recall that $\mathfrak{q}$ is a time shift operator, i.e., $\mathfrak{q}d_i(k) = d_i(k+1)$. Thus, the equation (4.22) can be written as

$$\begin{aligned}\left[r_{d_i}(1),\, r_{d_i}(2),\, \dots,\, r_{d_i}(T)\right] &= -\bar{N}\bar{E}_2 \begin{bmatrix} d_i(1) & \dots & d_i(T-d_N-1) \\ d_i(2) & \dots & d_i(T-d_N) \\ \vdots & \ddots & \vdots \\ d_i(d_N+2) & \dots & d_i(T) \end{bmatrix} \begin{bmatrix} \ell_1 \\ \vdots \\ \ell_{T-d_N-1} \end{bmatrix} \\ &= -\bar{N}\bar{E}_2 D_i \Gamma. \end{aligned} \tag{4.23}$$

To ensure the existence of D_i, we assume that the length of data T is greatly larger than $d_N + 1$, i.e., $T \gg d_N + 1$. With (4.23), the $\mathcal{L}_2$ norm of r_{d_i} as considered in Problem 2 is formulated into the quadratic form

$$\|r_{d_i}\|_{\mathcal{L}_2}^2 = \bar{N}\Phi_i\bar{N}^\top, \quad \Phi_i = \bar{E}_2 D_i \Gamma (\bar{E}_2 D_i \Gamma)^\top. \tag{4.24}$$

It is worth emphasizing that Φ_i is positive semi-definite since $\|r_{d_i}\|_{\mathcal{L}_2}^2 = \bar{N}\Phi_i\bar{N}^\top \geq 0$ for all non-zero $\bar{N}$.

Now, we can present the design method of the fault detection filter in the presence of non-decoupled disturbances in the following theorem.

Theorem 4.3.3 (Filter design: QP)**.** *Consider the unified state-space model of the inverter-based microgrid system* (4.11)*, Assumption* (4.2.1) *with the two-dimensional disturbance, and the structure of the fault detection filter in* (4.13)*. Given the degree d_N, a stable $a(\mathfrak{q})$ and multiple instances of disturbance $d_i = [d_i(1),\dots,d_i(T)]$ for $i \in \{1,\dots,m\}$ with the length $T \gg d_N$, the conditions* (4.18), (4.19)*, and* (4.16b) *in Problem 2 are satisfied by solving the following optimization problem*

$$\begin{aligned} &\min_{\bar{N}} \ \bar{N}\bar{\Phi}\bar{N}^\top - \|\bar{N}\bar{L}\bar{H}(1)\|_\infty \\ &\text{s.t. } \bar{N}\bar{E}_1 = 0, \end{aligned} \tag{4.25}$$

where $\bar{\Phi} = \frac{1}{m}\sum_{i=1}^{m}\Phi_i$,

$$\bar{E}_1 = \begin{bmatrix} E_{10} & E_{11} & 0 & \dots & 0 \\ 0 & E_{10} & E_{11} & 0 & \vdots \\ \vdots & 0 & \ddots & \ddots & 0 \\ 0 & \dots & 0 & E_{10} & E_{11} \end{bmatrix}.$$

Proof. The first term in the objective function, i.e., $\bar{N}\bar{\Phi}\bar{N}^\top$, relates to the condition (4.19), which ensures that the effects of different instances of disturbances on the residual are bounded. We show the derivation process of the quadratic form of $\|r_{d_i}\|^2_{\mathcal{L}_2}$ in (4.22)-(4.24). The second term in the objective function, i.e., $-\|\bar{N}\bar{L}\bar{H}(1)\|_\infty$, relates to the condition (4.16b), which is introduced to ensure the sensitivity of residual to the faulty mode. The constraint $\bar{N}\bar{E}_1 = 0$ related to the condition (4.18) is used to decouple the internal state x from the residual. One can show through the multiplication rule of polynomial matrices that $N(\mathfrak{q})E_1(\mathfrak{q},0) = 0 \Leftrightarrow \bar{N}\bar{E}_1 = 0$. This completes the proof. □

Note that one can view the optimization problem (4.25) as a set of $(d_N+2)(n_x+n_d)$ QP problems by replacing $\|\bar{N}\bar{L}\bar{H}(1)\|_\infty$ with $\bar{N}\bar{L}\bar{H}(1)v_i$ (or $-\bar{N}\bar{L}\bar{H}(1)v_i$) as analyzed before. Recall that $v_i = [0,\dots,1,\dots,0]^\top$. In addition, the matrix Φ_i is positive semi-definite, and thus the derived QP problems are convex and tractable. We further derive an approximate analytical solution to (4.25) in the following corollary.

Corollary 4.3.4 (Approximate analytical solution)**.** *Consider the optimization problem* (4.25)*. There exists an approximate analytical solution given by the following form:*

$$\bar{N}^*(\gamma) = \frac{1}{2\gamma}\left(\bar{L}\bar{H}(1)v_i^*\right)^\top\left(\gamma^{-1}\bar{\Phi} + \bar{E}_1\bar{E}_1^\top\right)^{-1}, \tag{4.26}$$

where $v_i^* = \arg\max_{i\in\{1,\dots,(d_N+2)(n_x+n_d)\}}|\bar{N}^*(\gamma)\bar{L}\bar{H}(1)v_i|$ *and* $\gamma \in \mathbb{R}_+$ *is the Lagrange multiplier. The solution* $\bar{N}^*(\gamma)$ *provides an approximate solution to* (4.25) *and will converge to the optimal solution as* γ *tends to* ∞*.*

Proof. The Lagrange function of (4.25) is

$$\mathcal{L}(\bar{N},\gamma) = \bar{N}\bar{\Phi}\bar{N}^\top - \|\bar{N}\bar{L}\bar{H}(1)\|_\infty + \gamma\|\bar{N}\bar{E}_1\|_2^2.$$

Since the optimization problem (4.25) can be viewed as a set of QP problems by replacing the term $\|\bar{N}\bar{L}\bar{H}(1)\|_\infty$ with $\bar{N}\bar{L}\bar{H}(1)v_i$, the set of the Lagrange functions is

$$\mathcal{L}_i(\bar{N},\gamma) = \bar{N}\bar{\Phi}\bar{N}^\top - \bar{N}\bar{L}\bar{H}(1)v_i + \gamma\|\bar{N}\bar{E}_1\|_2^2. \tag{4.27}$$

By taking the partial derivative of $\mathcal{L}_i(\bar{N},\gamma)$, we have

$$\frac{\partial\mathcal{L}_i(\bar{N},\gamma)}{\partial\bar{N}} = 2\bar{N}\bar{\Phi} + 2\gamma\bar{N}\bar{E}_1\bar{E}_1^\top - (\bar{L}\bar{H}(1)v_i)^\top.$$

4

Setting the partial derivative to zero leads to

$$\bar{N}_i^* = \frac{1}{2\gamma}\left(\bar{L}\bar{H}(1)v_i\right)^\top\left(\gamma^{-1}\bar{\Phi}+\bar{N}\bar{E}_1\bar{E}_1^\top\right)^{-1},$$

which is an admissible solution to the problem with the dual function (4.27). By choosing v_i for $i \in \{1,\dots,(d_N+2)(n_x+n_d)\}$ which maximizes $|\bar{N}\bar{L}\bar{H}(1)v_i|$, we obtain (4.26), i.e.,

$$\bar{N}^* = \frac{1}{2\gamma}\left(\bar{L}\bar{H}(1)v_i^*\right)^\top\left(\gamma^{-1}\bar{\Phi}+\bar{N}\bar{E}_1\bar{E}_1^\top\right)^{-1},$$

where $v_i^* = \arg\max_{i\in\{1,\dots,(d_N+2)(n_x+n_d)\}}|\bar{N}^*(\gamma)\bar{L}\bar{H}(1)v_i|$. By penalizing the equality constraint, we obtain the dual function, i.e., $g_i(\gamma) := \inf_{\bar{N}}\mathcal{L}_i(\bar{N},\gamma)$. It holds that

$$\sup_{\gamma\geq 0} g_i(\gamma) = \lim_{\gamma\to\infty}\mathcal{L}_i(\bar{N},\gamma).$$

Substituting $\bar{N}^*$ into the dual function leads to

$$\begin{cases} \max\limits_{\gamma} & -\frac{1}{4\gamma}\left(\bar{L}\bar{H}(1)v_i^*\right)^\top\left(\gamma^{-1}\bar{\Phi}+\bar{N}\bar{E}_1\bar{E}_1^\top\right)^{-1}\left(\bar{L}\bar{H}(1)v_i^*\right), \\ \text{s.t.} & \gamma \geq 0. \end{cases}$$

This quadratic negative (semi-)definite problem reaches its maximum when γ tends to infinity. This completes the proof. □

Remark 4.3.5 (Average objective function)**.** *To ensure that the derived fault detection filter is robust to the disturbance, we consider m different disturbance patterns d_i for $i \in \{1,\dots,m\}$ and take the average effects of all d_i on the residual as the objective function in* (4.25)*. An alternative way is to consider the worst-case scenario as the objective function, i.e.,* $\max_{i\in\{1,\dots,m\}}\bar{N}\Phi_i\bar{N}^\top$*. The average objective function is, however, of interest if one requires to train the filter with a large number of disturbance patterns. This is due to the fact that the computational complexity of the derived quadratic programming problem is independent of the number of disturbance patterns m with the average objective function.*

Remark 4.3.6 (Online updating of coefficients)**.** *In [107], the authors construct the objective function using the model mismatch data to ensure that the derived filter is robust to the mismatch. Compared to [107], we further derive an approximate analytical solution to the optimization problem* (4.25)*. With the analytical solution, one can update the coefficients of the filter online with new data without the need to re-solve* (4.25)*. This is a significant improvement over [107].*

Remark 4.3.7 (Approximate analytical solution with γ)**.** *The Lagrange multiplier γ is introduced in* (4.25) *to penalize the equality constraint $\bar{N}\bar{E}_1 = 0$, and in the ideal case, γ tends to infinity as stated in Corollary 4.3.4. However, for a bounded γ, the equality constraint cannot be strictly satisfied, which is why we refer to the solution* (4.26) *as an approximate analytical solution. Additionally, to ensure that $\bar{N}\bar{E}_1$ is sufficiently close to zero, γ should be large enough while remaining numerically bounded for practical considerations.*

To detect the fault, we introduce the power of the residual $r(k)$ as the evaluation function, i.e., $J(r) = r(k)^2$ for $k \in \mathbb{N}$. Let J_{th} be the detection threshold. Then, we can consider the following detection logic:

$$\begin{cases} J(r) \leq J_{th} & \Rightarrow \quad \text{no faults,} \\ J(r) > J_{th} & \Rightarrow \quad \text{faults.} \end{cases}$$

It is worth emphasizing that false alarms are inevitable due to the random nature of the residual. We show the computation method of the threshold and the false alarm rate in the following proposition.

Proposition 4.3.8 (Probabilistic performance)**.** *Assume that the disturbance patterns follow the iid. distribution. Consider the system* (4.11)*, the filter* $\mathbb{F}(\mathfrak{q})$ *obtained by using* (4.25) *with the corresponding solution* $\bar{N}^*$*, and the evaluation function* $J(r) = r(k)^2$ *for* $k \in N$*. Given a scalar* $\lambda \geq 1$*, if we set the threshold* J_{th} *as*

$$J_{th} = \frac{\lambda}{T} \bar{N}^* \bar{\Phi} \bar{N}^{*\top}, \tag{4.28}$$

the false alarm rate in the steady state satisfies

$$\begin{aligned} &\lim_{k\to\infty} \mathbf{Pr}\{J(r(k)) > J_{th} | f = 0\} \\ =&\lim_{T,k,m\to\infty} \mathbf{Pr}\left\{ r(k)^2 > \frac{\lambda}{T} \bar{N}^* \left(\frac{1}{m} \sum_{i=1}^{m} \Phi_i \right) \bar{N}^{*\top} \middle| f = 0 \right\} \leq \frac{1}{\lambda}. \end{aligned} \tag{4.29}$$

Proof. Since the disturbance d comes from a prescribed probability space and each disturbance pattern follows iid distribution, the residual in the healthy mode can be viewed as a random variable on the same probability space as d, i.e., $r = -a^{-1}(\mathfrak{q}) N(\mathfrak{q}) E_2[d]$. It is proven in [53, Theorem 4.11] that the empirical average error

$$e_m = \frac{1}{m} \sum_{i=1}^{m} \|r_{d_i}\|_{\mathcal{L}_2}^2 - \mathbf{E}\left[\|r\|_{\mathcal{L}_2}^2 \right],$$

satisfies the strong law of large numbers, i.e., $\lim_{m\to\infty} e_m = 0$ almost surely. Therefore, it holds that

$$\lim_{T,m\to\infty} \frac{\lambda}{T} \bar{N}^* \left(\frac{1}{m} \sum_{i=1}^{m} \Phi_i \right) \bar{N}^{*\top} = \lim_{T,m\to\infty} \frac{\lambda}{T} \frac{1}{m} \sum_{i=1}^{m} \|r_{d_i}\|_{\mathcal{L}_2}^2 = \lim_{T\to\infty} \frac{\lambda}{T} \mathbf{E}\left[\|r\|_{\mathcal{L}_2}^2 \right] = \lambda \lim_{k\to\infty} \mathbf{E}[r(k)^2].$$

According to Markov inequality, the false alarm rate in the steady state satisfies

$$\lim_{k\to\infty} \mathbf{Pr}\{r(k)^2 > \lambda \mathbf{E}[r(k)^2] | f = 0\} \leq \frac{1}{\lambda}.$$

This completes the proof. □

4.4 Simulation Results

In this section, we validate the performance of the fault detection filters through numerical simulations. The optimization problems are solved through the YALMIP toolbox [126]. Consider the inverter-based microgrid system depicted in Figure 4.1. We refer to the parameters and initial conditions in [164], which are presented in Table 4.1 and Table 4.2, respectively. The reference voltage (operating point) of the microgrid is $v^*_{odq} = [381, 0]^\top$ and the FCL parameter is $\tau_{dq} = [35, 0.7]^\top$, which are assumed to be constant during the experiment. The sampling period is 0.1 ms and the simulation time is 500 ms.

Table 4.1: Microgrid parameters.

Parameter	Value	Parameter	Value
f	50 Hz	R_{LOAD}	12 Ω
L_f	0.1 mH	K_P^c	28
R_f	0.1 Ω	K_I^c	5
C_f	30μ F	K_P^v	0.1
L_c	1 mH	K_I^v	170
R_c	0.03 Ω	F	0.75
ω	314.1		

Table 4.2: Initial conditions.

Parameter	Value	Parameter	Value
v_{od}	380.8	i_{ld}	11.4
v_{oq}	0	i_{lq}	-5.5×10^3
i_{od}	11.4	v_{bd}	379.5
i_{oq}	0.4	v_{bq}	-6
ϕ_d	0.13	γ_d	0.0115
ϕ_q	0	γ_q	0

4.4.1 Scenario 1: Perfect Setting

We first consider the perfect setting with one-dimensional disturbances that can be fully decoupled, as described in Remark 4.2.2. We set the matrix $B_d = [\mathbf{0}_{1\times8}\ [1\ 1]]^\top$. The disturbance is zero for $k \leq 1000$ and, subsequently, it follows a signal given by

$$d(k) = \alpha_0 + \sum_{i=1}^{\eta} \alpha_i \sin(\omega_i k + \psi_i),\ k > 1000.$$

Specifically, the constant $\alpha_0 \in \mathbb{R}$ represents an abrupt change, while the sinusoidal terms capture the short-term load fluctuations with amplitudes α_i, angular frequencies $\omega_i \in \mathbb{R}_+$, and phases $\psi_i \in \mathbb{R}$ [53]. It is worth emphasizing that we deliberately select the parameters of B_d and magnitude of d to make the output currents similar in the faulty mode and under the effect of the disturbance, which increases the difficulty of fault detection.

To design the fault detection filter in the form of (4.13), we fix the degree of $N(\mathfrak{q})$ to be $d_N = 10$, set $\gamma = 0.5$, and choose a stable denominator $a(\mathfrak{q})$ with a degree larger than d_N. We then apply Proposition 4.3.1 to construct the fault detection filter for inverter-based microgrid systems with the disturbance that can be fully decoupled. The detection threshold is set to $J_{th} = 1 \times 10^{-5}$. The simulation results are presented in Figure 4.2 and Figure 4.3.

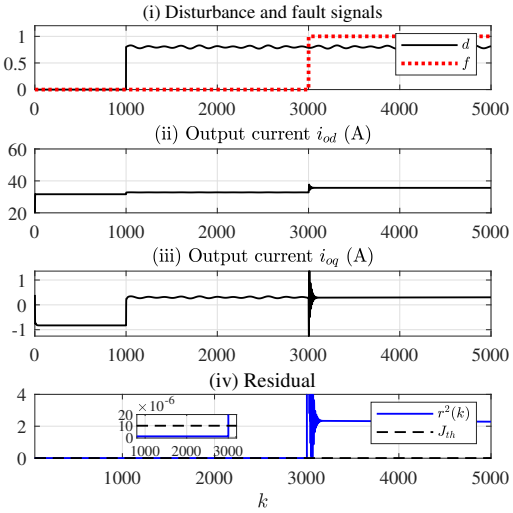

Figure 4.2: Diagnosis results in a perfect setting with small load fluctuations.

Figure 4.2 presents the diagnosis results when a decoupled disturbance has small load fluctuations, i.e.,

$$d(k) = 0.8 + 0.02\sin(k/30) + 0.01\sin(k/40) + 0.01\sin(k/60).$$

As shown in Figure 4.2 (i), the disturbance d and the ground fault f occur at $k = 1001$ and $k = 3001$, respectively. However, d and f have similar effects on the output currents i_{od} and i_{oq} from Figure 4.2 (ii) and (iii), which only exhibit minor variations. This makes it challenging to detect the occurrence of the ground fault and distinguish it from the disturbance only through the output currents.

In contrast, Figure 4.2 (iv) illustrates that the residual is insensitive to the disturbance and stays below the threshold until the fault happens. The power value of the residual $r^2(k)$ exceeds the threshold at $k = 3002$, resulting in the detection of the fault within 0.1 ms. We further consider a decoupled disturbance with larger load fluctuations, i.e.,

$$d(k) = 0.8 + 0.2\sin(k/30) + 0.3\sin(k/40) + 0.2\sin(k/60).$$

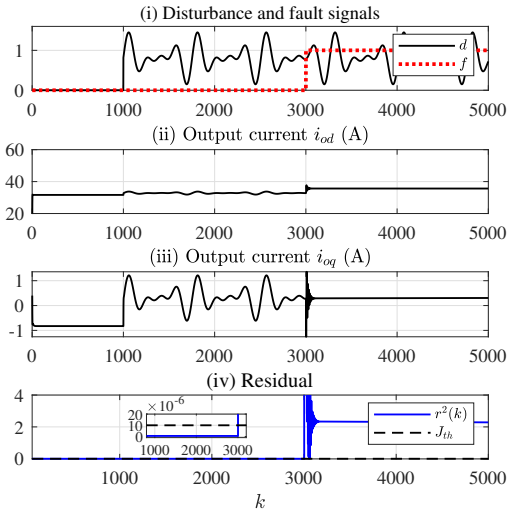

Figure 4.3: Diagnosis results in a perfect setting with large load fluctuations.

Figure 4.3 displays the diagnosis results and the analysis process is analogous to the previous one.

4.4.2 Scenario 2: Non-decoupled Disturbance

In this subsection, we consider two-dimensional disturbances that cannot be fully decoupled. The matrix $B_d = []\mathbf{0}_{2\times 8}\ \mathrm{diag}([0.5\ 0.5])]^\top$. To capture the disturbance, following [53], we denote the space of disturbance patterns by

$$d(k) = \begin{bmatrix} \alpha_{d,0} + \sum_{i=1}^{\eta} \alpha_{d,i} \sin(\omega_{d,i} k + \psi_{d,i}) \\ \alpha_{q,0} + \sum_{i=1}^{\eta} \alpha_{q,i} \sin(\omega_{q,i} k + \psi_{q,i}) \end{bmatrix},$$

where the parameters $(\alpha_{d,i})_{i=0}^{\eta}$, $(\alpha_{q,i})_{i=0}^{\eta}$, $(\omega_{d,i})_{i=1}^{\eta}$, $(\omega_{q,i})_{i=1}^{\eta}$, $(\psi_{d,i})_{i=1}^{\eta}$, $(\psi_{q,i})_{i=1}^{\eta}$, and η are random variables and follow uniform distributions in certain bounds. We generate 30 disturbance patterns (i.e., $m = 30$ in (4.19)) and choose the time horizon $T = 50$. Again, we fix $d_N = 10$ and choose a stable denominator $a(\mathfrak{q})$. With the above settings, we can generate the matrix $\bar{\Phi}$ in the objective function of the optimization problem (4.25). We construct robust fault detection filters by using Theorem 4.3.3 to deal with the fault detection problem for inverter-based microgrid systems with non-decoupled disturbances. The simulation results are presented in Figures 4.4-4.6.

Figure 4.4 provides the diagnosis result by using (4.25) in the presence of a non-decoupled disturbance with small load fluctuations. Let $U(l_1, l_2)$ denote a uniform distribution taking values between l_1 and l_2. Then, for disturbances with small load fluctuations, the parameters of the disturbance d are $\alpha_{d,0}, \alpha_{q,0} \sim U[1,2]$, $\alpha_{d,i}, \alpha_{q,i} \sim U[0, 0.05]$, $\omega_{d,i}, \omega_{q,i} \sim U[1/80, 1/40]$, and $\psi_{d,i}, \psi_{q,i} \sim U[0, 100]$. We compute the threshold $J_{th} = 0.0018$ based on (4.28) with $\lambda = 3$.

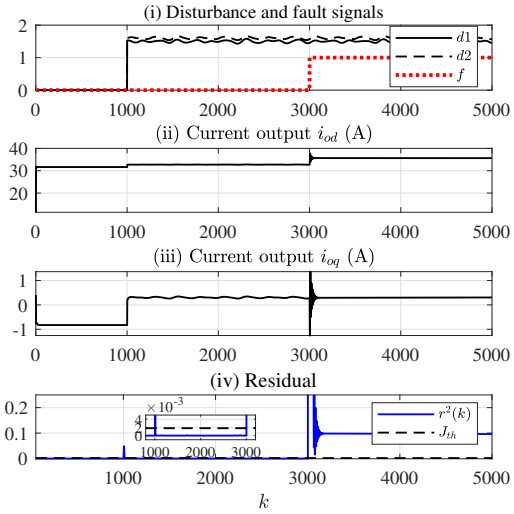

Figure 4.4: Diagnosis results with non-decoupled disturbances and small load fluctuations.

As shown in Figure 4.4 (i), the disturbance d and the ground fault f happen at $k = 1001$ and $k = 3001$, respectively. However, it is difficult to distinguish d and f through the output currents from Figure 4.4 (ii) and (iii). The power value of the residual $r^2(k)$ is shown in Figure 4.4 (iv), one can see that $r^2(k)$ remains below the threshold in the presence of non-decoupled disturbances until the occurrence of the fault at $k = 3001$. This suggests that the proposed filter effectively suppresses the effects of disturbances on the residual. Although there is a spike in the residual caused by the transient response of the step signal in the disturbance, it disappears quickly. After the fault happens, the value of $r^2(k)$ immediately exceeds the threshold and remains significantly higher than zero. This indicates that the fault is successfully detected and is distinguishable from the disturbance through the residual. To further verify the robustness of the fault detection filter to disturbances, we opted for a non-decoupled disturbance with larger fluctuations, where $\alpha_{d,0}, \alpha_{q,0} \sim U[0.5, 1]$, $\alpha_{d,i}, \alpha_{q,i} \sim U[0, 0.5]$, $\omega_{d,i}.\omega_{q,i} \sim U[1/60, 1/30]$, and $\psi_{d,i}, \psi_{q,i} \sim U[0, 100]$. Since the disturbance patterns vary, it is necessary to regenerate the matrix $\bar{\Phi}$ and redesign the filter using (4.25). We calculated the threshold $J_{th} = 0.0091$ based on (4.28) with $\lambda = 10$. The diagnosis results in the presence of large load fluctuations are presented in Figure 4.5. The analysis process is similar to the previous one and, therefore, omitted here. In Figure 4.6, we show that the approximate analytical solutions in (4.26) with larger γ have better diagnosis performance.

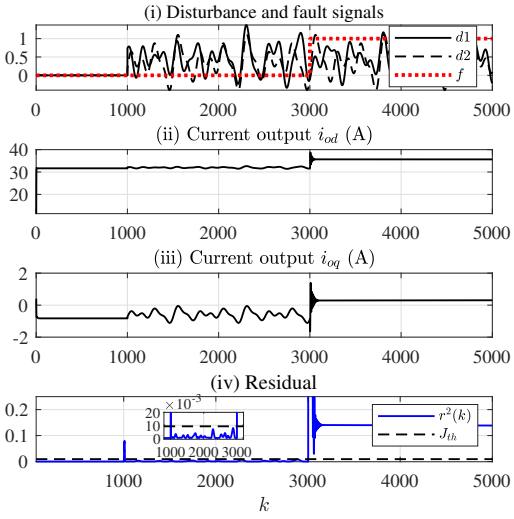

Figure 4.5: Diagnosis results with non-decoupled disturbances and large load fluctuations.

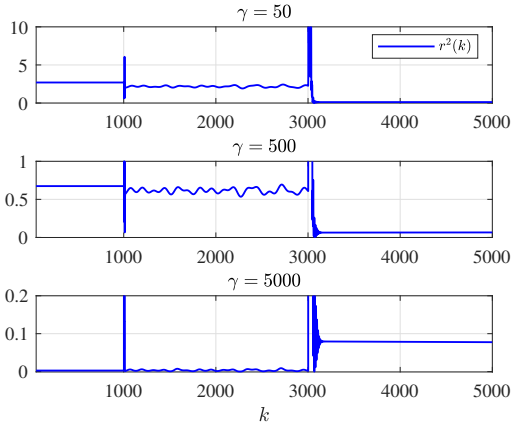

Figure 4.6: Diagnosis results by using approximate solutions (4.26) with different γ.

4.5 Conclusions

In this chapter, we proposed diagnosis strategies for the detection of ground faults in inverter-based microgrid systems with decoupled and non-decoupled disturbances, respectively. Our strategies involve developing fault detection filters to deal with disturbances and ensure fault sensitivity. To achieve this, we reformulate the filter design problem into tractable optimization problems, which enable us to efficiently optimize the filter parameters and meet the desired performance criteria. Simulation results on an inverter-based microgrid system that works in the islanded mode show the effectiveness of the proposed approaches. In future work, we first will consider designing the denominator of the filter for better dynamic performance. The second direction will be focused on extending the proposed approaches to more complex and realistic settings, such as considering the presence of multiple converters that introduce nonlinearity into the model.

5

Conclusions and Recommendations

This thesis aims to improve the reliability and safety of industrial systems by designing novel and effective model-based fault diagnosis schemes. Motivated by the fact that a scalable diagnosis system can effectively reduce the computational complexity when dealing with complex modern industrial systems, we opt to design residual generators in the framework of differential-algebraic equations, which results in residual generators with the possibly lower order. Furthermore, we develop an optimization framework to determine the parameters of residual generators to achieve certain diagnosis requirements including decoupling faults, suppressing disturbances, and enhancing fault sensitivity within a specific frequency range. Additionally, we propose evaluation methods for residuals and threshold determination methods to provide probabilistic guarantees on false alarms and missing detection rates. We apply these fault diagnosis methods to building radiant systems, multi-area power systems, and microgrid systems to validate their performance.

In what follows, we summarize the results of this thesis and present some future research directions.

First problem

Summary. In this part, we study a diagnosis scheme to reliably detect the active mode of discrete-time, switched affine systems in the presence of measurement noise and asynchronous switching. The proposed scheme consists of two parts: (i) the construction of a bank of filters, and (ii) the introduction of a residual/threshold-based diagnosis rule. By combining residual generation and $\mathcal{H}_2$ norm approaches, we formulate an optimization problem to design an optimal bank of filters that minimizes the noise contribution to the residuals. The diagnosis performance is also analyzed. Specifically, we determine diagnosis thresholds that provide probabilistic false-alarm guarantees on the mode detection performance and compute the estimate of diagnosis time.

Future research directions. There are several directions related to this project that can be further explored.

- **Active fault diagnosis.** In order to distinguish between matched and unmatched residuals, we set the transfer function from the reference signal to the matched residual to zero, while ensuring that the steady-state gain of the transfer function from the reference signal to the remaining unmatched residuals is greater than or equal to 1. However, matched and unmatched residuals may overlap when the reference signal is small. One potential solution is to utilize the concept of active fault diagnosis, which involves designing input sequences that can reliably separate the unmatched residuals from the matched residual with a high probability.

- **Controller design and stochastic stability analysis.** Stochastic noise introduces randomness into the delay between the active mode and its corresponding controller, which can impact system performance. As a result, it is meaningful to design controllers that are resilient to random delays and analyze the stability of asynchronously switched systems. Note that we have obtained the distribution of delay times in our result, which can also be useful in this context.

Second problem

Summary. To address the conservatism involved in traditional fault diagnosis methods that are designed for the entire frequency domain, we introduce the frequency information of faults into the design of fault detection and estimation filters. We first develop an exact optimization framework to solve the fault detection filter that simultaneously decouples unknown inputs, suppresses noise, and enhances fault sensitivity in the finite frequency domain. A threshold determination method that provides probabilistic guarantees on false alarms and fault detection rates is proposed too. It is worth emphasizing that the proposed design approach allows for residuals of arbitrary dimensions, which is a significant improvement over previous methods. Second, we adjust the constraints in the proposed optimization framework and obtain the design method for the fault estimation filter. To reduce computational complexity, we further relax fault estimation conditions stated in the constraints and formulate a quadratic programming problem to obtain the desired fault estimation filter.

Future research directions. There are several directions related to this project that can be further explored.

- **Fault-tolerant control.** After obtaining diagnosis results, it is natural to consider designing a fault-tolerant control system that utilizes the estimate of faults to compensate for the performance degradation caused by faults. However, as mentioned in [168], there exists a robustness interaction between the fault estimation filter and fault-tolerant controller. Specifically, the uncertainties, disturbances, and noise will affect the fault estimation performance, and the fault estimation error will further affect the performance of the fault-tolerant controller. Therefore, it is of interest to find a framework to achieve an integrated design of the fault estimation filter and fault-tolerant controller.

- **Fault diagnosis for nonlinear systems.** Given that nonlinearity is ubiquitous in practical systems, it is intriguing to explore the extension of optimization-based fault diagnosis methods derived in the framework of differential-algebraic equations to nonlinear systems while considering faults in the finite frequency domain.

Third problem

Summary. The last problem we solve is more application-oriented. We consider ground fault detection for inverter-based microgrid systems. Different from previous results, we consider disturbances that cannot be fully decoupled here. To tackle this challenge, we leverage available disturbance patterns to train the fault detection filter and enhance its resilience to disturbances. We formulate the design problem as a quadratic programming problem, which has an approximate analytical solution with arbitrary precision. Additionally, we establish a threshold to ensure the desired probabilistic diagnosis performance.

Future research directions. There are several directions related to this project that can be further explored.

- **More realistic settings.** We consider an inverter-based microgrid that operates in isolated mode and has a single converter with balanced ground faults. However, it is worth noting that in practice, faults in microgrids are often unbalanced and grids usually involve multiple converters and synchronous machines. Therefore, extending the current approach to more realistic settings is valuable.

- **Application on hardware.** To validate the effectiveness of the proposed detection technique, we conducted simulations using MATLAB. However, it would be valuable to further test the approach on a practical microgrid system.

We also mention several other research directions to extend the results of this thesis.

- **Attack resilient system design.** Modern industrial systems are vulnerable to attacks due to the existence of various wireless communication devices. The fault diagnosis methods developed here may not be fully effective in detecting cyber-attacks because they are intentionally designed to be covert. As a result, it is necessary to model attack signals to account for all potential signals and to design controllers and filters capable of maintaining system security under attacks.

  Considering the different characteristics of attack signals and fault signals, it is necessary to construct novel metrics to jointly characterize the impact and detectability of attacks. We can then improve the filter design approach based on the proposed metrics to simultaneously suppress the impact and enhance the detectability of attacks.

- **Data-driven and learning-based fault diagnosis.** Our results are focused on model-based fault diagnosis methods. However, in engineering practice, the analytical model of systems may be difficult to obtain. A workable solution is to use data-driven methods to approximate the model mismatches or uncertainties.

  Note that pure data-driven methods developed primarily in the machine learning literature neglect knowledge about the underlying dynamics of systems. Therefore, we can combine our model-based methods with data-driven methods to develop a data-assisted model-based diagnosis method that makes full use of the available information.

- **Fault diagnosis for distributed systems.** Large-scale infrastructures, including electric power systems, water distribution networks, and transportation systems,

are interconnected both physically and through communication networks. This interconnection increases the vulnerability of these infrastructures to potential attacks or failures.

It would be beneficial and worthwhile to expand the diagnostic methods developed in this study to distributed systems. For example, we can design a local diagnosis filter for each subsystem and obtain the local diagnostic decision based on the interconnection with neighboring subsystems to improve fault detectability in distributed systems.

Bibliography

References

[1] Steven X Ding. *Model-based fault diagnosis techniques: design schemes, algorithms, and tools*. Springer Science & Business Media, 2008.

[2] Zhiwei Gao, Carlo Cecati, and Steven X Ding. A survey of fault diagnosis and fault-tolerant techniques—part I: Fault diagnosis with model-based and signal-based approaches. *IEEE Transactions on Industrial Electronics*, 62(6):3757–3767, 2015.

[3] M Bin Shams, H Budman, and T Duever. Finding a trade-off between observability and economics in the fault detection of chemical processes. *Computers & Chemical Engineering*, 35(2):319–328, 2011.

[4] Pouyan Pourbeik, Prabha S Kundur, and Carson W Taylor. The anatomy of a power grid blackout-root causes and dynamics of recent major blackouts. *IEEE Power and Energy Magazine*, 4(5):22–29, 2006.

[5] Husam Kharoufah, John Murray, Glenn Baxter, and Graham Wild. A review of human factors causations in commercial air transport accidents and incidents: From to 2000–2016. *Progress in Aerospace Sciences*, 99:1–13, 2018.

[6] Stephen Frank, Xin Jin, Daniel Studer, and Amanda Farthing. Assessing barriers and research challenges for automated fault detection and diagnosis technology for small commercial buildings in the united states. *Renewable and Sustainable Energy Reviews*, 98:489–499, 2018.

[7] R Vilela, JC Metrolho, and JC Cardoso. Machine and industrial monitorization system by analysis of acoustic signatures. In *Proceedings of the 12th IEEE Mediterranean Electrotechnical Conference (IEEE Cat. No. 04CH37521)*, volume 1, pages 277–279. IEEE, 2004.

[8] Dirk van Schrick. Remarks on terminology in the field of supervision, fault detection and diagnosis. *IFAC Proceedings Volumes*, 30(18):959–964, 1997.

[9] Mogens Blanke, Michel Kinnaert, Jan Lunze, Marcel Staroswiecki, and Jochen Schröder. *Diagnosis and fault-tolerant control*, volume 2. Springer, 2006.

[10] Steven X Ding. Integrated design of feedback controllers and fault detectors. *Annual Reviews in Control*, 33(2):124–135, 2009.

[11] Inseok Hwang, Sungwan Kim, Youdan Kim, and Chze Eng Seah. A survey of fault detection, isolation, and reconfiguration methods. *IEEE Transactions on Control Systems Technology*, 18(3):636–653, 2009.

[12] Paul M Frank. Fault diagnosis in dynamic systems using analytical and knowledge-based redundancy: A survey and some new results. *Automatica*, 26(3):459–474, 1990.

[13] Peter W Tse, YH Peng, , and Richard Yam. Wavelet analysis and envelope detection for rolling element bearing fault diagnosis—their effectiveness and flexibilities. *J. Vib. Acoust.*, 123(3):303–310, 2001.

[14] Pablo Lezana, Ricardo Aguilera, and José Rodríguez. Fault detection on multicell converter based on output voltage frequency analysis. *IEEE Transactions on Industrial Electronics*, 56(6):2275–2283, 2009.

[15] Qiao SUN and Ying Tang. Singularity analysis using continuous wavelet transform for bearing fault diagnosis. *Mechanical Systems and Signal Processing*, 16(6):1025–1041, 2002.

[16] Khalid F Al-Raheem, Asok Roy, KP Ramachandran, David K Harrison, and Steven Grainger. Application of the laplace-wavelet combined with ann for rolling bearing fault diagnosis. *Journal of Vibration and Acoustics*, 130(5), 2008.

[17] Zhi Ke Peng and FL Chu. Application of the wavelet transform in machine condition monitoring and fault diagnostics: a review with bibliography. *Mechanical Systems and Signal Processing*, 18(2):199–221, 2004.

[18] Zhipeng Feng, Ming Liang, and Fulei Chu. Recent advances in time-frequency analysis methods for machinery fault diagnosis: A review with application examples. *Mechanical Systems and Signal Processing*, 38(1):165–205, 2013.

[19] Bo Li, M-Y Chow, Yodyium Tipsuwan, and James C Hung. Neural-network-based motor rolling bearing fault diagnosis. *IEEE Transactions on Industrial Electronics*, 47(5):1060–1069, 2000.

[20] Jonathan M Vinson and Lyle H Ungar. Dynamic process monitoring and fault diagnosis with qualitative models. *IEEE Transactions on Systems, Man, and Cybernetics*, 25(1):181–189, 1995.

[21] Masao Iri, Katsuaki Aoki, Eiji O'Shima, and H Matsuyama. An algorithm for diagnosis of system failures in the chemical process. *Computers & Chemical Engineering*, 3(1-4):489–493, 1979.

[22] Jian-Da Wu, Yu-Hsuan Wang, and Mingsian R Bai. Development of an expert system for fault diagnosis in scooter engine platform using fuzzy-logic inference. *Expert Systems with Applications*, 33(4):1063–1075, 2007.

[23] Venkat Venkatasubramanian, Raghunathan Rengaswamy, Surya N Kavuri, and Kewen Yin. A review of process fault detection and diagnosis: Part III: Process history based methods. *Computers & Chemical Engineering*, 27(3):327–346, 2003.

[24] Gao Zhiwei, Carlo Cecati, Steven X Ding, et al. A survey of fault diagnosis and fault-tolerant techniques—part II: Fault diagnosis with knowledge-based and hybrid/active approaches. *IEEE Transactions on Industrial Electronics*, 2015.

[25] Steven X Ding. *Advanced methods for fault diagnosis and fault-tolerant control*. Springer, 2021.

[26] Ruqiang Yan, Robert X Gao, and Xuefeng Chen. Wavelets for fault diagnosis of rotary machines: A review with applications. *Signal processing*, 96:1–15, 2014.

[27] Purushottam Gangsar and Rajiv Tiwari. Signal based condition monitoring techniques for fault detection and diagnosis of induction motors: A state-of-the-art review. *Mechanical Systems and Signal Processing*, 144:106908, 2020.

[28] Yuanfang Chi, Yanjie Dong, Jane Wang, F Richard Yu, and Victor CM Leung. Knowledge-based fault diagnosis in industrial internet of things: A survey. *IEEE Internet of Things Journal*, 2022.

[29] Richard Vernon Beard. *Failure accomodation in linear systems through self-reorganization.* PhD thesis, Massachusetts Institute of Technology, 1971.

[30] Jie Chen, Ron J Patton, and Hong-Yue Zhang. Design of unknown input observers and robust fault detection filters. *International Journal of Control*, 63(1):85–105, 1996.

[31] Zhiwei Gao, Xiaoxu Liu, and Michael ZQ Chen. Unknown input observer-based robust fault estimation for systems corrupted by partially decoupled disturbances. *IEEE Transactions on Industrial Electronics*, 63(4):2537–2547, 2015.

[32] Andrea Cristofaro and Tor Arne Johansen. Fault tolerant control allocation using unknown input observers. *Automatica*, 50(7):1891–1897, 2014.

[33] Christopher Edwards, Sarah K Spurgeon, and Ron J Patton. Sliding mode observers for fault detection and isolation. *Automatica*, 36(4):541–553, 2000.

[34] Chee Pin Tan and Christopher Edwards. Sliding mode observers for detection and reconstruction of sensor faults. *Automatica*, 38(10):1815–1821, 2002.

[35] Hong Wang and Steve Daley. Actuator fault diagnosis: an adaptive observer-based technique. *IEEE Transactions on Automatic Control*, 41(7):1073–1078, 1996.

[36] Qinghua Zhang. Adaptive observer for multiple-input-multiple-output (mimo) linear time-varying systems. *IEEE Transactions on Automatic Control*, 47(3):525–529, 2002.

[37] Christian Commault, Jean-Michel Dion, Olivier Sename, and Reza Motyeian. Observer-based fault detection and isolation for structured systems. *IEEE Transactions on Automatic Control*, 47(12):2074–2079, 2002.

[38] Paul M Frank. Enhancement of robustness in observer-based fault detection. *International Journal of Control*, 59(4):955–981, 1994.

[39] EYEY Chow and Alan Willsky. Analytical redundancy and the design of robust failure detection systems. *IEEE Transactions on Automatic Control*, 29(7):603–614, 1984.

[40] Xianchun Ding, Limin Guo, and Torsten Jeinsch. A characterization of parity space and its application to robust fault detection. *IEEE Transactions on Automatic Control*, 44(2):337–343, 1999.

[41] Janos Gertler. *Fault detection and diagnosis in engineering systems*. CRC press, 1998.

[42] Xiao He, Zidong Wang, Yang Liu, and Dong-Hua Zhou. Least-squares fault detection and diagnosis for networked sensing systems using a direct state estimation approach. *IEEE Transactions on Industrial Informatics*, 9(3):1670–1679, 2013.

[43] Zhiwei Gao. Fault estimation and fault-tolerant control for discrete-time dynamic systems. *IEEE Transactions on Industrial Electronics*, 62(6):3874–3884, 2015.

[44] Erik Frisk and Mattias Nyberg. A minimal polynomial basis solution to residual generation for fault diagnosis in linear systems. *Automatica*, 37(9):1417–1424, 2001.

[45] Mattias Nyberg and Erik Frisk. Residual generation for fault diagnosis of systems described by linear differential-algebraic equations. *IEEE Transactions on Automatic Control*, 51(12):1995–2000, 2006.

[46] Carsten Scherer, Pascal Gahinet, and Mahmoud Chilali. Multiobjective output-feedback control via LMI optimization. *IEEE Transactions on Automatic Control*, 42(7):896–911, 1997.

[47] Maiying Zhong, Steven X Ding, James Lam, and Haibo Wang. An LMI approach to design robust fault detection filter for uncertain LTI systems. *Automatica*, 39(3):543–550, 2003.

[48] Xiaobo Li and Kemin Zhou. A time domain approach to robust fault detection of linear time-varying systems. *Automatica*, 45(1):94–102, 2009.

[49] Xiao He, Zidong Wang, and DH Zhou. Robust fault detection for networked systems with communication delay and data missing. *Automatica*, 45(11):2634–2639, 2009.

[50] Ralf Seliger and Paul M Frank. Fault-diagnosis by disturbance decoupled nonlinear observers. In *the 30th IEEE Conference on Decision and Control*, pages 2248–2253, 1991.

[51] Mouhacine Benosman. A survey of some recent results on nonlinear fault tolerant control. *Mathematical Problems in Engineering*, 2010, 2010.

[52] Riccardo MG Ferrari, Thomas Parisini, and Marios M Polycarpou. Distributed fault detection and isolation of large-scale discrete-time nonlinear systems: An adaptive approximation approach. *IEEE Transactions on Automatic Control*, 57(2):275–290, 2011.

[53] Peyman Mohajerin Esfahani and John Lygeros. A tractable fault detection and isolation approach for nonlinear systems with probabilistic performance. *IEEE Transactions on Automatic Control*, 61(3):633–647, 2015.

[54] Hongtian Chen, Zhigang Liu, Cesare Alippi, Biao Huang, and Derong Liu. Explainable intelligent fault diagnosis for nonlinear dynamic systems: From unsupervised to supervised learning. *IEEE Transactions on Neural Networks and Learning Systems*, 2022.

[55] Hongtian Chen, Linlin Li, Chao Shang, and Biao Huang. Fault detection for nonlinear dynamic systems with consideration of modeling errors: A data-driven approach. *IEEE Transactions on Cybernetics*, 2022.

[56] Steven X Ding, Ping Zhang, A Naik, Eve L Ding, and Biao Huang. Subspace method aided data-driven design of fault detection and isolation systems. *Journal of Process Control*, 19(9):1496–1510, 2009.

[57] Jin Wang and S Joe Qin. Closed-loop subspace identification using the parity space. *Automatica*, 42(2):315–320, 2006.

[58] A Akhenak, E Duviella, L Bako, and S Lecoeuche. Online fault diagnosis using recursive subspace identification: Application to a dam-gallery open channel system. *Control Engineering Practice*, 21(6):797–806, 2013.

[59] Yiming Wan, Tamas Keviczky, Michel Verhaegen, and Fredrik Gustafsson. Data-driven robust receding horizon fault estimation. *Automatica*, 71:210–221, 2016.

[60] Yiming Wan, Tamás Keviczky, and Michel Verhaegen. Fault estimation filter design with guaranteed stability using markov parameters. *IEEE Transactions on Automatic Control*, 63(4):1132–1139, 2017.

[61] Theodora Kourti and John F MacGregor. Process analysis, monitoring and diagnosis, using multivariate projection methods. *Chemometrics and Intelligent Laboratory Systems*, 28(1):3–21, 1995.

[62] Ricardo Dunia and S Joe Qin. Joint diagnosis of process and sensor faults using principal component analysis. *Control Engineering Practice*, 6(4):457–469, 1998.

[63] S Joe Qin. Statistical process monitoring: basics and beyond. *Journal of Chemometrics: A Journal of the Chemometrics Society*, 17(8-9):480–502, 2003.

[64] Chris Van Der Ploeg, Mohsen Alirezaei, Nathan Van De Wouw, and Peyman Mohajerin Esfahani. Multiple faults estimation in dynamical systems: Tractable design and performance bounds, 2020.

[65] Agnar Höskuldsson. Pls regression methods. *Journal of Chemometrics*, 2(3):211–228, 1988.

[66] John F MacGregor and Theodora Kourti. Statistical process control of multivariate processes. *Control Engineering Practice*, 3(3):403–414, 1995.

[67] Shen Yin. *Data-driven design of fault diagnosis systems*. PhD thesis, Duisburg, Essen, Universität Duisburg-Essen, Diss., 2012, 2012.

[68] Steven X Ding. *Data-driven design of fault diagnosis and fault-tolerant control systems*. Springer, 2014.

[69] Jong-Min Lee, ChangKyoo Yoo, Sang Wook Choi, Peter A Vanrolleghem, and In-Beum Lee. Nonlinear process monitoring using kernel principal component analysis. *Chemical Engineering Science*, 59(1):223–234, 2004.

[70] Yingwei Zhang, Hong Zhou, S Joe Qin, and Tianyou Chai. Decentralized fault diagnosis of large-scale processes using multiblock kernel partial least squares. *IEEE Transactions on Industrial Informatics*, 6(1):3–10, 2009.

[71] KG Narendra, VK Sood, K Khorasani, and R Patel. Application of a radial basis function (rbf) neural network for fault diagnosis in a hvdc system. *IEEE Transactions on Power Systems*, 13(1):177–183, 1998.

[72] Yi-gang He, Yan-hong Tan, and Yi-chuang Sun. Wavelet neural network approach for fault diagnosis of analogue circuits. *IEE Proceedings-Circuits, Devices and Systems*, 151(4):379–384, 2004.

[73] Xiaoyue Chen, Jianzhong Zhou, Han Xiao, Ercheng Wang, Jian Xiao, and Huifeng Zhang. Fault diagnosis based on comprehensive geometric characteristic and probability neural network. *Applied Mathematics and Computation*, 230:542–554, 2014.

[74] Yaguo Lei, Bin Yang, Xinwei Jiang, Feng Jia, Naipeng Li, and Asoke K Nandi. Applications of machine learning to machine fault diagnosis: A review and roadmap. *Mechanical Systems and Signal Processing*, 138:106587, 2020.

[75] Thomas Cover and Peter Hart. Nearest neighbor pattern classification. *IEEE Transactions on Information Theory*, 13(1):21–27, 1967.

[76] Daphne Koller and Nir Friedman. *Probabilistic graphical models: principles and techniques*. MIT press, 2009.

[77] Chuan Li, René-Vinicio Sanchez, Grover Zurita, Mariela Cerrada, Diego Cabrera, and Rafael E Vásquez. Multimodal deep support vector classification with homologous features and its application to gearbox fault diagnosis. *Neurocomputing*, 168:119–127, 2015.

[78] Feng Jia, Yaguo Lei, Jing Lin, Xin Zhou, and Na Lu. Deep neural networks: A promising tool for fault characteristic mining and intelligent diagnosis of rotating machinery with massive data. *Mechanical Systems and Signal Processing*, 72:303–315, 2016.

[79] Yann LeCun, Yoshua Bengio, and Geoffrey Hinton. Deep learning. *Nature*, 521(7553):436–444, 2015.

[80] Feng Jia, Yaguo Lei, Liang Guo, Jing Lin, and Saibo Xing. A neural network constructed by deep learning technique and its application to intelligent fault diagnosis of machines. *Neurocomputing*, 272:619–628, 2018.

[81] Haidong Shao, Hongkai Jiang, Huiwei Zhao, and Fuan Wang. A novel deep autoencoder feature learning method for rotating machinery fault diagnosis. *Mechanical Systems and Signal Processing*, 95:187–204, 2017.

[82] Meng Ma, Chuang Sun, and Xuefeng Chen. Deep coupling autoencoder for fault diagnosis with multimodal sensory data. *IEEE Transactions on Industrial Informatics*, 14(3):1137–1145, 2018.

[83] Xiao-hui He, Dong Wang, Yan-feng Li, Chun-hua Zhou, et al. A novel bearing fault diagnosis method based on gaussian restricted boltzmann machine. *Mathematical Problems in Engineering*, 2016, 2016.

[84] Haidong Shao, Hongkai Jiang, Fuan Wang, and Yanan Wang. Rolling bearing fault diagnosis using adaptive deep belief network with dual-tree complex wavelet packet. *ISA Transactions*, 69:187–201, 2017.

[85] Haidong Shao, Hongkai Jiang, Xun Zhang, and Maogui Niu. Rolling bearing fault diagnosis using an optimization deep belief network. *Measurement Science and Technology*, 26(11):115002, 2015.

[86] Alex Krizhevsky, Ilya Sutskever, and Geoffrey E Hinton. Imagenet classification with deep convolutional neural networks. *Communications of the ACM*, 60(6):84–90, 2017.

[87] MM Manjurul Islam and Jong-Myon Kim. Automated bearing fault diagnosis scheme using 2d representation of wavelet packet transform and deep convolutional neural network. *Computers in Industry*, 106:142–153, 2019.

[88] Sheng Guo, Tao Yang, Wei Gao, and Chen Zhang. A novel fault diagnosis method for rotating machinery based on a convolutional neural network. *Sensors*, 18(5):1429, 2018.

[89] Dezun Zhao, Tianyang Wang, and Fulei Chu. Deep convolutional neural network based planet bearing fault classification. *Computers in Industry*, 107:59–66, 2019.

[90] Ruonan Liu, Guotao Meng, Boyuan Yang, Chuang Sun, and Xuefeng Chen. Dislocated time series convolutional neural architecture: An intelligent fault diagnosis approach for electric machine. *IEEE Transactions on Industrial Informatics*, 13(3):1310–1320, 2016.

[91] Shaobo Li, Guokai Liu, Xianghong Tang, Jianguang Lu, and Jianjun Hu. An ensemble deep convolutional neural network model with improved ds evidence fusion for bearing fault diagnosis. *Sensors*, 17(8):1729, 2017.

[92] Levent Eren, Turker Ince, and Serkan Kiranyaz. A generic intelligent bearing fault diagnosis system using compact adaptive 1d cnn classifier. *Journal of Signal Processing Systems*, 91:179–189, 2019.

[93] Luyang Jing, Ming Zhao, Pin Li, and Xiaoqiang Xu. A convolutional neural network based feature learning and fault diagnosis method for the condition monitoring of gearbox. *Measurement*, 111:1–10, 2017.

[94] Wei Zhang, Xiang Li, and Qian Ding. Deep residual learning-based fault diagnosis method for rotating machinery. *ISA transactions*, 95:295–305, 2019.

[95] Duy-Tang Hoang and Hee-Jun Kang. A survey on deep learning based bearing fault diagnosis. *Neurocomputing*, 335:327–335, 2019.

[96] Jingwei Dong, Arman Sharifi Kolarijani, and Peyman Mohajerin Esfahani. Multi-mode diagnosis for switched affine systems with noisy measurement. *Automatica*, 151:110898, 2023.

[97] Venkat Venkatasubramanian, Raghunathan Rengaswamy, Kewen Yin, and Surya N Kavuri. A review of process fault detection and diagnosis: Part I: Quantitative model-based methods. *Computers & Chemical Engineering*, 27(3):293–311, 2003.

[98] Ali Zolghadri. Advanced model-based FDIR techniques for aerospace systems: Today challenges and opportunities. *Progress in Aerospace Sciences*, 53:18–29, 2012.

[99] James Weimer, José Araujo, Mani Amoozadeh, Seyed Alireza Ahmadi, Henrik Sandberg, and Karl Henrik Johansson. Parameter-invariant actuator fault diagnostics in cyber-physical systems with application to building automation. In *Control of Cyber-Physical Systems*, pages 179–196. Springer, 2013.

[100] Laurent Bako. Identification of switched linear systems via sparse optimization. *Automatica*, 47(4):668–677, 2011.

[101] Henrik Ohlsson and Lennart Ljung. Identification of switched linear regression models using sum-of-norms regularization. *Automatica*, 49(4):1045–1050, 2013.

[102] G Ackerson and K Fu. On state estimation in switching environments. *IEEE Transactions on Automatic Control*, 15(1):10–17, 1970.

[103] Hai Lin and Panos J Antsaklis. Stability and stabilizability of switched linear systems: a survey of recent results. *IEEE Transactions on Automatic control*, 54(2):308–322, 2009.

[104] Shuai Yuan, Lixian Zhang, Bart De Schutter, and Simone Baldi. A novel lyapunov function for a non-weighted $\mathcal{L}_2$ gain of asynchronously switched linear systems. *Automatica*, 87:310–317, 2018.

[105] David Henry and Ali Zolghadri. Design and analysis of robust residual generators for systems under feedback control. *Automatica*, 41(2):251–264, 2005.

[106] Francesca Boem, Riccardo MG Ferrari, and Thomas Parisini. Distributed fault detection and isolation of continuous-time non-linear systems. *European Journal of Control*, 17(5-6):603–620, 2011.

[107] Kaikai Pan, Peter Palensky, and Peyman Mohajerin Esfahani. Dynamic anomaly detection with high-fidelity simulators: A convex optimization approach. *IEEE Transactions on Smart Grid*, 13(2):1500–1515, 2021.

[108] Meriem Halimi, Gilles Millérioux, and Jamal Daafouz. Model-based modes detection and discernibility for switched affine discrete-time systems. *IEEE Transactions on Automatic Control*, 60(6):1501–1514, 2014.

[109] Ferdinand Küsters and Stephan Trenn. Switch observability for switched linear systems. *Automatica*, 87:121–127, 2018.

[110] Vincent Cocquempot, Touria El Mezyani, and Marcel Staroswiecki. Fault detection and isolation for hybrid systems using structured parity residuals. In *the 5th Asian Control Conference*, volume 2, pages 1204–1212. IEEE, 2004.

[111] Dan Wang and Kai Yew Lum. Adaptive unknown input observer approach for aircraft actuator fault detection and isolation. *International Journal of Adaptive Control and Signal Processing*, 21(1):31–48, 2007.

[112] Diego Mincarelli, Alessandro Pisano, Thierry Floquet, and Elio Usai. Uniformly convergent sliding mode-based observation for switched linear systems. *International Journal of Robust and Nonlinear Control*, 26(7):1549–1564, 2016.

[113] ZhiHui Zhang, Shujiang Li, Hua Yan, and QuanYong Fan. Sliding mode switching observer-based actuator fault detection and isolation for a class of uncertain systems. *Nonlinear Analysis: Hybrid Systems*, 33:322–335, 2019.

[114] Joseph K Scott, Rolf Findeisen, Richard D Braatz, and Davide M Raimondo. Input design for guaranteed fault diagnosis using zonotopes. *Automatica*, 50(6):1580–1589, 2014.

[115] G Roberto Marseglia and Davide M Raimondo. Active fault diagnosis: A multi-parametric approach. *Automatica*, 79:223–230, 2017.

[116] Farshad Harirchi and Necmiye Ozay. Guaranteed model-based fault detection in cyber–physical systems: A model invalidation approach. *Automatica*, 93:476–488, 2018.

[117] Francesca Boem, Stefano Riverso, Giancarlo Ferrari-Trecate, and Thomas Parisini. Plug-and-play fault detection and isolation for large-scale nonlinear systems with stochastic uncertainties. *IEEE Transactions on Automatic Control*, 64(1):4–19, 2018.

[118] XiaoHeng Chang and GuangHong Yang. New results on output feedback $\mathcal{H}_\infty$ control for linear discrete-time systems. *IEEE Transactions on Automatic Control*, 59(5):1355–1359, 2013.

[119] Kaikai Pan, Peter Palensky, and Peyman Mohajerin Esfahani. From static to dynamic anomaly detection with application to power system cyber security. *IEEE Transactions on Power Systems*, 35(2):1584–1596, 2019.

[120] Roman Vershynin. *High-dimensional probability: An introduction with applications in data science*, volume 47. Cambridge university press, 2018.

[121] Paulo Rosa and Carlos Silvestre. On the distinguishability of discrete linear time-invariant dynamic systems. In *2011 50th IEEE Conference on Decision and Control and European Control Conference*, pages 3356–3361. IEEE, 2011.

[122] Yang Liu, Zidong Wang, Xiao He, and Dong-Hua Zhou. Filtering and fault detection for nonlinear systems with polynomial approximation. *Automatica*, 54:348–359, 2015.

[123] Maurıcio C De Oliveira, José C Geromel, and Jacques Bernussou. Extended $\mathcal{H}_2$ and $\mathcal{H}_\infty$ norm characterizations and controller parametrizations for discrete-time systems. *International Journal of Control*, 75(9):666–679, 2002.

[124] Carl D Meyer. *Matrix analysis and applied linear algebra*, volume 71. Siam, 2000.

[125] Chris Van der Ploeg, Mohsen Alirezaei, Nathan Van De Wouw, and Peyman Mohajerin Esfahani. Multiple faults estimation in dynamical systems: Tractable design and performance bounds. *IEEE Transactions on Automatic Control*, 2022.

[126] J. Löfberg. Yalmip : A toolbox for modeling and optimization in matlab. In *Proceedings of the CACSD Conference*, Taipei, Taiwan, 2004.

[127] Heng Wang and G-H Yang. A finite frequency domain approach to fault detection for linear discrete-time systems. *International Journal of Control*, 81(7):1162–1171, 2008.

[128] Jian Liu, Jian Liang Wang, and Guang-Hong Yang. An LMI approach to minimum sensitivity analysis with application to fault detection. *Automatica*, 41(11):1995–2004, 2005.

[129] Tetsuya Iwasaki and Shinji Hara. Generalized KYP lemma: Unified frequency domain inequalities with design applications. *IEEE Transactions on Automatic Control*, 50(1):41–59, 2005.

[130] Zhenhua Wang, Peng Shi, and Cheng-Chew Lim. $\mathcal{H}_-/\mathcal{H}_\infty$ fault detection observer in finite frequency domain for linear parameter-varying descriptor systems. *Automatica*, 86:38–45, 2017.

[131] Wentao Tang, Zhenhua Wang, and Yi Shen. Fault detection and isolation for discrete-time descriptor systems based on $\mathcal{H}_-/\mathcal{L}_\infty$ observer and zonotopic residual evaluation. *International Journal of Control*, 93(8):1867–1878, 2020.

[132] Weixin Han, Pan Long, and Bin Xu. Fault detection for uncertain polynomial fuzzy systems using $\mathcal{H}_-/\mathcal{L}_\infty$ observer and ellipsoidal analysis. *IEEE Transactions on Fuzzy Systems*, 2022.

[133] Halim Alwi and Christopher Edwards. Robust fault reconstruction for linear parameter varying systems using sliding mode observers. *International Journal of Robust and Nonlinear Control*, 24(14):1947–1968, 2014.

[134] Zhiwei Gao, Steven X Ding, and Y Ma. Robust fault estimation approach and its application in vehicle lateral dynamic systems. *Optimal Control Applications and Methods*, 28(3):143–156, 2007.

[135] Henrik Niemann and Jakob Stoustrup. Design of fault detectors using $\mathcal{H}_\infty$ optimization. In *Proceedings of the 39th IEEE Conference on Decision and Control (Cat. No. 00CH37187)*, volume 5, pages 4327–4328. IEEE, 2000.

[136] Jianfei Dong and Michel Verhaegen. Identification of fault estimation filter from I/O data for systems with stable inversion. *IEEE Transactions on Automatic Control*, 57(6):1347–1361, 2011.

[137] Steven Gillijns. Kalman filtering techniques for system inversion and data assimilation. *Katholieke universiteit leuven*, 2007.

[138] Ming Hou and Ron J Patton. Input observability and input reconstruction. *Automatica*, 34(6):789–794, 1998.

[139] Ke Zhang, Bin Jiang, Peng Shi, and Jinfa Xu. Analysis and design of robust $\mathcal{H}_\infty$ fault estimation observer with finite-frequency specifications for discrete-time fuzzy systems. *IEEE Transactions on Cybernetics*, 45(7):1225–1235, 2014.

[140] Zhenhua Wang, Peng Shi, and Cheng-Chew Lim. Robust fault estimation observer in the finite frequency domain for descriptor systems. *International Journal of Control*, 92(7):1590–1599, 2019.

[141] Jovan Stefanovski and Đani Juričić. Input estimation over frequency region in presence of disturbances. *IEEE Transactions on Automatic Control*, 64(12):5074–5079, 2019.

[142] Chao Shang, Steven X Ding, and Hao Ye. Distributionally robust fault detection design and assessment for dynamical systems. *Automatica*, 125:109434, 2021.

[143] Huijun Gao and Xianwei Li. $\mathcal{H}_\infty$ filtering for discrete-time state-delayed systems with finite frequency specifications. *IEEE Transactions on Automatic Control*, 56(12):2935–2941, 2011.

[144] Chris van der Ploeg, Emilia Silvas, Nathan van de Wouw, and Peyman Mohajerin Esfahani. Real-time fault estimation for a class of discrete-time linear parameter-varying systems. *IEEE Control Systems Letters*, 6:1988–1993, 2021.

[145] Guangtao Ran, Jian Liu, Chuanjiang Li, Hak-Keung Lam, Dongyu Li, and Hongtian Chen. Fuzzy-model-based asynchronous fault detection for markov jump systems with partially unknown transition probabilities: an adaptive event-triggered approach. *IEEE Transactions on Fuzzy Systems*, 30(11):4679–4689, 2022.

[146] Stephen Boyd, Laurent El Ghaoui, Eric Feron, and Venkataramanan Balakrishnan. *Linear matrix inequalities in system and control theory*. SIAM, 1994.

[147] Lu Wang and Jianbo Su. Disturbance rejection control for non-minimum phase systems with optimal disturbance observer. *ISA Transactions*, 57:1–9, 2015.

[148] Muhammad Waseem Altaf, Mohammad Taufiqul Arif, Shama Naz Islam, and Md Enamul Haque. Microgrid protection challenges and mitigation approaches-a comprehensive review. *IEEE Access*, 2022.

[149] M Amin Zamani, Amirnaser Yazdani, and Tarlochan S Sidhu. A communication-assisted protection strategy for inverter-based medium-voltage microgrids. *IEEE Transactions on Smart Grid*, 3(4):2088–2099, 2012.

[150] Kexing Lai, Mahesh S Illindala, and Mohammed A Haj-ahmed. Comprehensive protection strategy for an islanded microgrid using intelligent relays. In *2015 IEEE Industry Applications Society Annual Meeting*, pages 1–11. IEEE, 2015.

[151] Hamed Karimi, Ghazanfar Shahgholian, Bahador Fani, Iman Sadeghkhani, and Majid Moazzami. A protection strategy for inverter-interfaced islanded microgrids with looped configuration. *Electrical Engineering*, 101(3):1059–1073, 2019.

[152] Dispersed Generation Photovoltaics and Energy Storage. Ieee application guide for ieee std 1547™, ieee standard for interconnecting distributed resources with electric power systems. *IEEE std*, pages 1547–2, 2009.

[153] Tom Loix, Thomas Wijnhoven, and Geert Deconinck. Protection of microgrids with a high penetration of inverter-coupled energy sources. In *2009 CIGRE/IEEE PES Joint Symposium Integration of Wide-Scale Renewable Resources Into the Power Delivery System*, pages 1–6. IEEE, 2009.

[154] Erik Casagrande, Wei Lee Woon, Hatem H Zeineldin, and Davor Svetinovic. A differential sequence component protection scheme for microgrids with inverter-based distributed generators. *IEEE Transactions on Smart Grid*, 5(1):29–37, 2013.

[155] SR Samantaray, Geza Joos, and Innocent Kamwa. Differential energy based microgrid protection against fault conditions. In *2012 IEEE PES Innovative Smart Grid Technologies (ISGT)*, pages 1–7. IEEE, 2012.

[156] Eric Sortomme, SS Venkata, and Joydeep Mitra. Microgrid protection using communication-assisted digital relays. *IEEE Transactions on Power Delivery*, 25(4):2789–2796, 2009.

[157] Xinyao Li, Adam Dyśko, and Graeme M Burt. Traveling wave-based protection scheme for inverter-dominated microgrid using mathematical morphology. *IEEE Transactions on Smart Grid*, 5(5):2211–2218, 2014.

[158] Sohrab Mirsaeidi, Dalila Mat Said, Mohammad Wazir Mustafa, and Mohammad Hafiz Habibuddin. A protection strategy for micro-grids based on positive-sequence component. *IET Renewable Power Generation*, 9(6):600–609, 2015.

[159] Siavash Beheshtaein, Mehdi Savaghebi, Juan Carlos Vasquez, and Josep M Guerrero. A hybrid algorithm for fault locating in looped microgrids. In *2016 IEEE Energy Conversion Congress and Exposition (ECCE)*, pages 1–6. IEEE, 2016.

[160] Hashim A Al Hassan, Andrew Reiman, Gregory F Reed, Zhi-Hong Mao, and Brandon M Grainger. Model-based fault detection of inverter-based microgrids and a mathematical framework to analyze and avoid nuisance tripping and blinding scenarios. *Energies*, 11(8):2152, 2018.

[161] Houshang Karimi, Amirnaser Yazdani, and Reza Iravani. Negative-sequence current injection for fast islanding detection of a distributed resource unit. *IEEE Transactions on Power Electronics*, 23(1):298–307, 2008.

[162] Mohammad Pirani, Mehdi Hosseinzadeh, Joshua A Taylor, and Bruno Sinopoli. Optimal active fault detection in inverter-based grids. *IEEE Transactions on Control Systems Technology*, 2022.

[163] Ron J Patton and Jie Chen. On eigenstructure assignment for robust fault diagnosis. *International Journal of Robust and Nonlinear Control: IFAC-Affiliated Journal*, 10(14):1193–1208, 2000.

[164] Nagaraju Pogaku, Milan Prodanovic, and Timothy C Green. Modeling, analysis and testing of autonomous operation of an inverter-based microgrid. *IEEE Transactions on Power Electronics*, 22(2):613–625, 2007.

[165] Stefan Leitner, Mehrdad Yazdanian, Ali Mehrizi-Sani, and Annette Muetze. Small-signal stability analysis of an inverter-based microgrid with internal model-based controllers. *IEEE Transactions on Smart Grid*, 9(5):5393–5402, 2017.

[166] Robert H Park. Two-reaction theory of synchronous machines generalized method of analysis-part I. *Transactions of the American Institute of Electrical Engineers*, 48(3):716–727, 1929.

[167] Yinliang Xu. Robust finite-time control for autonomous operation of an inverter-based microgrid. *IEEE Transactions on Industrial Informatics*, 13(5):2717–2725, 2017.

[168] Jianglin Lan and Ron J Patton. A new strategy for integration of fault estimation within fault-tolerant control. *Automatica*, 69:48–59, 2016.